UNIVERSITY OF OKLAHOMA

GRADUATE COLLEGE

EVALUATING THE PERFORMANCE OF METHODS FOR DUAL-FUNCTION RADAR COMMUNICATIONS

A THESIS

SUBMITTED TO THE GRADUATE FACULTY

in partial fulfillment of the requirements for the

Degree of

MASTER OF SCIENCE

By

MIKAL COLE
Norman, Oklahoma
2022

EVALUATING THE PERFORMANCE OF METHODS FOR DUAL-FUNCTION RADAR COMMUNICATIONS

A THESIS APPROVED FOR THE
SCHOOL OF ELECTRICAL AND COMPUTER ENGINEERING

BY THE COMMITTEE CONSISTING OF

Dr. Justin Metcalf, Chair

Dr. Nathan Goodman

Dr. Samuel Cheng

Acknowledgments

I would like to thank my research adviser Professor Justin Metcalf for all of the help and direction he has given me throughout my time at the University of Oklahoma. I thank Dr. Nathan Goodman and Dr. Samuel Cheng for agreeing to be on my thesis committee. I would also like to thank my family who has supported me throughout my life.

I thank the Defense Advanced Research Projects Agency (DARPA) under Grant HR0011-20-1-0007 for sponsoring this work.

Table of Contents

List of Figures

Abstract

Dual-Function Radar Communications (DFRC), where a radar and communications function is performed by the same antenna or array, has recently begun to be investigated as a means of alleviating or coping with spectrum congestion [1]. O'Connor and O'Donoughue [2] investigated continuous wave DFRC and this thesis focuses on extending O'Connor and O'Donoughue's treatment to pulsed radar operations.

Timesharing, aperture partitioning, and simultaneous dual-beam (SDB) are compared by spectral efficiency across the amount of power allocated to the communications function, distance, and pulse repetition frequency (PRF). Each DFRC method is also evaluated on its performance on parameter estimators, beamwidth, and detection effects.

Chapter 1

Introduction

1.1 Overview

Modern radars need to perform multiple functions simultaneously and these functions compete for time, energy, and computational resources. Some of these tasks can include:

- Search
- Tracking
- Target classification
- Communications
- Imaging
- Waveform selection
- Interference mitigation

These tasks must be controlled by some sort of scheduler which must, by some metric, select the next task, interrupt the current task, or change some mode of array operation.

1.2 Motivation

With more and more devices utilizing the electromagnetic spectrum for sensing and communication purposes, the spectrum is becoming more crowded leading to interference effects becoming more common and spectrum sharing becoming a necessity.

One way of dealing with a congested spectrum is the use of dual-function radar and communications (DFRC) where a radar performs both sensing and communications functions. Therefore, determining some sort of metric of performance, especially for digital arrays where more advanced techniques are available, is important to arrive at an optimal DFRC method given the environment presented to the system. Concerning DFRC, channel capacity and spectral efficiency have been used as a metric to determine when to use timesharing, simultaneous dual-beam (SDB), or aperture partitioning as DFRC methods. However, spectral efficiency or capacity as a metric for DFRC performance is incomplete as of now.

1.3 Research Objective

This thesis seeks to expand on communications, tracking, and radar performance metrics of dual or multi-functional, digital, phased array radars. This will provide a framework for future work for radars operating in a congested spectrum and for future metrics for evaluating radar performance or capability. Furthermore this thesis will investigate the effects of array element number, beam-steering, search and detection requirements, and effects of interferers and how these, combined with DFRC, affect the performance of the communications or sensing functions.

1.4 Outline of the Dissertation

To this end, following the Introduction,

Chapter 2 provides an introduction and review of literature relating to resource management and concepts that will be used for later chapters.

Chapter 3 starts expanding continuous wave DFRC [2] spectral efficiency analysis across the radar beam fraction of power (α) to look at how distance affects the optimal method.

Chapter 4 first expands on the spectral efficiency analysis of DFRC for pulsed radar and how some methods are no longer optimal as in the continuous wave case with later sections looking at how PRF affects performance.

Chapter 5 quantifies the changes in beamwidth for aperture partitioning and SDB for certain situations for its impact on other radar parameters such as tracking effects, search cells, and certain estimators.

Chapter 6 focuses on how each DFRC method may affect the Cramer-Rao Lower Bound (CRLB) for range, frequency, and angle of arrival estimators.

Chapter 7 implements the beamwidth effects into van Keuk and Blackman's [3] paper on track management.

Chapter 8 investigates how the probability of detecting a target with known SNR changes across α for two detector models.

Chapter 9 concludes the dissertation with a brief look into radar capacity measures and mutual information of a detector for searching scenarios.

Chapter 2

Spectral Efficiency of Dual Function Radar Communications

The Shannon capacity of an additive white Gaussian noise (AWGN) channel is [2], [4]

$$C = B \log_2(1 + \frac{\chi}{B}). \tag{2.1}$$

where χ is the signal-to-noise ratio (SNR) and B is the bandwidth. Another way to parameterize capacity is in terms of the spectral efficiency, measured in bits/s/Hz. The spectral efficiency is therefore defined as [2]

$$SE = \frac{C}{B} = \log_2(1 + \frac{\chi}{B}) = \log_2(1 + F) \tag{2.2}$$

where F is the figure of merit, the ratio of the SNR to the bandwidth.

The DFRC array may use three fundamental techniques to send the two beams of radar and communications. The first case considered is the SDB technique where multiple beams (two in this thesis) are simultaneously emitted from an array capable of digital beamforming. The second case, which may be considered the baseline (i.e., traditional technique) is timesharing. Timesharing means the radar and communi-

cations beams are transmitted sequentially, with each beam using the entire array. For the timesharing case, if radar gets a fraction α of the total transmit time, then the communications beam gets a fraction $\beta = 1 - \alpha$ of the transmit time. Then the spectral efficiency of timesharing is

$$SE_{ts} = \beta \log_2(1 + F). \tag{2.3}$$

The spectral efficiency for simultaneous dual-beam, if the communications beam is allocated a fraction β of the effective radiated power, is [2]

$$SE_{sdb} = \log_2(1 + \beta F). \tag{2.4}$$

The final technique for DFRC is the aperture partitioning, or sub-arraying approach. In this case some number $a = [1, 2, \ldots, N]$ of antenna elements are used radar, while $b = N - a$ elements are used for communications. It was found in [2] that, if radar gets a fraction α of the effective radiated power, the fraction available to the communication's beam is $(1 - \sqrt{\alpha})^2$ and the resulting spectral efficiency would be [2]

$$SE_{ap} = \log_2(1 + (1 - \sqrt{\alpha})^2 F). \tag{2.5}$$

Throughout this thesis, the difference between spectral efficiencies of two DFRC methods will be plotted as way of comparing the two methods. For example, in Figure 2.5, all traces apart from the $F = 1$ trace are positive, meaning SDB has a higher

spectral efficiency than timesharing at $F = 10, 100$, and 1000.

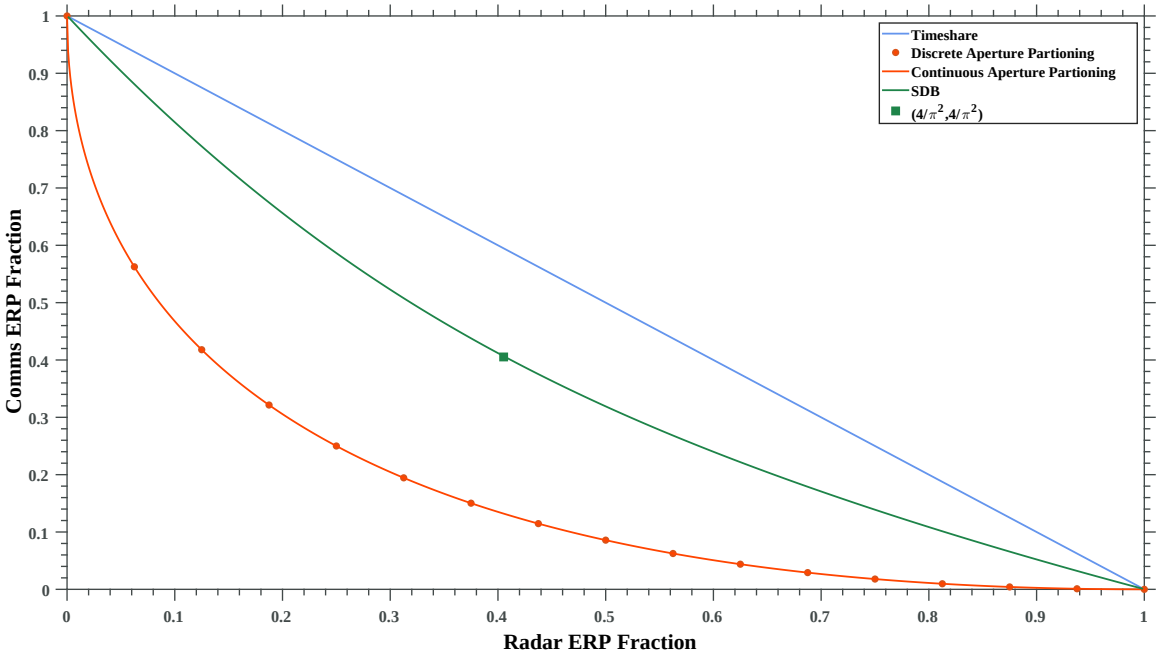

Figure 2.1: The communication beam's effective radiated power as a function of the radar beam's allocated ERP for each method of DFRC.

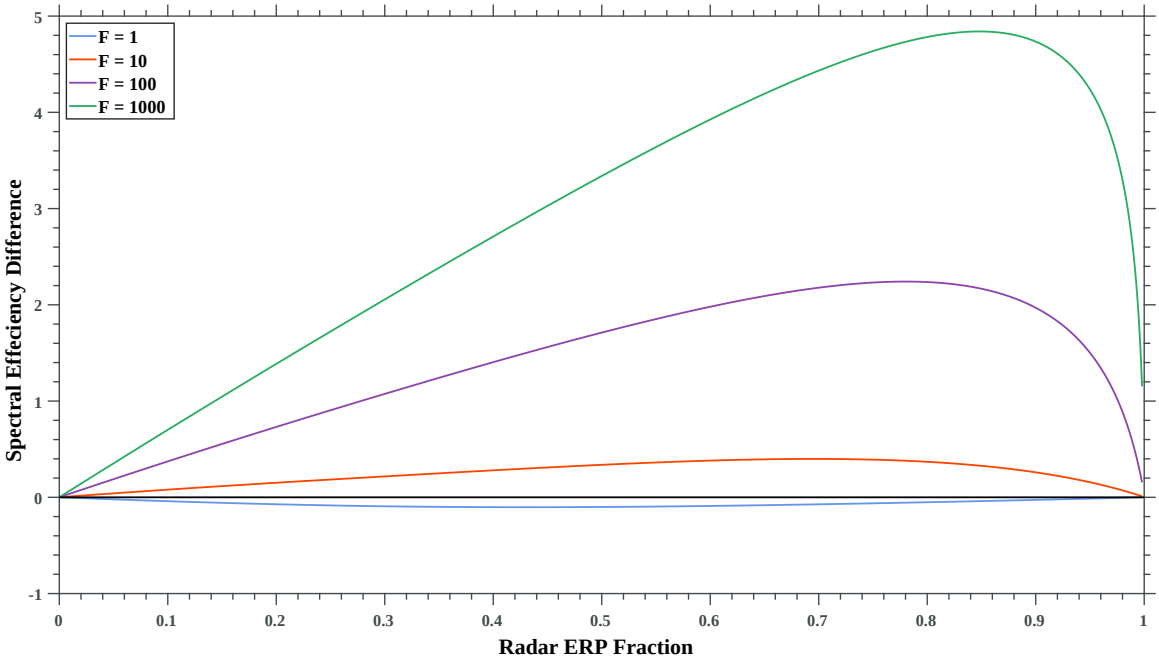

Figure 2.2: Spectral efficiency difference between simultaneous dual-beam and timesharing showing a slight advantage for timesharing in low F situations.

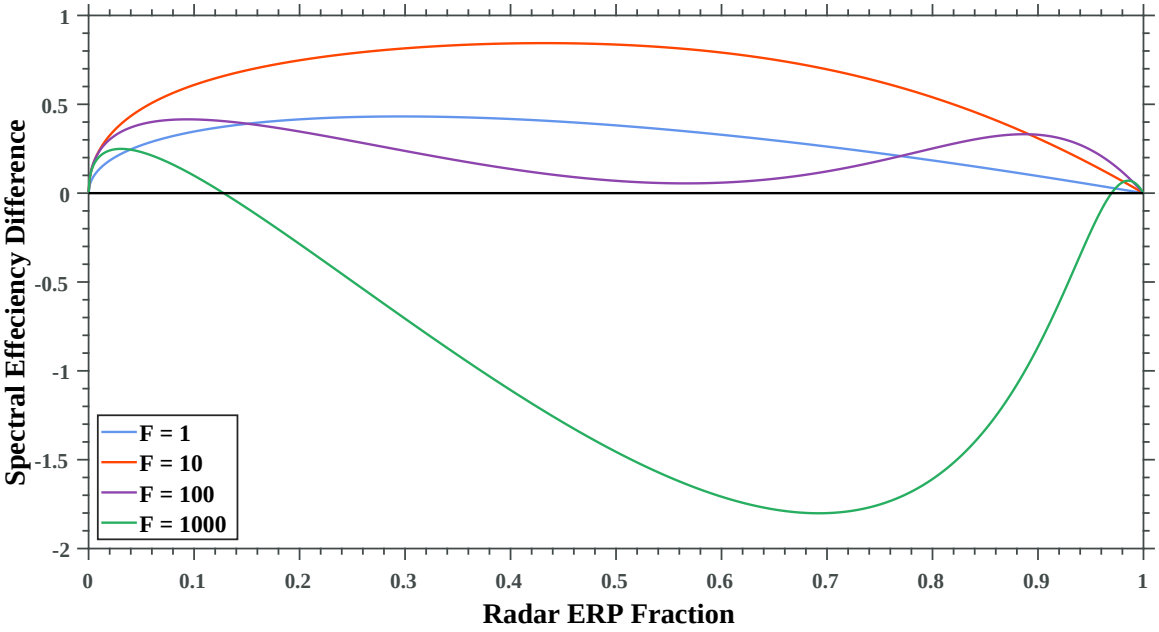

Figure 2.3: Spectral Efficiency Difference between timesharing and aperture-partitioning; not taking the number of array elements into account.

Figure 2.4 shows the effective radiated power (ERP) for the communications beam as a function of the radar beam's ERP for each of the methods. for a ULA with $N = 16$ elements. Note that the point $((4/\pi^2, 4/\pi^2)$ is the limit of SDB performance [2]. This figure correspond to Figure 2 in [2], with the exception of the aperture partitioning trace. In [2] it was assumed that the aperture partitioning could be parameterized along a continuous power curve. However, in practice each antenna element has a peak transmitted power. Therefore, we add a discretization of the aperture partitioning curve, where it is assumed that each antenna element may provide an identical power to it's assigned beam. Figures 2.5 and 2.6 are similar to Figures 8 and 9 in [2], and provide an initial examination of the comparative performance of timesharing as compared to SDB and aperture partitioning. This analysis provides a focal point for the developments in this thesis.

Chapter 3

Spectral Efficiency Analysis

This chapter focuses on covering and extending the work of [2] to show some instances of how array size affects available spectral efficiencies for aperture partitioning, how range affects spectral efficiency, and a brief example involving capacity instead of spectral efficiency for a 100MHz radar.

3.1 Simultaneous Dual-Beams from an Digital-at-Every-Element

O'Donoughue [5], introduced a method to simultaneously emit two different waveforms (radar and communications) at different angles from a digital-at-every-element array (i.e., an array with a unique waveform generator behind every antenna element). He investigated the performance tradeoffs of this approach using the loss of signal power, peak-to-average-power ratio (PAPR), and other metrics. The following equations in this section cover the necessary components of [5] to obtain the normalized power of the communications beam (β) as a function of the normalized power of the radar beam (α). This simultaneous dual-beam (SDB) algorithm will be one of the key emission techniques studied in the remainder of this thesis.

The discretized radar and communications waveforms are given by the column vectors $\boldsymbol{p}_r$ and $\boldsymbol{p}_c$ respectively. The steering vectors for the radar and communications

beams are

$$\boldsymbol{x}_r = \begin{bmatrix} 1 & e^{j\frac{2\pi}{\lambda}d\sin(\theta_r)} & \dots & e^{j\frac{2\pi}{\lambda}(N-1)d\sin(\theta_r)} \end{bmatrix}^T, \tag{3.1}$$

$$\boldsymbol{x}_c = \begin{bmatrix} 1 & e^{j\frac{2\pi}{\lambda}d\sin(\theta_c)} & \dots & e^{j\frac{2\pi}{\lambda}(N-1)d\sin(\theta_c)} \end{bmatrix}^T, \tag{3.2}$$

for an array of N elements. The steering vector is used to get the array emission in a given direction from the final signal matrix. The discretized transmit waveform for the N^{th} antenna with K samples is given by

$$\boldsymbol{s}_n = \begin{bmatrix} s_n(0) & \dots & s_n(K-1) \end{bmatrix}^T. \tag{3.3}$$

$$\tag{3.4}$$

These can be arranged into a $K \times N$ matrix,

$$\boldsymbol{S} = \begin{bmatrix} \boldsymbol{s}_0 & \dots & \boldsymbol{s}_{N-1} \end{bmatrix}, \tag{3.5}$$

to represent the entire emission from the digital array. The radar and communications signal matrices are given by

$$\boldsymbol{S}_r = \boldsymbol{p}_r \boldsymbol{x}_r^T, \tag{3.6}$$

$$\boldsymbol{S}_c = \boldsymbol{p}_c \boldsymbol{x}_c^T. \tag{3.7}$$

Given a scale factor δ, the combined matrix is formed as

$$\boldsymbol{S} = \boldsymbol{B} \odot (\sqrt{\delta}\boldsymbol{S}_r + \sqrt{1-\delta}\boldsymbol{S}_c), \tag{3.8}$$

with $\odot$ being the Hadamard product and $\boldsymbol{B}$ used to keep the transmitted energy

constant and is defined as

$$[\boldsymbol{B}]_{ij} = \frac{1}{|\sqrt{\delta}[\boldsymbol{S}_r]_{ij} + \sqrt{1-\delta}[\boldsymbol{S}_c]_{ij}|} \tag{3.9}$$

3.2 Comparing Timesharing and Aperture Partitioning for Continuous Wave Emissions

The initial analysis in [2] only considers continuous wave illumination and the two competing figures of merit of ERP and spectral efficiency. First, consider the impact of the size of the aperture on the spectral efficiency comparison between timesharing and aperture partitioning. Figures 3.1- 3.3 show the spectral efficiency difference for an array size of 8, 16, and 34 elements, respectively.

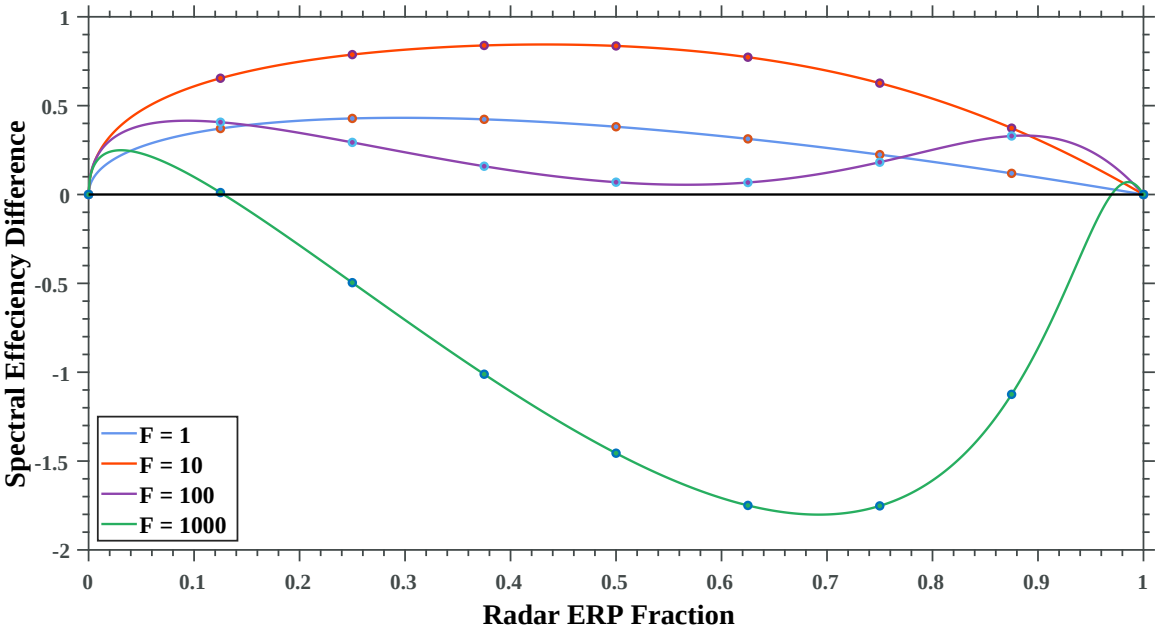

Figure 3.1: Spectral Efficiency Difference between timesharing and aperture-partitioning for an array with 8 elements.

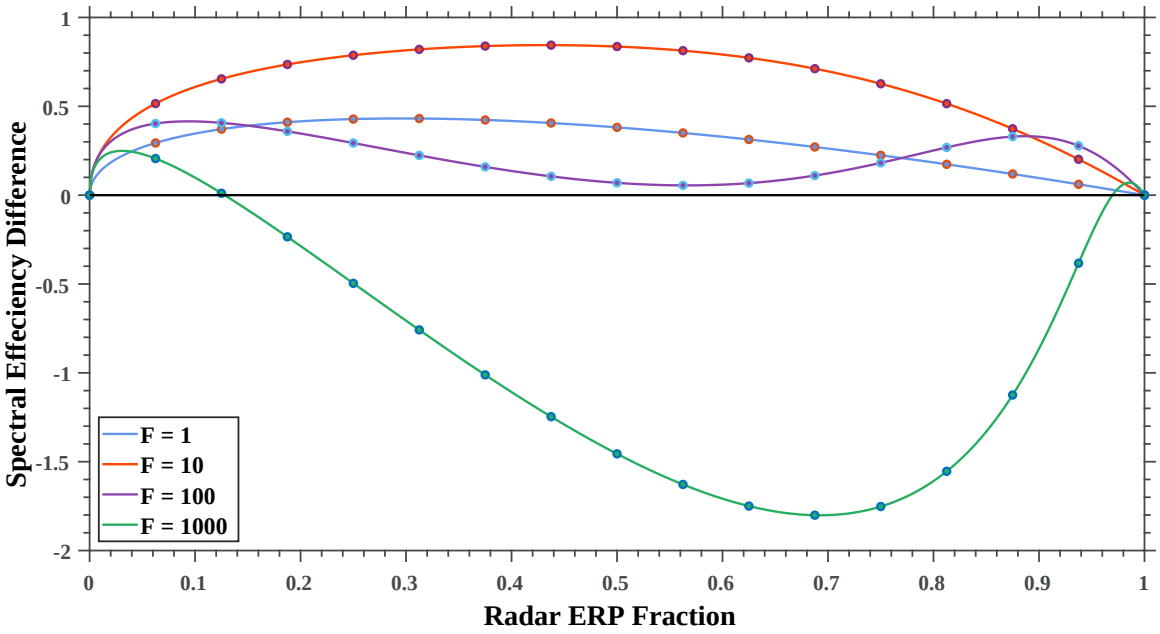

Figure 3.2: Spectral Efficiency Difference between timesharing and aperture-partitioning for an array with 16 elements.

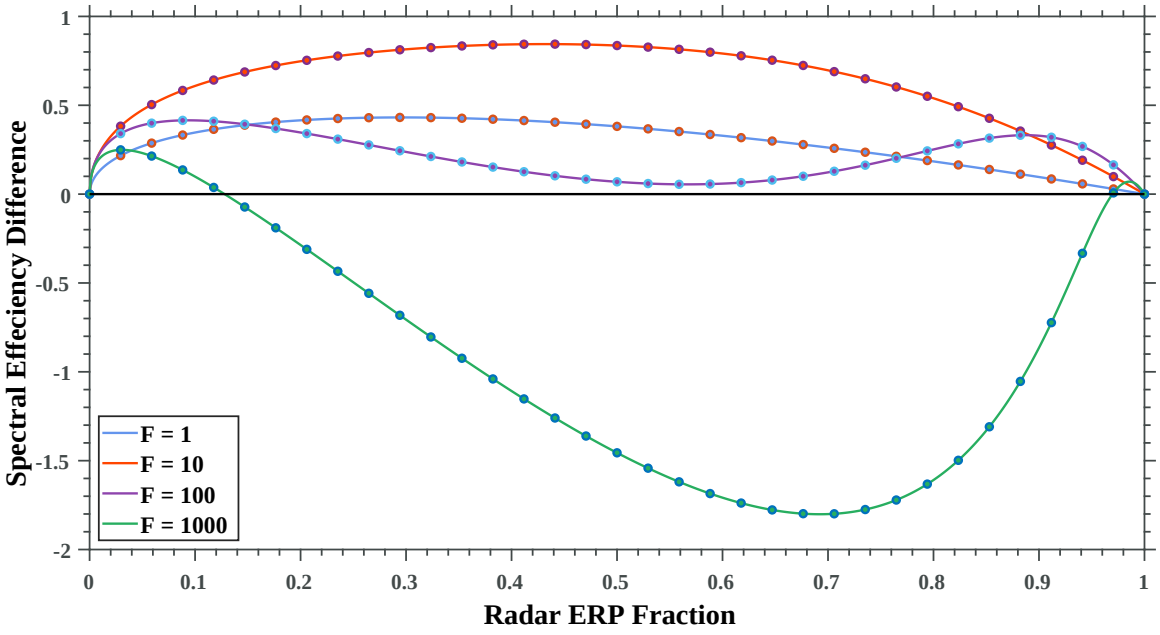

Figure 3.3: Spectral Efficiency Difference between timesharing and aperture-partitioning for an array with 34 elements.

As was previously shown in [2], timesharing is superior (from a spectral efficiency

perspective) to aperture partitioning at lower values of F for all values of α. Notice that for all array sizes the expression is unchanged, it is the discretization of the spectral difference that changes. Therefore, assuming that each antenna element can only transmit a set power (i.e., the amplifiers behind each antenna element is driven into saturation), an array with a minimum of 34 elements is needed for timesharing to be most effective near $\alpha = 1$ for a figure of merit of 1000 (30dB). It should be noted that only two elements will be dedicated to communications for the cases of high-radar ERP. However, for $F = 1000$ all intermediate values of α show aperture partitioning has a spectral efficiency advantage.

The use of the figure of merit F and reliance of spectral efficiency can make it challenging to draw conclusions about the impact of the relative advantages of timesharing as compared to aperture partitioning. To illustrate the comparison in a more intuitive way, Figures 3.4-3.6 show the communication's capacity at modest values of SNR (at full ERP) when the communication's bandwidth is 100MHz.

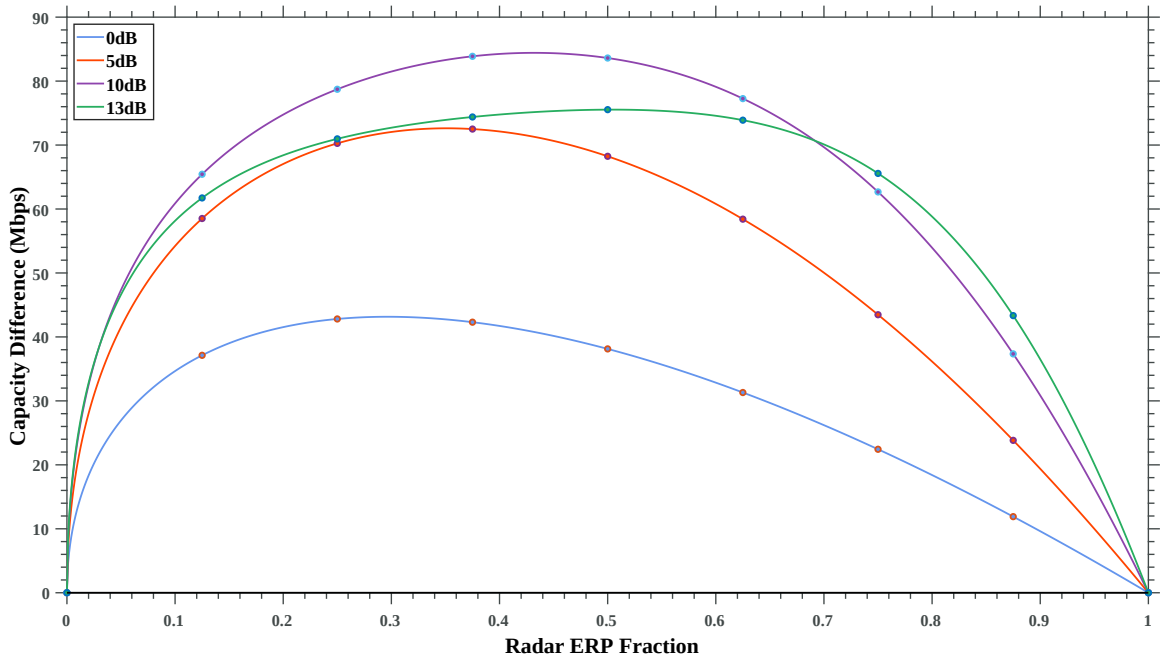

Figure 3.4: Capacity difference between timesharing and aperture-partitioning for an array with 8 elements and a bandwidth of 100MHz.

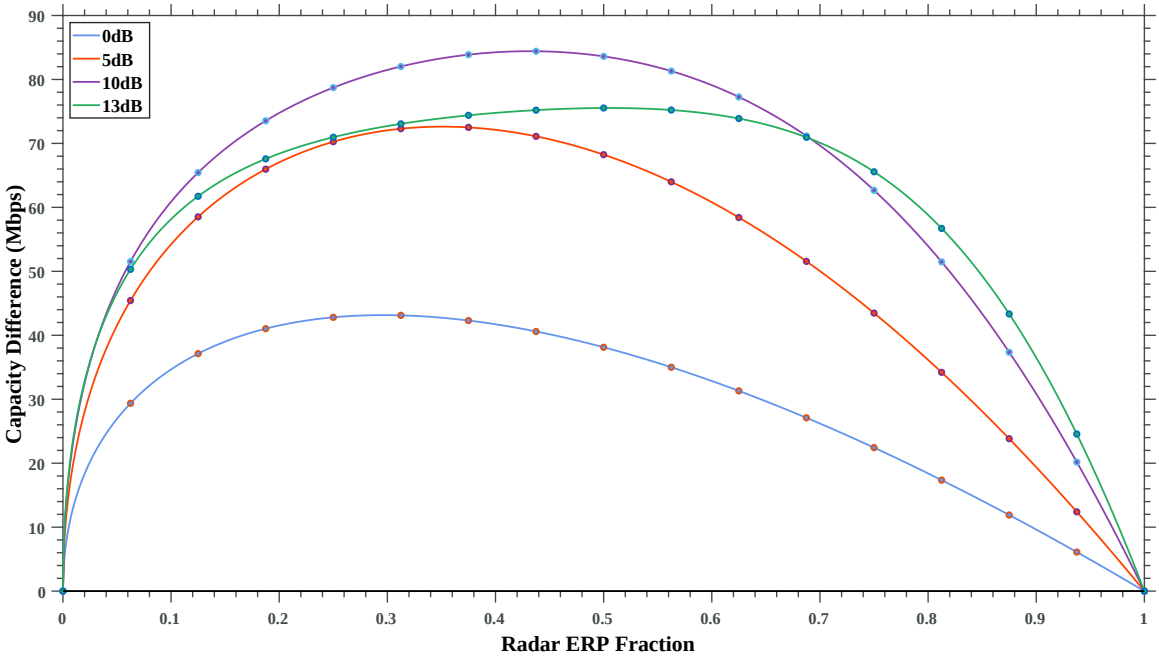

Figure 3.5: Capacity difference between timesharing and aperture-partitioning for an array with 16 elements and a bandwidth of 100MHz.

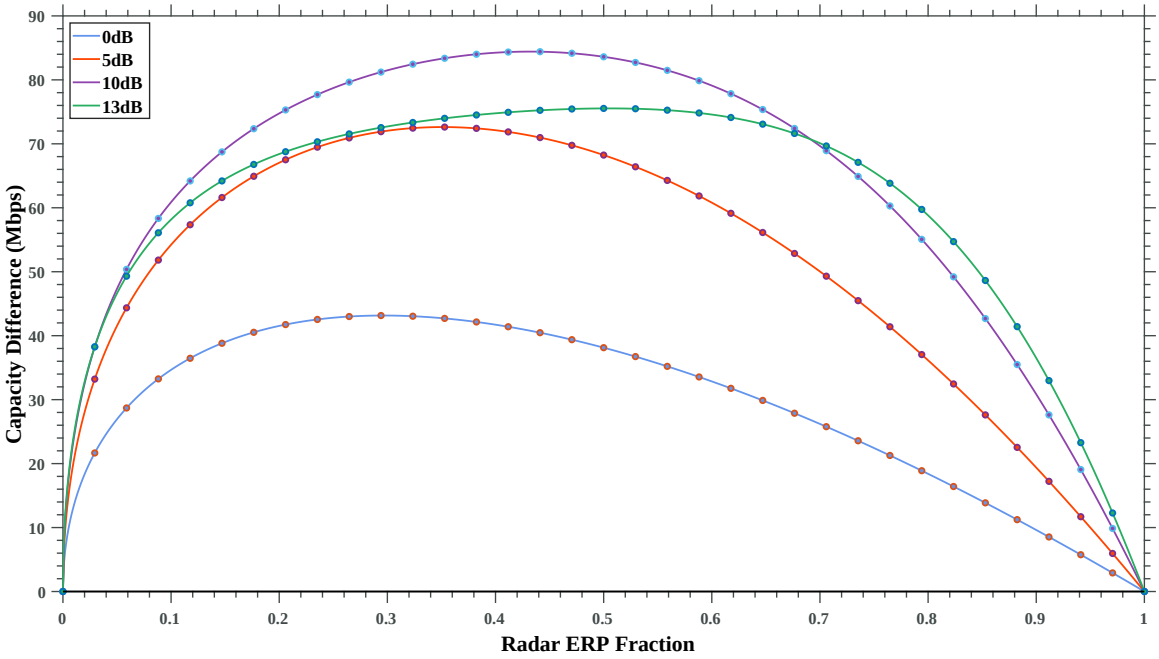

Figure 3.6: Capacity difference between timesharing and aperture-partitioning for an array with 34 elements and a bandwidth of 100MHz.

Next, Figures 3.7 and 3.8 illustrate the capacity differences between timesharing and aperture partitioning at higher SNRs for arrays with 8 and 16 elements; showing more interesting outcomes such as the continuing lessening of timesharing's advantage until it is outperformed by aperture partitioning for moderate values of α. The non-intuitive emergence of the power division where aperture partitioning gains an advantage can be seen to emerge at approximately 21 dB of SNR for both aperture sizes.

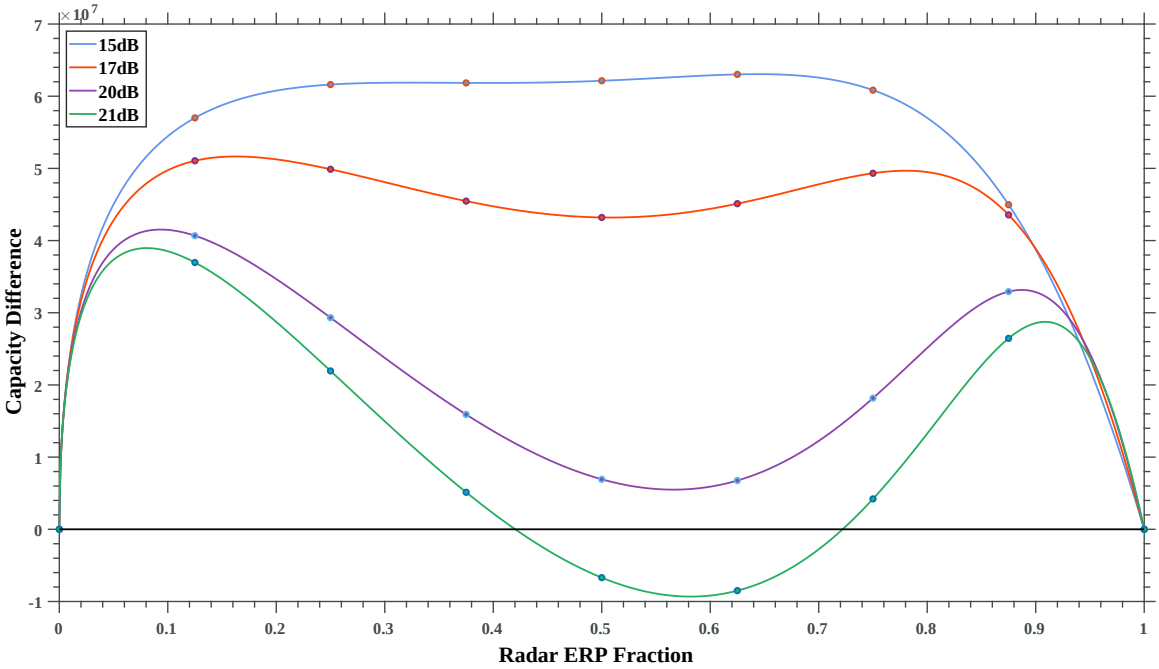

Figure 3.7: Higher SNR capacity difference between timesharing and aperture-partitioning for an array with 8 elements and a bandwidth of 100MHz.

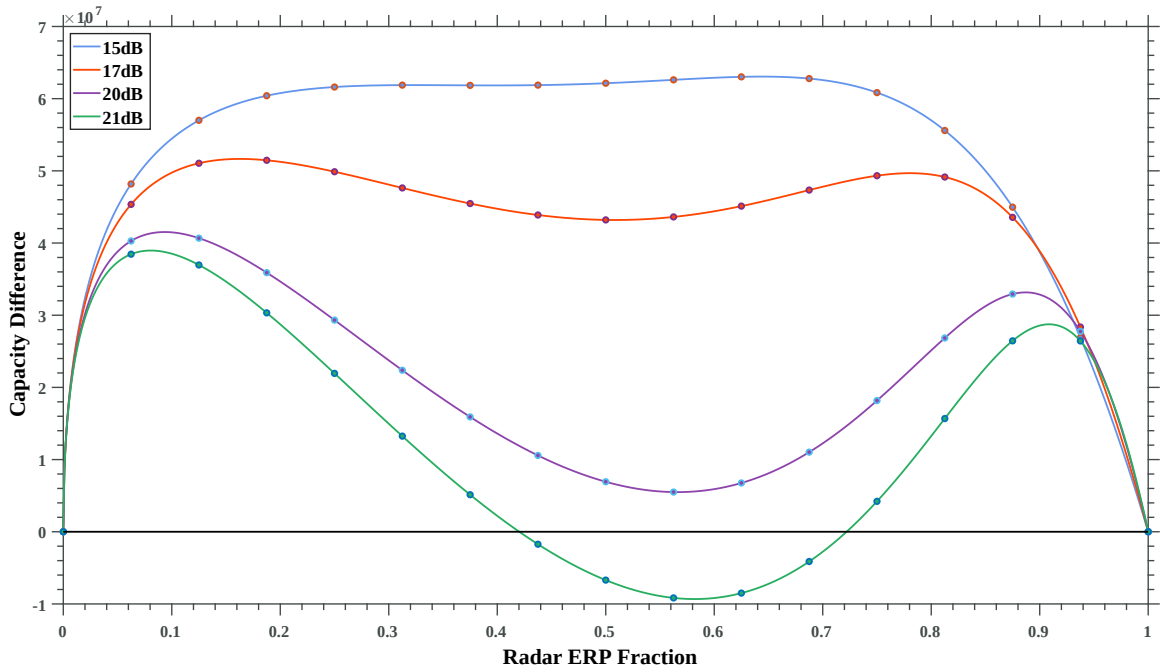

Figure 3.8: Higher SNR capacity difference between timesharing and aperture-partitioning for an array with 16 elements and a bandwidth of 100MHz.

3.3 Comparing SDB and Timesharing for Continuous Wave Emissions

Next, going back to spectral efficiency, SDB and timesharing are compared using the communication SNRs to better show the transition zone. It's important to note that we have retained the mathematical structure used in [2]. Consequently, for the comparison between timesharing and aperture partitioning, positive values of spectral efficiency difference corresponded to areas where timesharing was more spectrally efficient. In contrast, here positive values of the spectral efficiency difference correspond to regions where SDB is more spectrally efficient than timesharing. Figure 3.9 shows that for 10 dB SNR and above SDB is superior to timesharing for all values of α. However, around 5 dB SNR there are regions where timesharing becomes more efficient. This region is explored further in Figure 3.10. In Figure 3.10 it can be seen

that this transition point is at approximately 6 dB SNR.

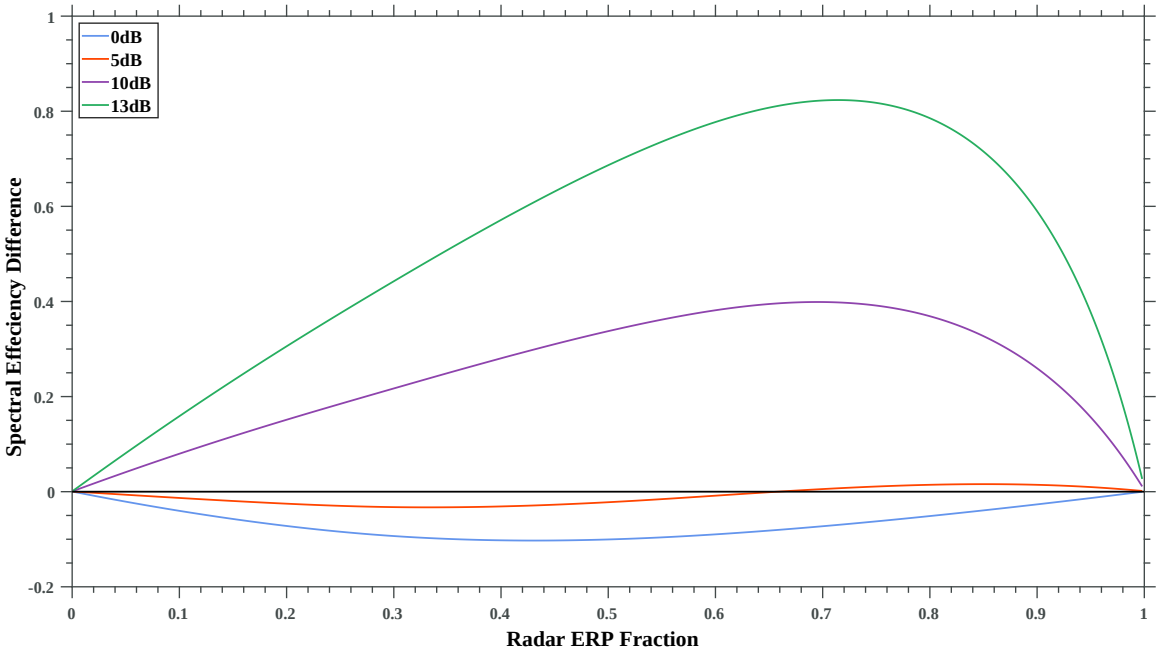

Figure 3.9: Spectral efficiency difference between SDB and timesharing for different receiver SNRs.

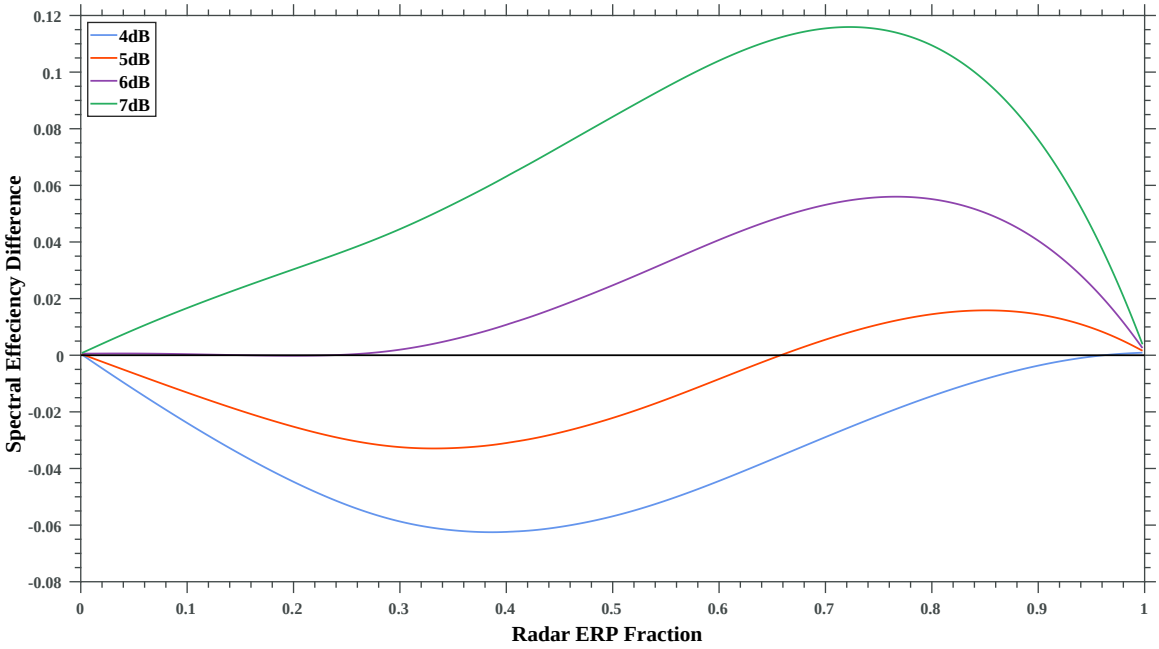

Figure 3.10: Spectral efficiency difference between SDB and timesharing for different receiver SNRs near the transition where SDB starts to beat timesharing.

3.4 Incorporating Friis' Transmission Equation

In the previous analysis, the comparison was conducted as a function of SNR or figure of merit F. However, these values abstract away practical concerns. Therefore, now the impact of propagation and range to the communications receiver is considered. The potential transmit power, P_t, for each case will be effectively parameterized by β. With G_t being the transmitting antenna gain, G_r being the receiving antenna gain, and R being the range between the antennas, the received power will be

$$P_r = \frac{P_t G_t G_r \lambda^2}{(4\pi R)^2} \tag{3.10}$$

and the SNR will be

$$\chi = \frac{P_t G_t G_r \lambda^2}{(4\pi R)^2 k_B T_e B F_n}, \tag{3.11}$$

where k_B is the Boltzmann constant, T_e is the effective noise temperature, and F_n is the system noise figure.

Since this first treatment is ignoring all path length-dependent losses apart from the distance from the transmitter to the receiver; an increase in distance by a factor of 2 would decrease the SNR by a factor of 4; pushing the optimal method of DFRC (in terms of capacity or spectral efficiency) at smaller distances to another method at further distances if the SNR at the receiver is high enough. Figures 3.11-3.25 illustrate the range-dependent spectral efficiency differencer (i.e., $SE_{ts} - SE_{ap}$), where the initial SNR is obtained at a range of 1000 meters (1 km). It will be seen that aperture partitioning and SDB are only advantageous, from a spectral efficiency perspective, at near-ranges. Timesharing becomes the optimal technique as ranges increase and

SNR decreases.

First, Figures 3.11-3.13 show the spectral efficiency comparison between timesharing and aperture partitioning as a function of range, with each Figure illustrating a different (i.e., increasing) radar ERP fraction. It can be seen that at modest SNRs, the timesharing method is always superior to the aperture partitioning method, but the advantage decreases as range increases (and therefore SNR decreases).

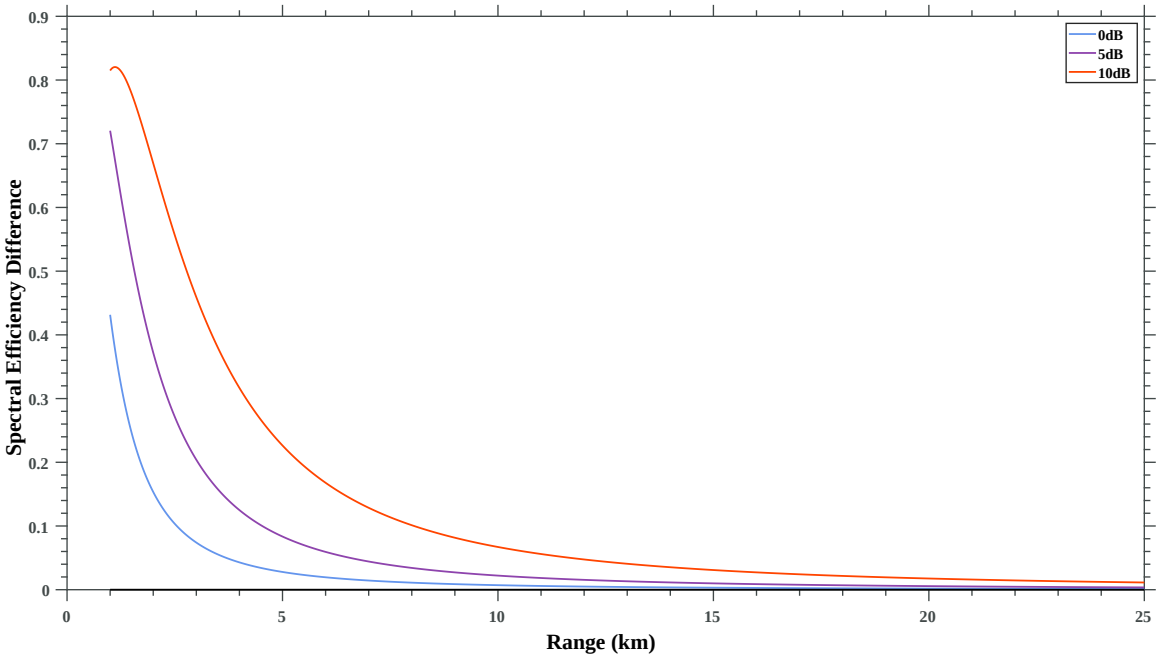

Figure 3.11: Plot showing the spectral efficiency difference between timesharing and aperture partitioning. The legend values are the SNR values at a range of 1000 meters. The radar ERP fraction (α) is fixed at 0.3.

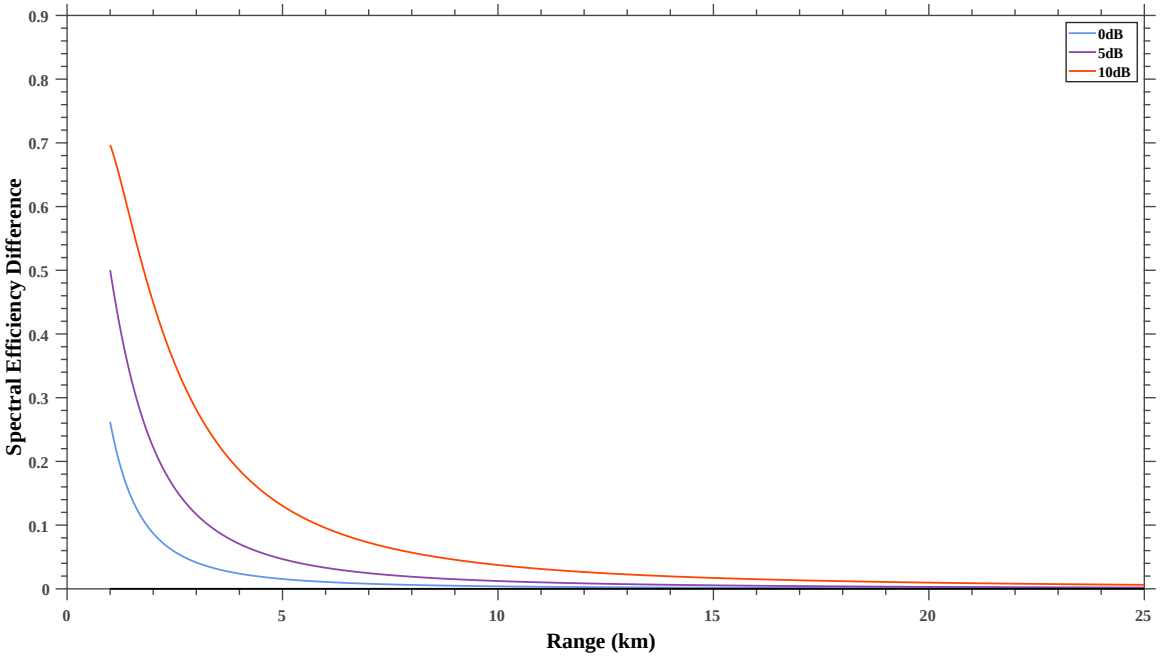

Figure 3.12: Plot showing the spectral efficiency difference between timesharing and aperture partitioning. The legend values are the SNR values at a range of 1000 meters. The radar ERP fraction (α) is fixed at 0.7.

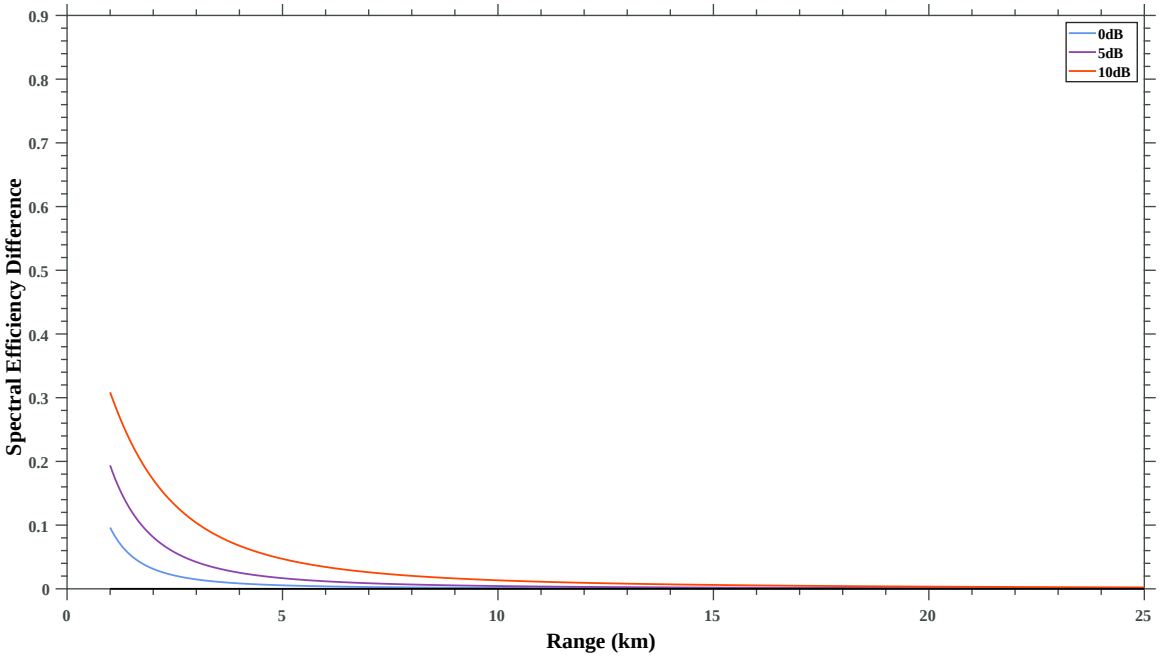

Figure 3.13: Plot showing the spectral efficiency difference between timesharing and aperture partitioning. The legend values are the SNR values at a range of 1000 meters. The radar ERP fraction (α) is fixed at 0.9.

Next, Figures 3.14-3.16 show the same scenario for higher SNRs, specifically where the communications SNR starts at 22, 25, or 28 dB at a range of 1 km. It is seen that for near ranges there are regions and selections of α where the aperture partitioning technique results in superior spectral efficiency.

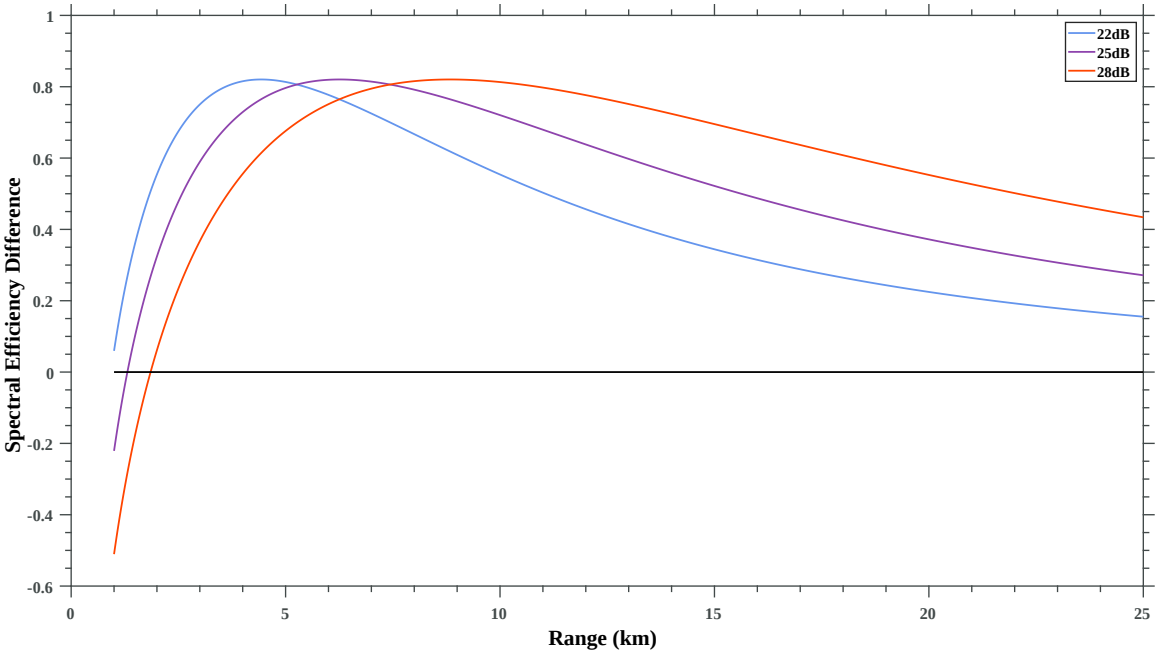

Figure 3.14: Plot showing the spectral efficiency difference between timesharing and aperture partitioning. The legend values are the SNR values at a range of 1000 meters. The radar ERP fraction (α) is fixed at 0.3.

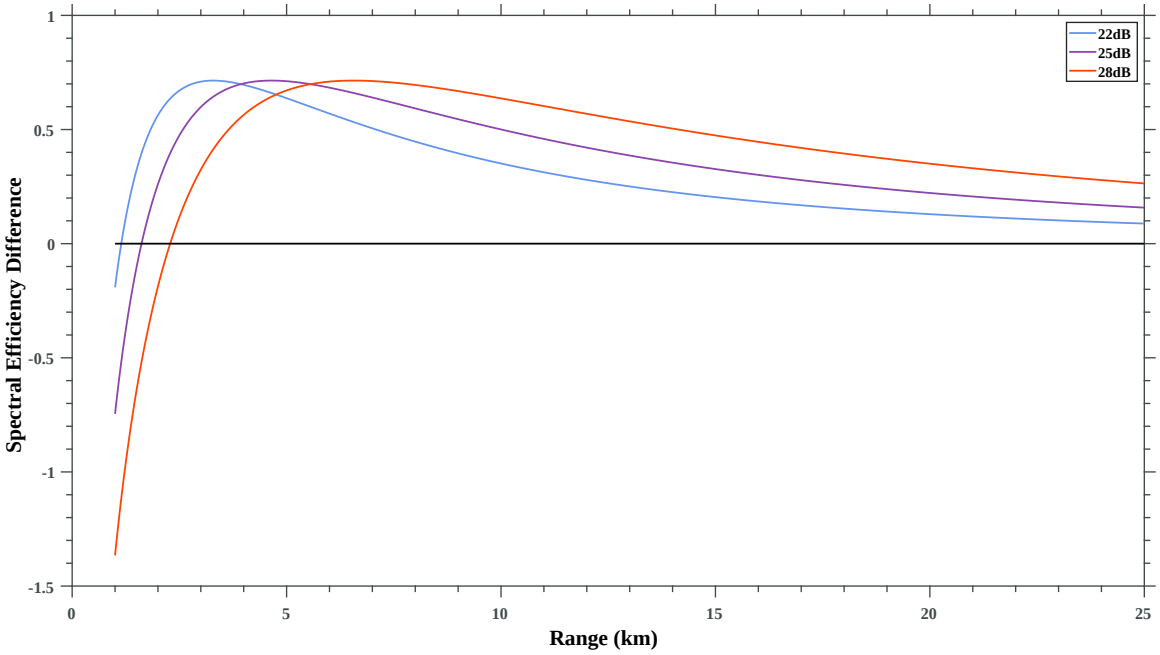

Figure 3.15: Plot showing the spectral efficiency difference between timesharing and aperture partitioning. The legend values are the SNR values at a range of 1000 meters. The radar ERP fraction (α) is fixed at 0.7.

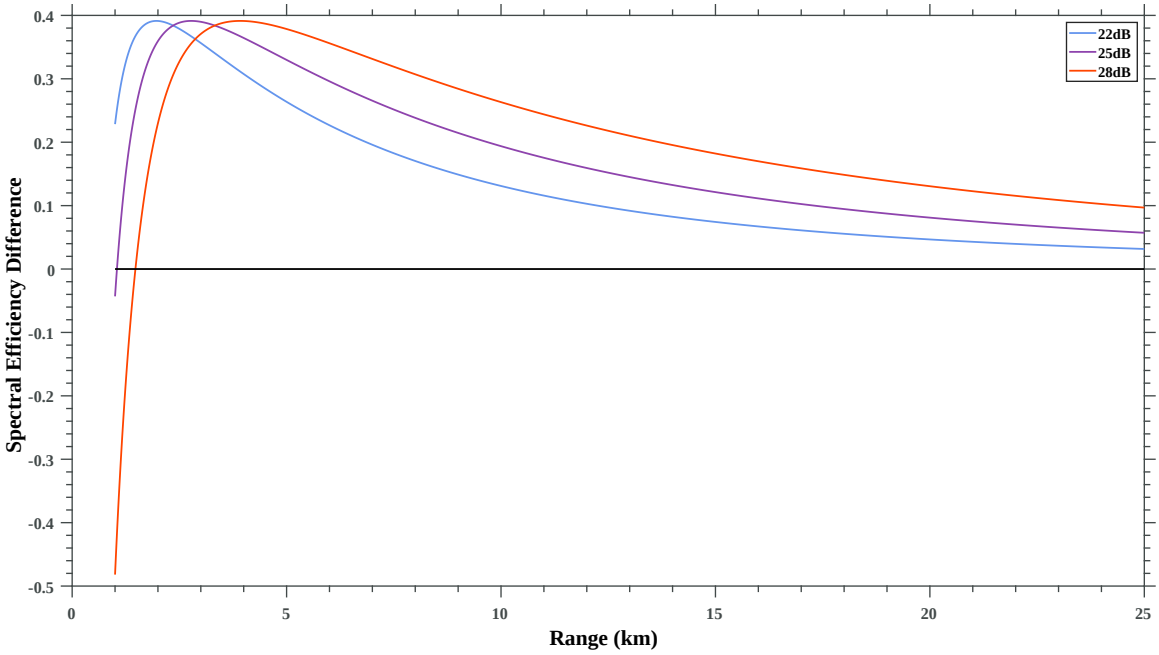

Figure 3.16: Plot showing the spectral efficiency difference between timesharing and aperture partitioning. The legend values are the SNR values at a range of 1000 meters. The radar ERP fraction (α) is fixed at 0.9.

The above plots show how timesharing becomes the more attractive option at intermediate ranges in terms of spectral efficiency as the range to the communications receiver decreases (with higher SNR slightly preferring timesharing). Any added path length-dependent losses will only further decrease the distance to where the difference between the two methods equals zero until aperture partitioning is always sub-optimal.

Next we examine how distance affects the spectral efficiency difference between SDB and timesharing ($SE_{sdb} - SE_{ts}$). Figures 3.17-3.19 show this metric for values of $\alpha = 0.3, 0.7, 0.9$, respectively, for cases of moderate to low SNR.

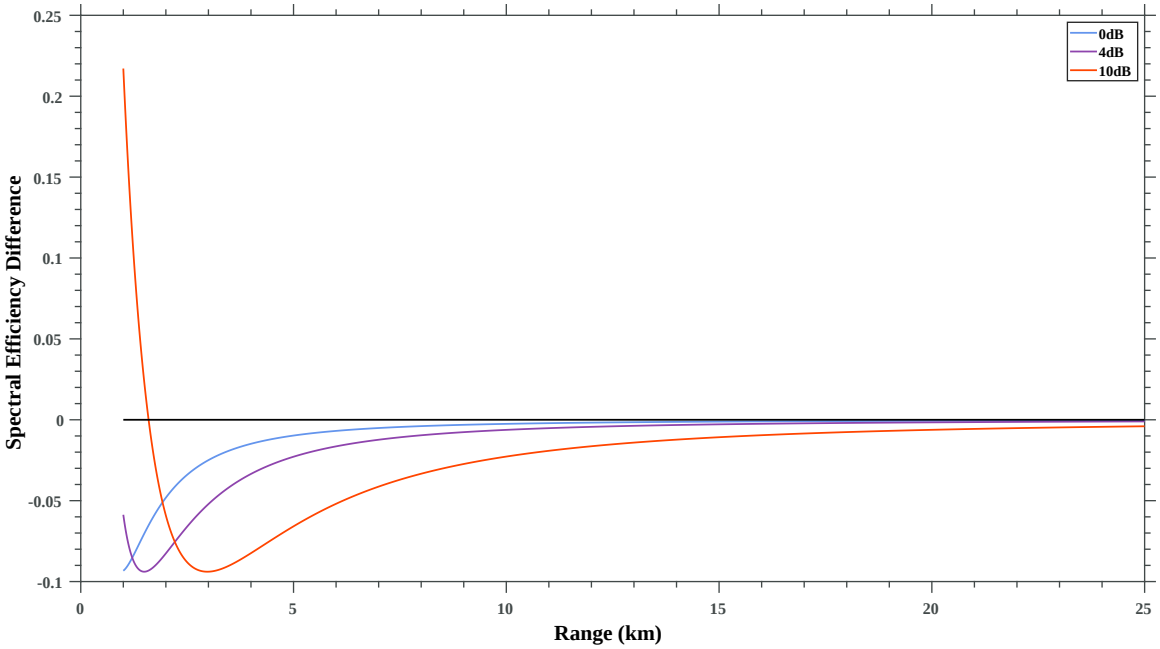

Figure 3.17: Plot showing the spectral efficiency difference between SDB and time-sharing. The legend values are the SNR values at a range of 1000 meters. The radar ERP fraction (α) is fixed at 0.3.

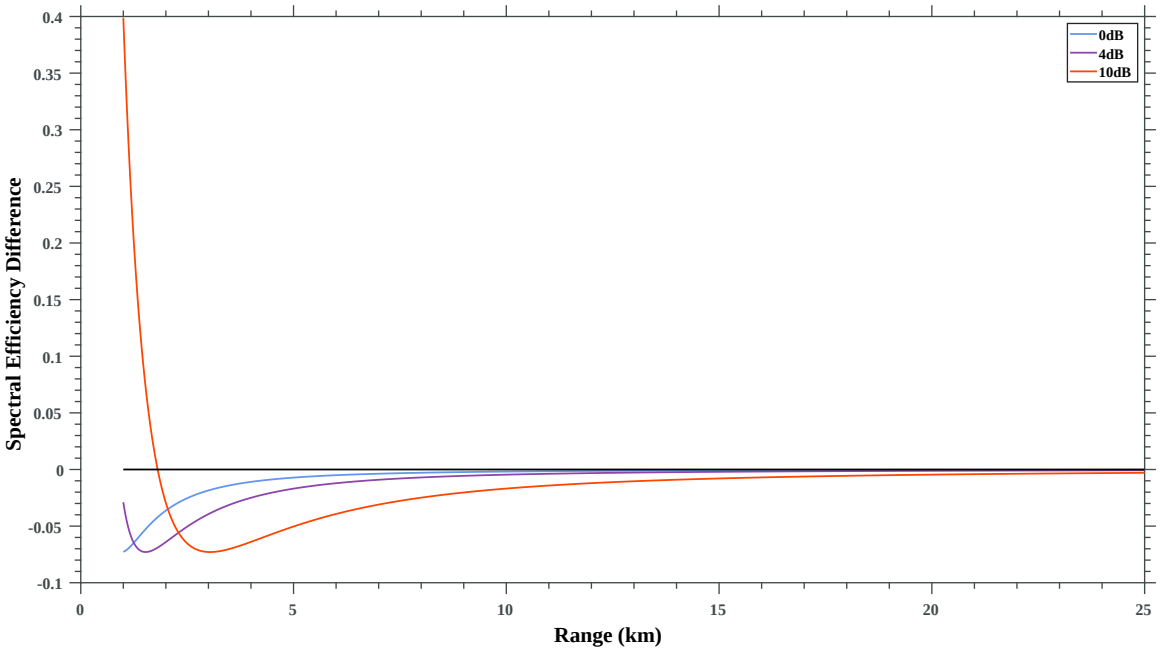

Figure 3.18: Plot showing the spectral efficiency difference between SDB and time-sharing. The legend values are the SNR values at a range of 1000 meters. The radar ERP fraction (α) is fixed at 0.7.

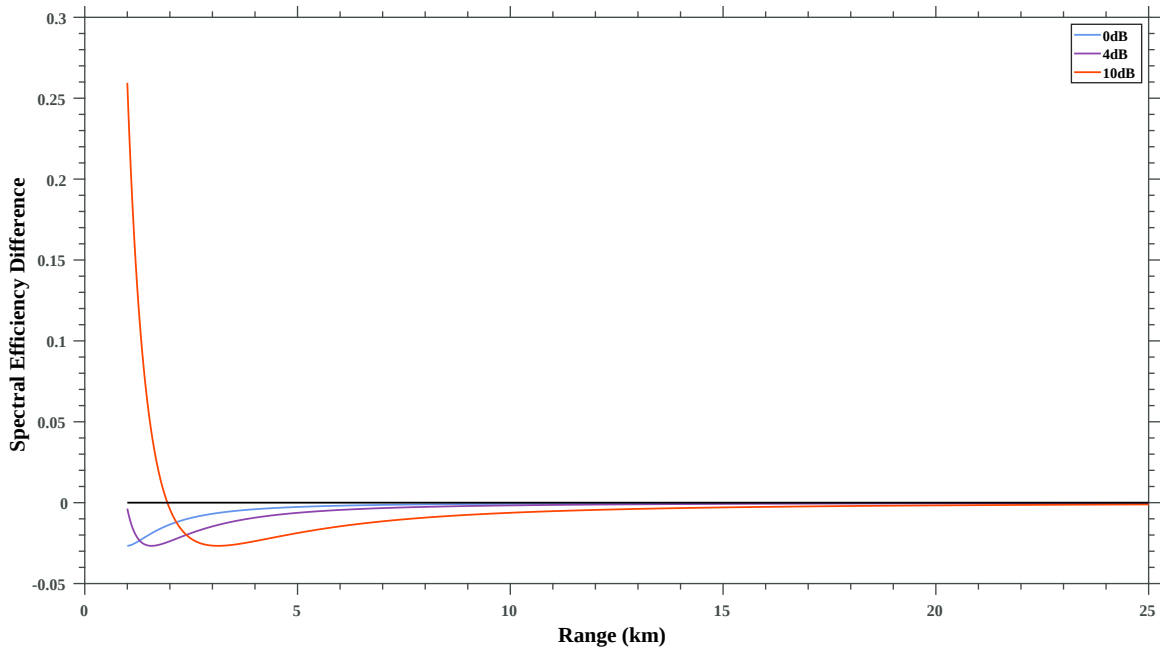

Figure 3.19: Plot showing the spectral efficiency difference between SDB and time-sharing. The legend values are the SNR values at a range of 1000 meters. The radar ERP fraction (α) is fixed at 0.9.

From examination of Figures 3.17-3.19 it can be seen that SDB is only superior at higher SNRs with SDB being the best choice at an SNR slightly over 4dB when $\alpha = 0.9$.

Next, these scenarios are repeated for higher SNRs in Figures 3.20-3.22.

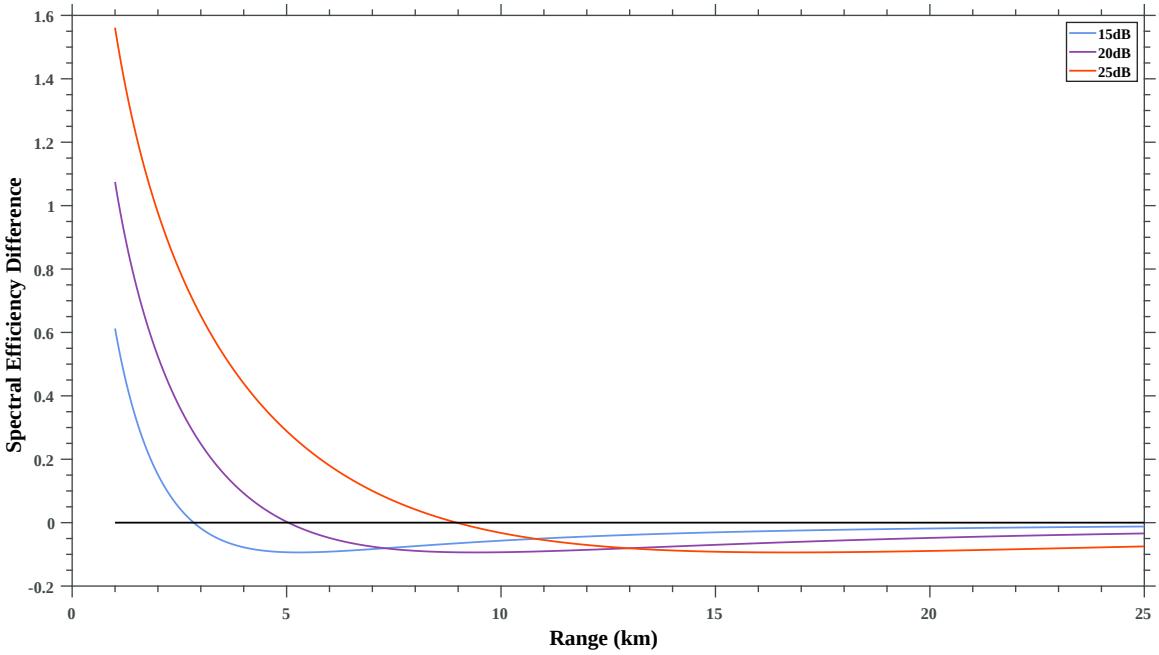

Figure 3.20: Plot showing the spectral efficiency difference between SDB and time-sharing. The legend values are the SNR values at a range of 1000 meters. The radar ERP fraction (α) is fixed at 0.3.

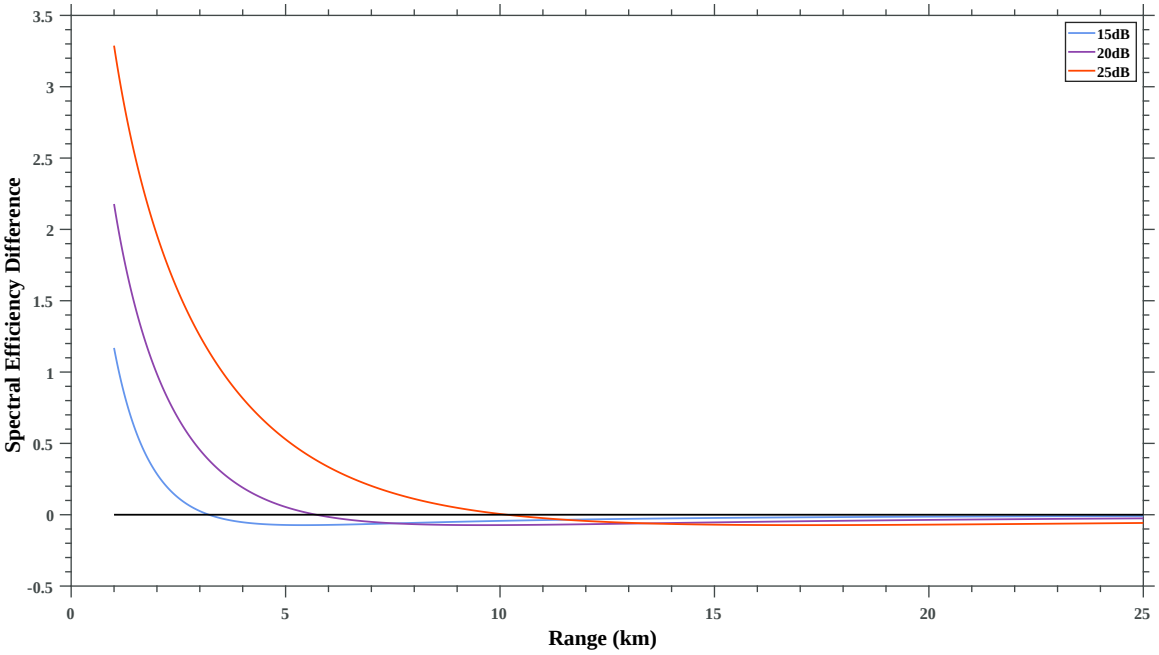

Figure 3.21: Plot showing the spectral efficiency difference between SDB and time-sharing. The legend values are the SNR values at a range of 1000 meters. The radar ERP fraction (α) is fixed at 0.7.

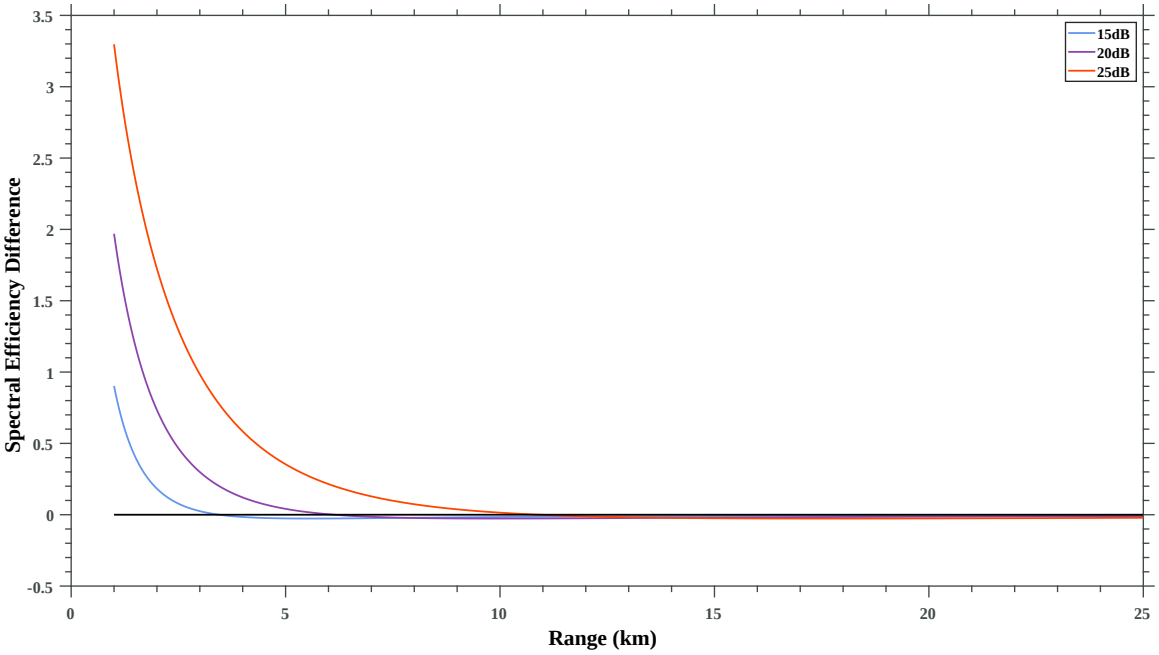

Figure 3.22: Plot showing the spectral efficiency difference between SDB and timesharing. The legend values are the SNR values at a range of 1000 meters. The radar ERP fraction (α) is fixed at 0.9.

At long distances, timesharing has an increased spectral efficiency in the range of approximately 0.005 to 0.02 bits/s/Hz. As an example, this range of spectral efficiency advantage yields an increase of 500kb/s to 2Mb/s in capacity at a bandwidth of 100MHz. Also, at higher α, the difference approaches zero.

Thus far both SDB and aperture partitioning have only been compared to the timesharing approach. Therefore, Figures 3.23-3.25 show the comparison in spectral efficiency of SDB as compared to aperture partitioning. It is seen that SDB has the higher capacity at all considered starting SNR, ranges, and values of α. However, both methods converge to the same efficiency as range increases and SNR decreases.

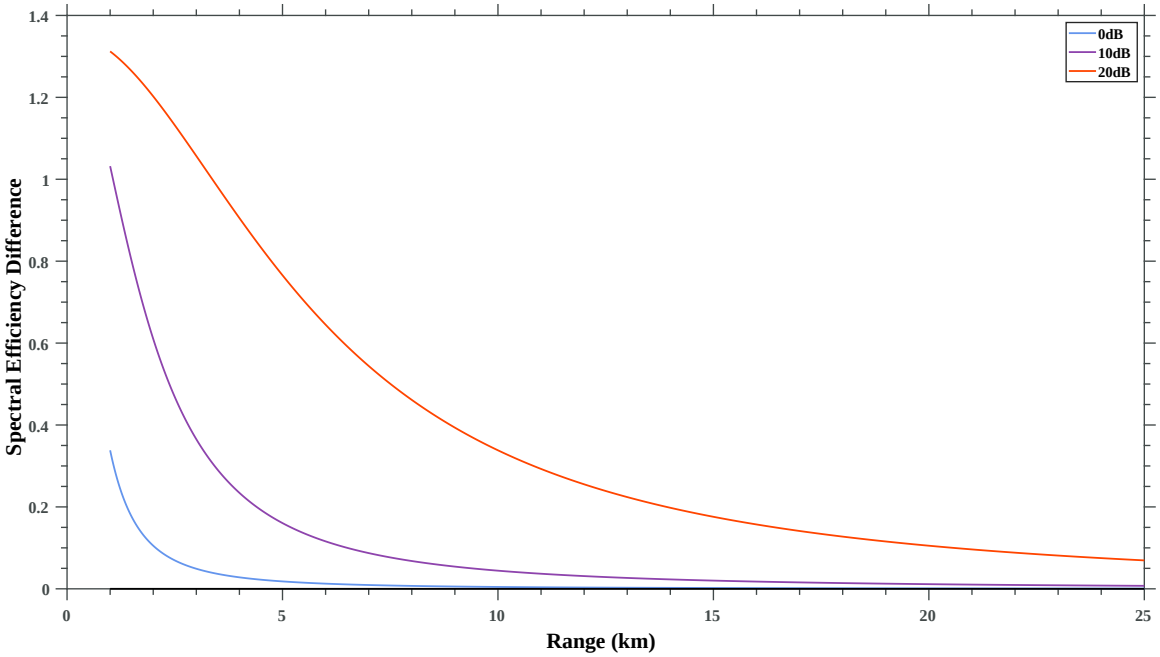

Figure 3.23: Plot showing the spectral efficiency difference between SDB and aperture-partitioning. The legend values are the SNR values at a range of 1000 meters. The radar ERP fraction (α) is fixed at 0.3.

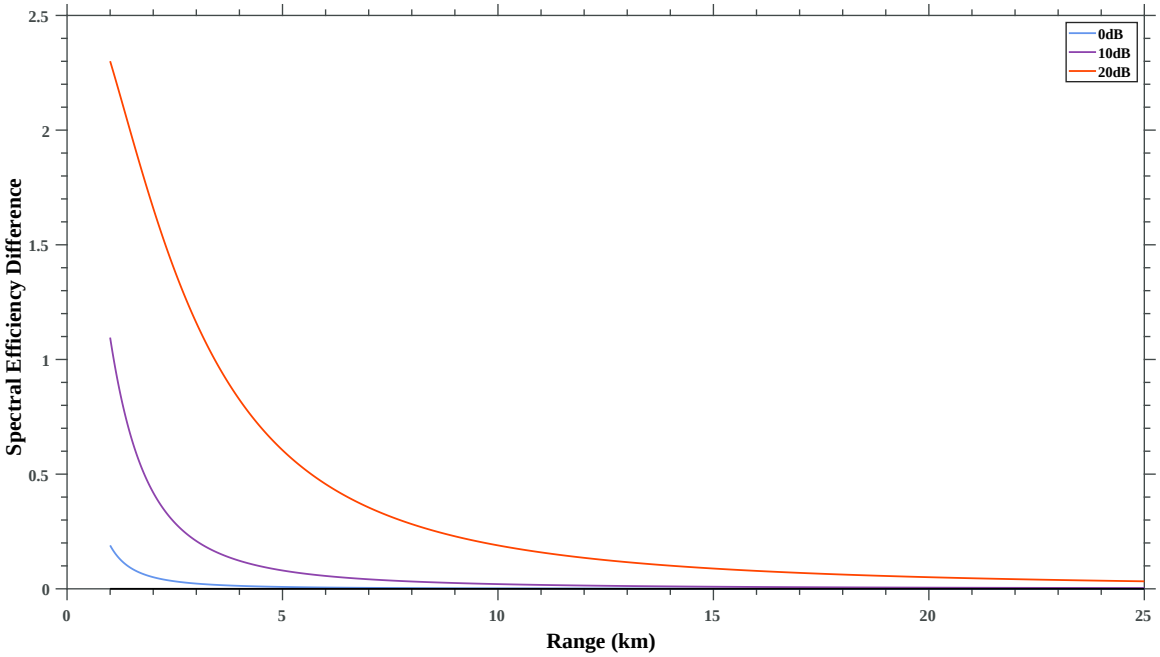

Figure 3.24: Plot showing the spectral efficiency difference between SDB and aperture-partitioning. The legend values are the SNR values at a range of 1000 meters. The radar ERP fraction (α) is fixed at 0.7.

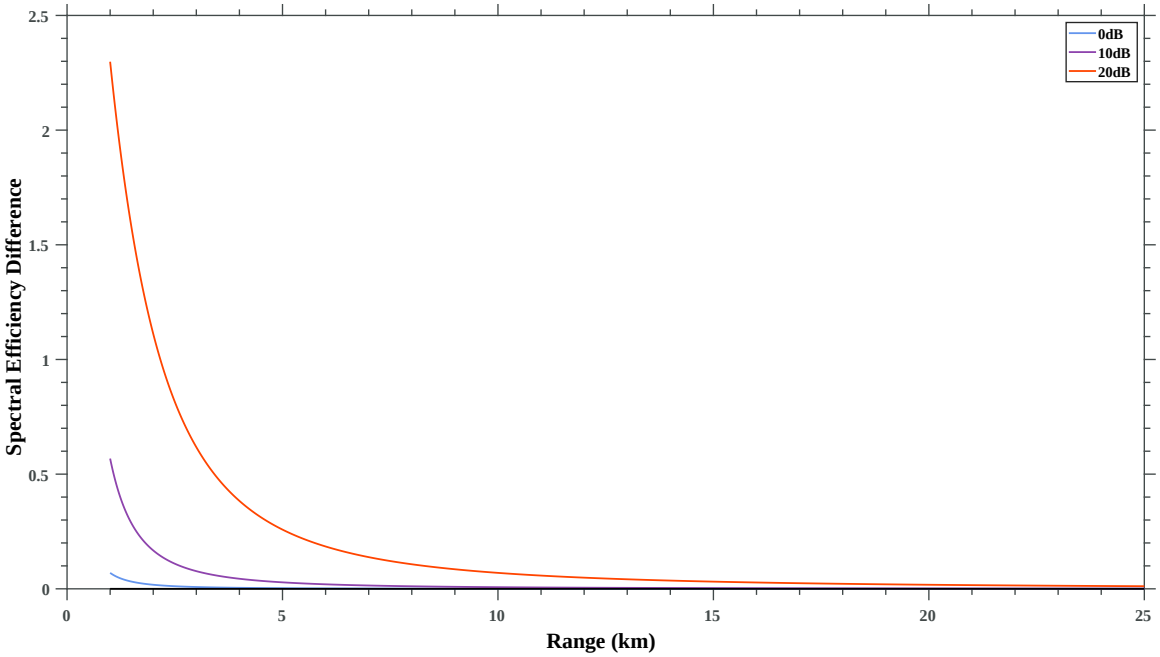

Figure 3.25: Plot showing the spectral efficiency difference between SDB and aperture-partitioning. The legend values are the SNR values at a range of 1000 meters. The radar ERP fraction (α) is fixed at 0.9.

Chapter 4

Pulsed Radar

Building off the SNR discussion of section 2.3, pulsed radar will affect the capacity or spectral efficiency of the communications beam depending on the radar duty cycle. These effects will be explored in later chapters with relevant equations being discussed here. The radar duty cycle is defined as

$$D = \frac{T_p}{PRI} = T_p PRF, \tag{4.1}$$

where T_p is the pulse width, PRI is the pulse repetition interval, and PRF is the pulse repetition frequency; it can be seen that the PRF will affect communications performance and so the effects of the PRF (ambiguities, number of pulses that hit a moving target, etc) will presumably be related to the communication's beam capacity or spectral efficiency.

In terms of duty cycle, the unambiguous range is [6]

$$R_{ua} = \frac{c}{2}(\frac{PRI}{T_p} - 1)T_p = \frac{cT_p}{2D}(1 - D) \approx \frac{cT_p}{2D}. \tag{4.2}$$

The PRF also affects the doppler resolution which is on the order of

$$\Delta F_D = \frac{PRF}{M} = \frac{D}{MT_p}, \tag{4.3}$$

where M is the number of pulses.

The analysis conducted in Chapter 3 was based on the results presented in [2], which considered only continuous emissions. However, high power digital arrays are often pulsed, with maximum pulse durations and duty cycles. Hence, the analysis is extended to consider pulsed operation of the radar and communications functions. Assuming a pulse duration of T_p and a pulse repetition interval of T_{PRI} the duty cycle limited timesharing spectral efficiency becomes

$$SE_{ts_p} = \beta D \log_2(1+F) = \beta \frac{T_p}{T_{PRI}} \log_2(1+F), \tag{4.4}$$

where D is the duty cycle of the aperture. It may also be the case that, during the communications portion of timesharing, the communications beam may be able to continuously transmit at full power making $SE_{ts_p} = SE_{ts}$. Otherwise, if full power constant transmission is not feasible and the communications beam may still continuously transmit with reduced power, then the spectral efficiency would become

$$SE_{ts_p} = \beta \log_2(1+\gamma F). \tag{4.5}$$

where γ is the fraction of full ERP given to the communications function and $\gamma = 1$ is equivalent to full power continuous transmission. If all DFRC methods are duty cycle limited then they are all scaled versions o f the continuous wave case; this will

not be covered in this thesis.

It is assumed that the communications beam will be forced to be pulsed along with the radar pulses for the aperture partitioning and SDB modes of DFRC leading to the spectral efficiency for aperture partitioning becoming

$$SE_{ap_p} = D \log_2(1 + (1 - \sqrt{\alpha})^2 F) \tag{4.6}$$

and the spectral efficiency for SDB becoming

$$SE_{sdb_p} = D \log_2(1 + \beta F). \tag{4.7}$$

4.1 Performance Across α

Since most of these expressions are just scaling the continuous wave case, the only interesting case is where timesharing may be allowed to continuously operate with varying transmit powers. If the communications beam is allowed to continuously transmit at full power, timesharing becomes much more favorable as seen in the following graphs with a PRF of 2000Hz.

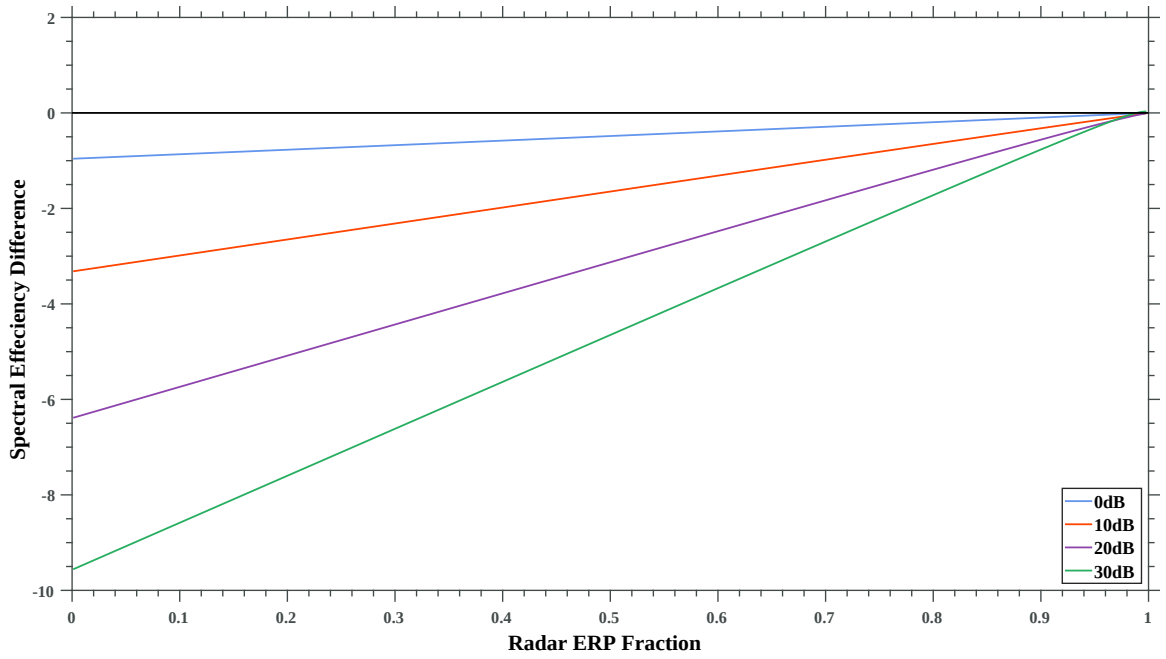

Figure 4.1: Spectral efficiency difference, $SE_{sdb_p} - SE_{ts_p}$, for $T_p = 20\mu s$, PRF $= 2000Hz$, a duty cycle of 0.04, and a communications beam continuously transmitting at full power.

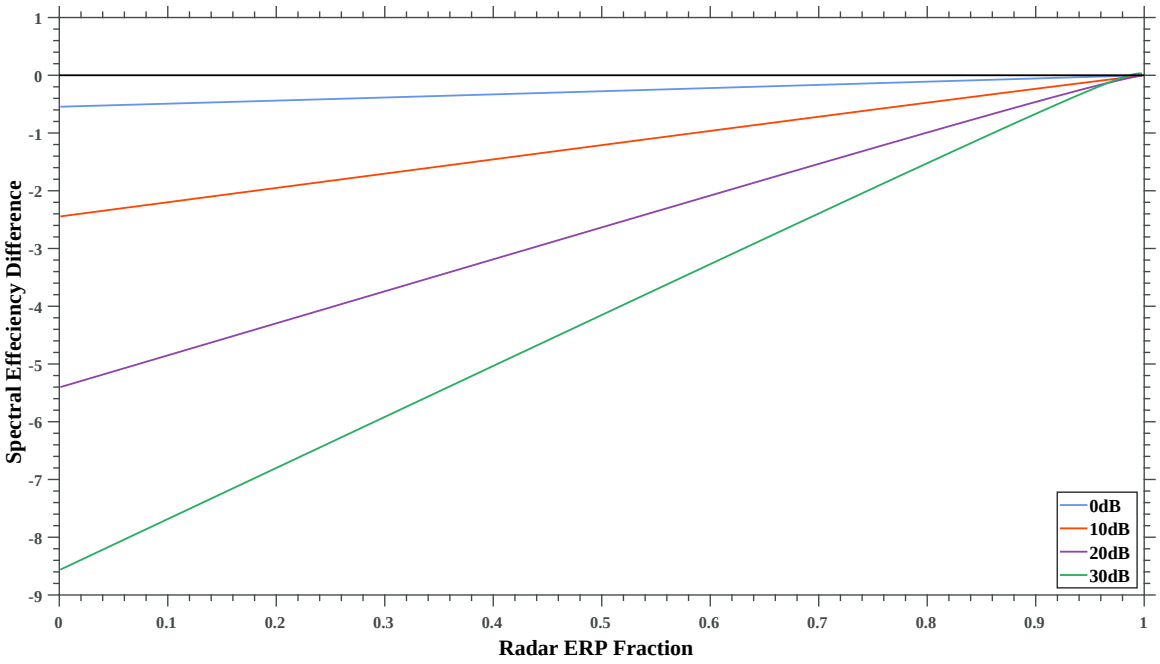

Figure 4.2: Spectral efficiency difference, $SE_{sdb_p} - SE_{ts_p}$, for $T_p = 20\mu s$, PRF = $2000Hz$, a duty cycle of 0.04, and a communications beam continuously transmitting at half power.

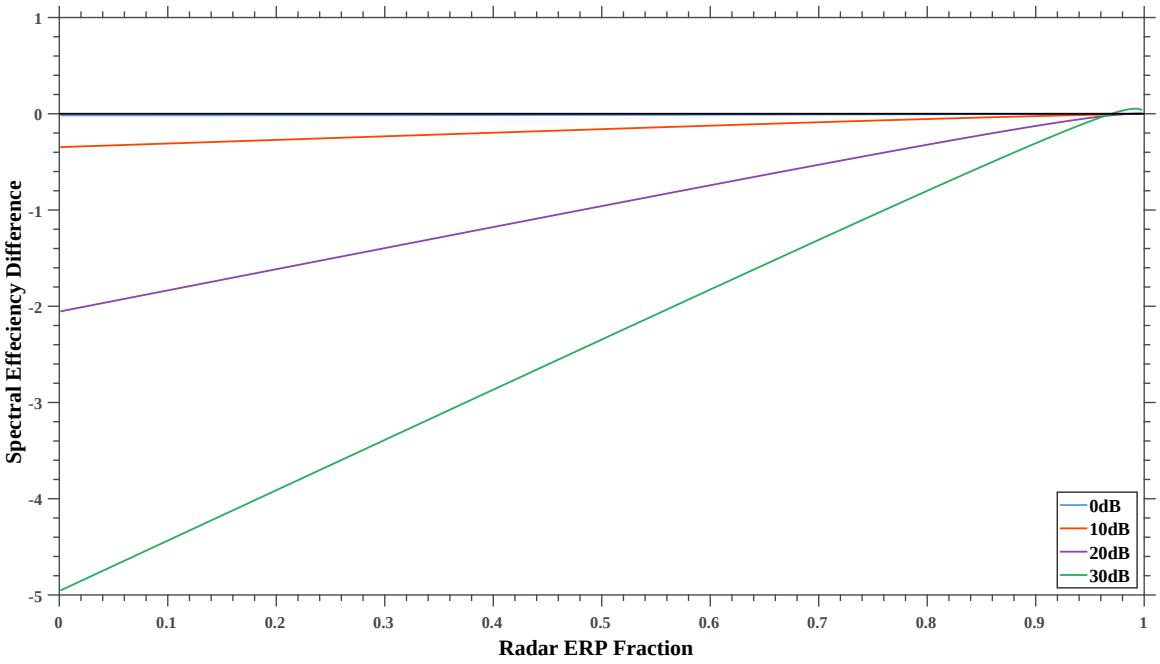

Figure 4.3: Spectral efficiency difference, $SE_{sdb_p} - SE_{ts_p}$, for $T_p = 20\mu s$, PRF = $2000Hz$, a duty cycle of 0.04, and a communications beam continuously transmitting at a fraction D of full power.

When the PRF is increased to 8000Hz, SDB becomes more viable if the radar beam is allocated the majority of the power as seen in the following plots.

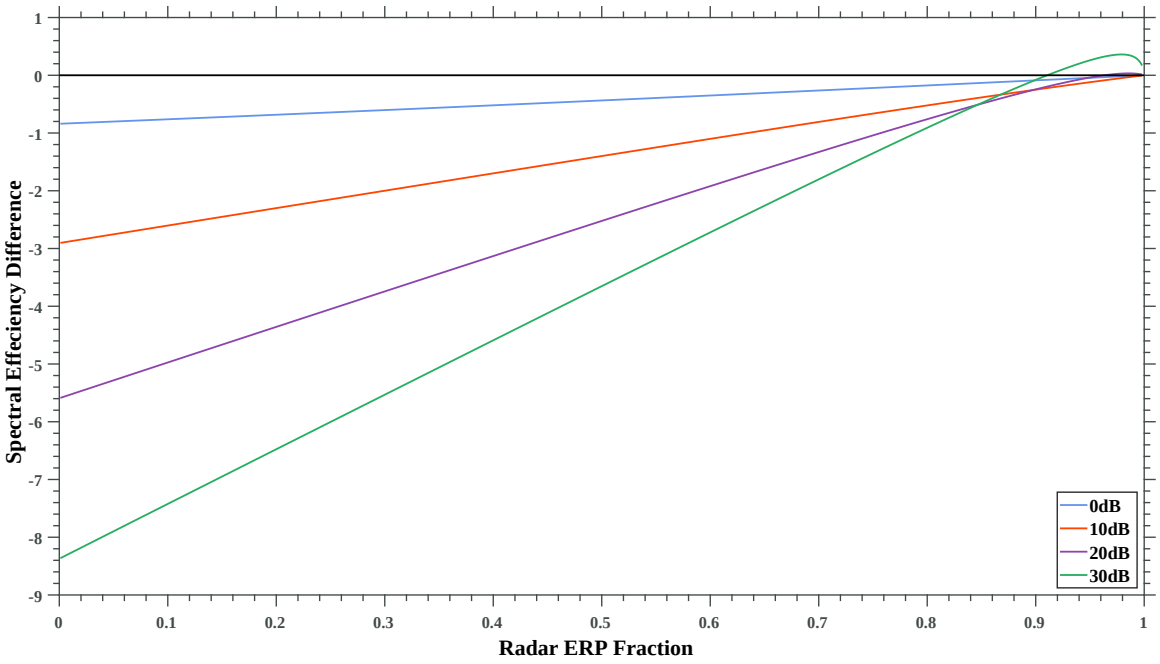

Figure 4.4: Spectral efficiency difference, $SE_{sdb_p} - SE_{ts_p}$, for $T_p = 20\mu s$, PRF = $8000Hz$, a duty cycle of 0.16, and a communications beam continuously transmitting at full power.

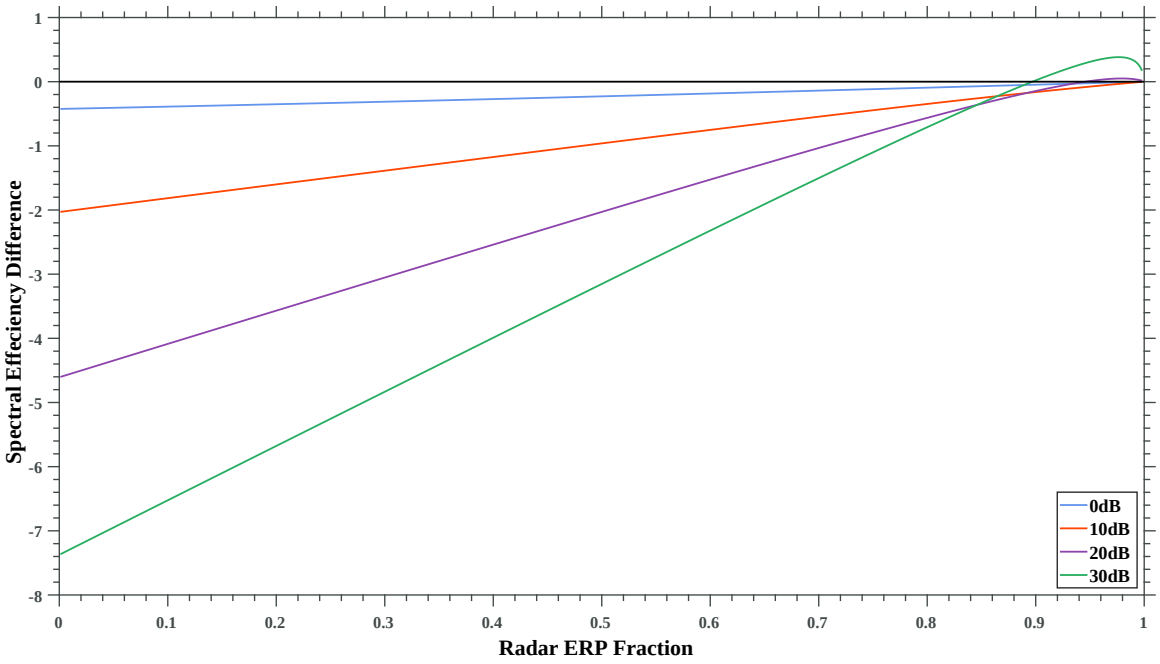

Figure 4.5: Spectral efficiency difference, $SE_{sdb_p} - SE_{ts_p}$, for $T_p = 20\mu s$, PRF = $8000Hz$, a duty cycle of 0.16, and a communications beam continuously transmitting at half power.

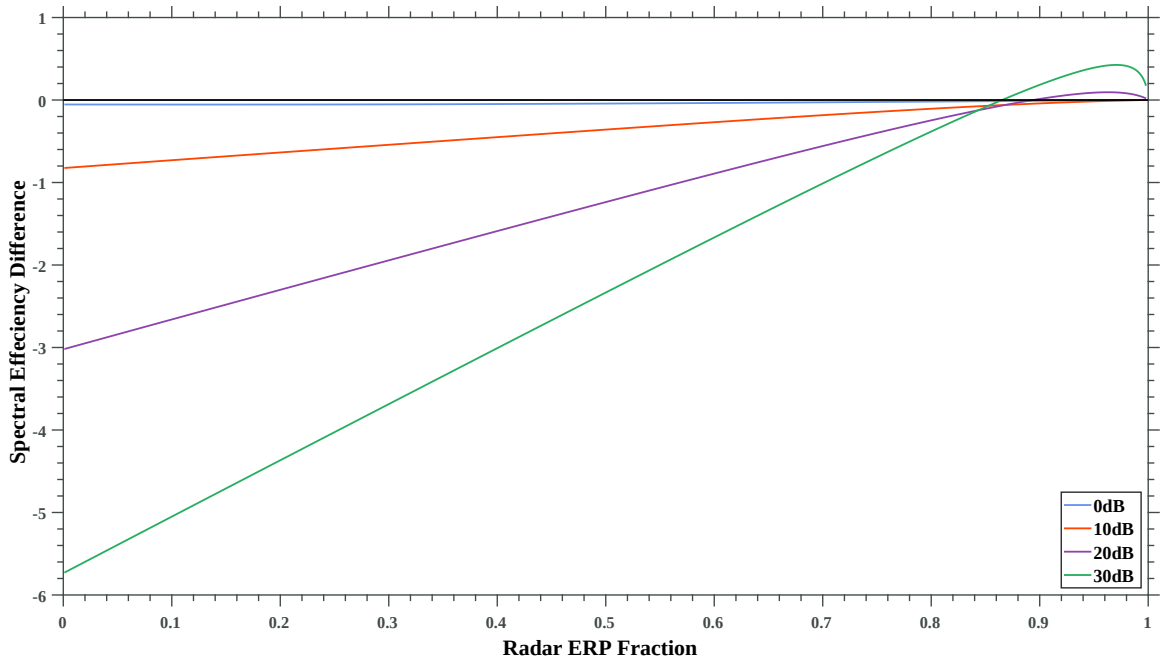

Figure 4.6: Spectral efficiency difference, $SE_{sdb_p} - SE_{ts_p}$, for $T_p = 20\mu s$, PRF = $8000Hz$, a duty cycle of 0.16, and a communications beam continuously transmitting at a fraction D of full power.

The previous six plots show how SDB is no longer the best across all radar ERP values and SNRs and only provides a spectral efficiency advantage over timesharing at higher α and higher SNRs. A key result is shown in Figure 4.6, which shows that timesharing's advantage largely holds even if the percentage of full power allocated to timesharing matches the duty cycle of the SDB emission. In other words, in this case the timesharing is limited to an identical power budget as the SDB emission.

As shown in the following plots, timesharing's advantage over aperture partitioning only increases when considering pulsed radar, as compared to the continuous wave case.

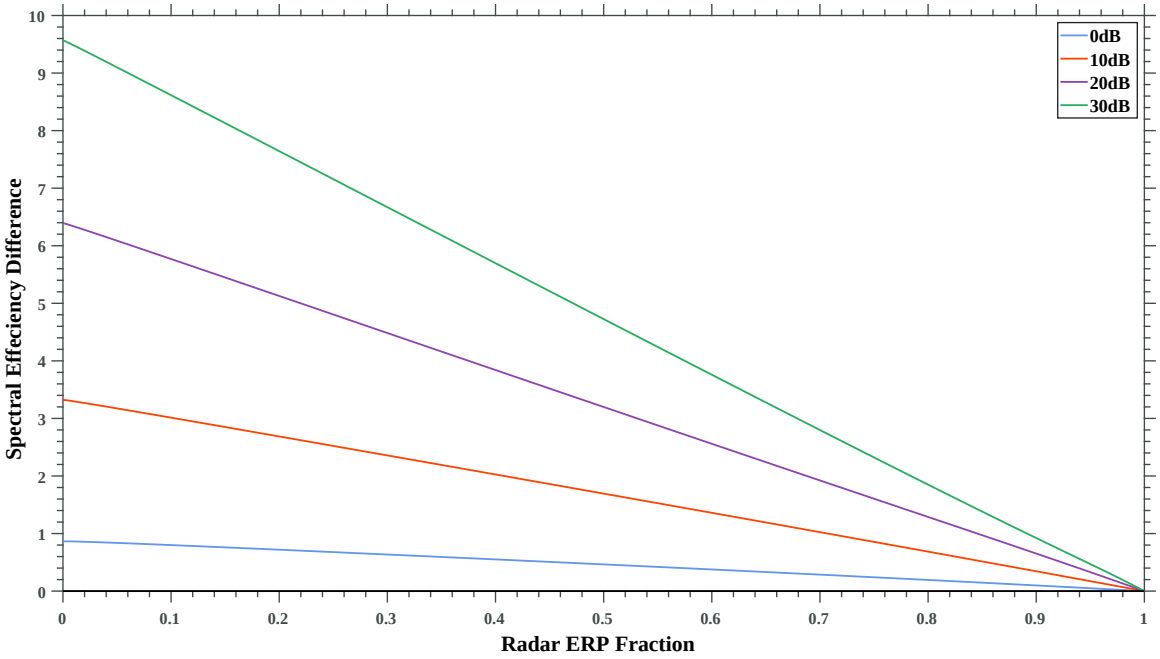

Figure 4.7: Spectral efficiency difference, $SE_{ts_p} - SE_{part_p}$, for $T_p = 20\mu s$, PRF $= 2000Hz$, a duty cycle of 0.04, and a communications beam continuously transmitting at full power.

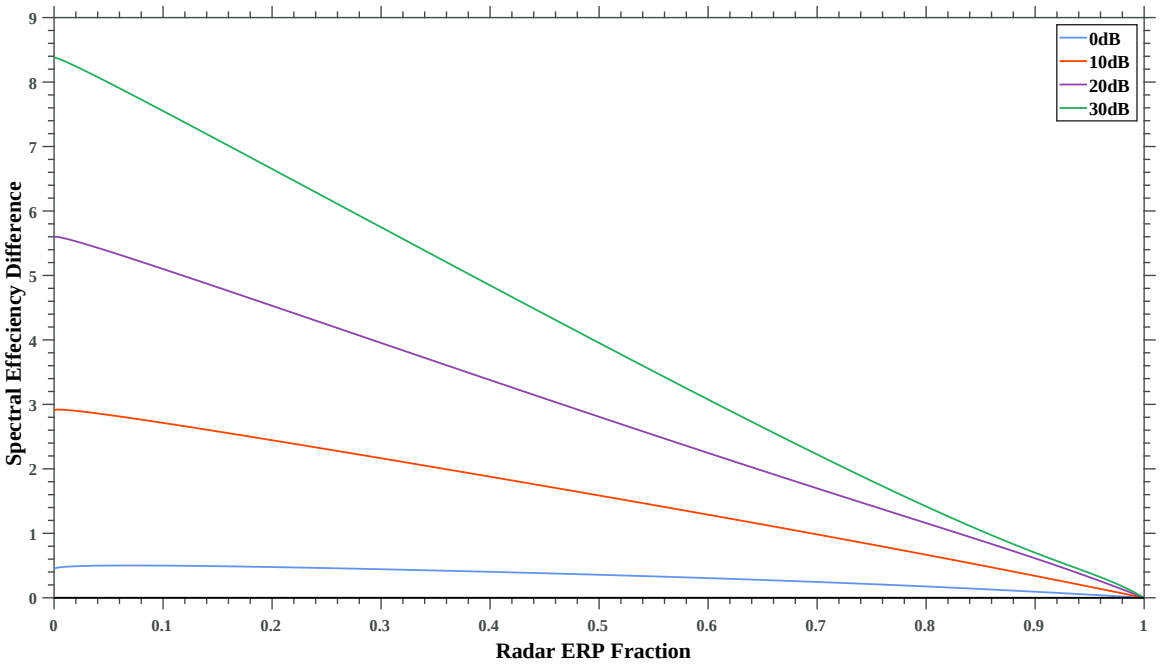

Figure 4.8: Spectral efficiency difference, $SE_{ts_p} - SE_{part_p}$, for $T_p = 20\mu s$, PRF = $8000Hz$, a duty cycle of 0.16, and a communications beam continuously transmitting at full power.

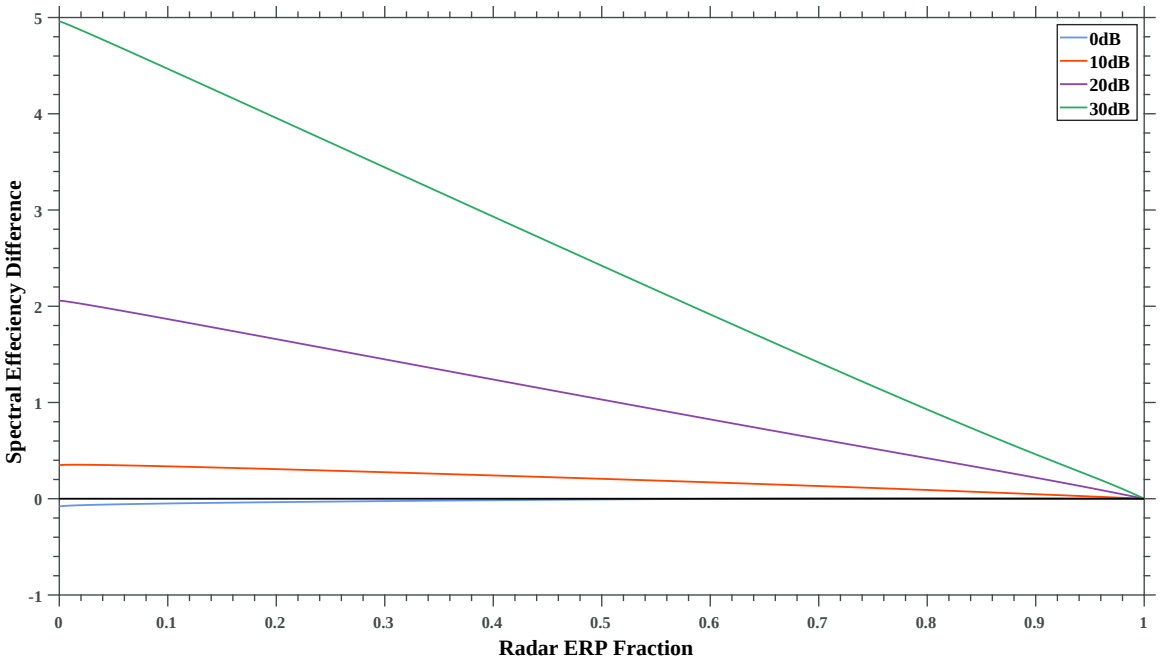

Figure 4.9: Spectral efficiency difference, $SE_{ts_p} - SE_{part_p}$, for $T_p = 20\mu s$, PRF = $2000Hz$, a duty cycle of 0.04, and a communications beam continuously transmitting at a fraction D of full power.

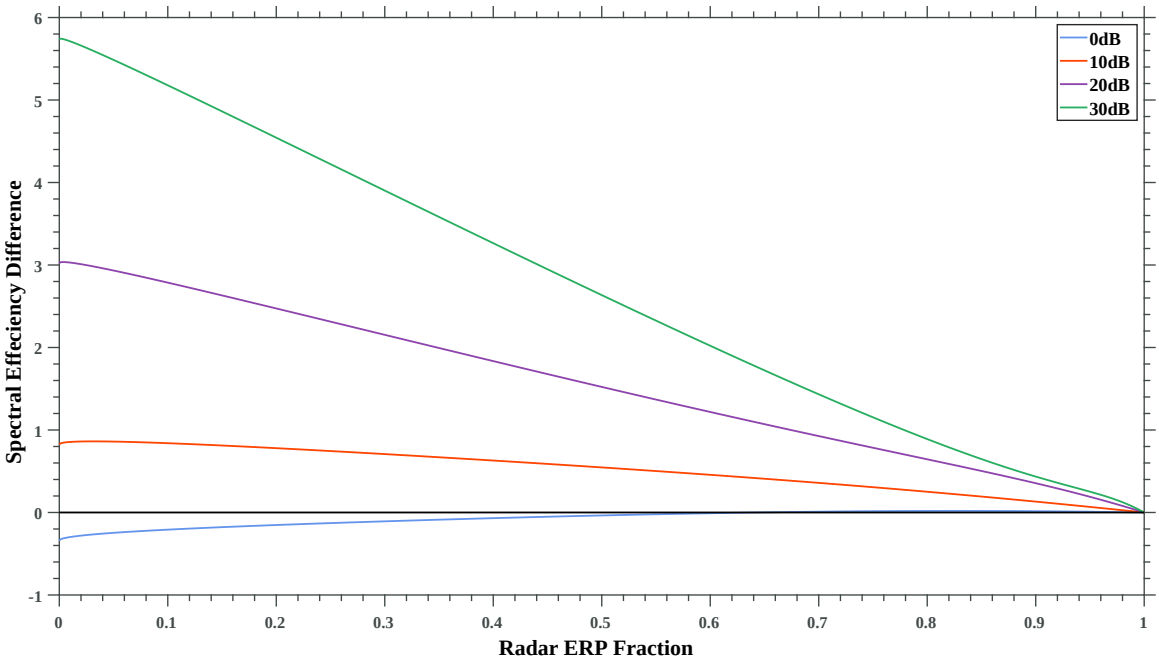

Figure 4.10: Spectral efficiency difference, $SE_{ts_p} - SE_{part_p}$, for $T_p = 20\mu s$, PRF = $8000Hz$, a duty cycle of 0.16, and a communications beam continuously transmitting at a fraction D of full power.

The results of considering pulsed radar operation show how the SDB mode of DFRC loses its large advantage in terms of the communication beam's spectral efficiency. Nonetheless, SDB remains viable for instances where the majority of power is allocated to the radar beam. When considering timesharing and aperture partitioning, aperture partitioning becomes a better choice at lower SNR and higher PRF values.

4.2 Performance Across Distance

Next the spectral efficiency difference is considered as a function of range. Allowing the communications beam to continuously transmit, even at reduced power, leads to timesharing consistently outperforming aperture partitioning as shown in the following plots. This result is consistent with those seen in Section 4.1.

4.2.1 Pulsed Spectral Efficiency Difference Between Time Sharing and Aperture Partitioning

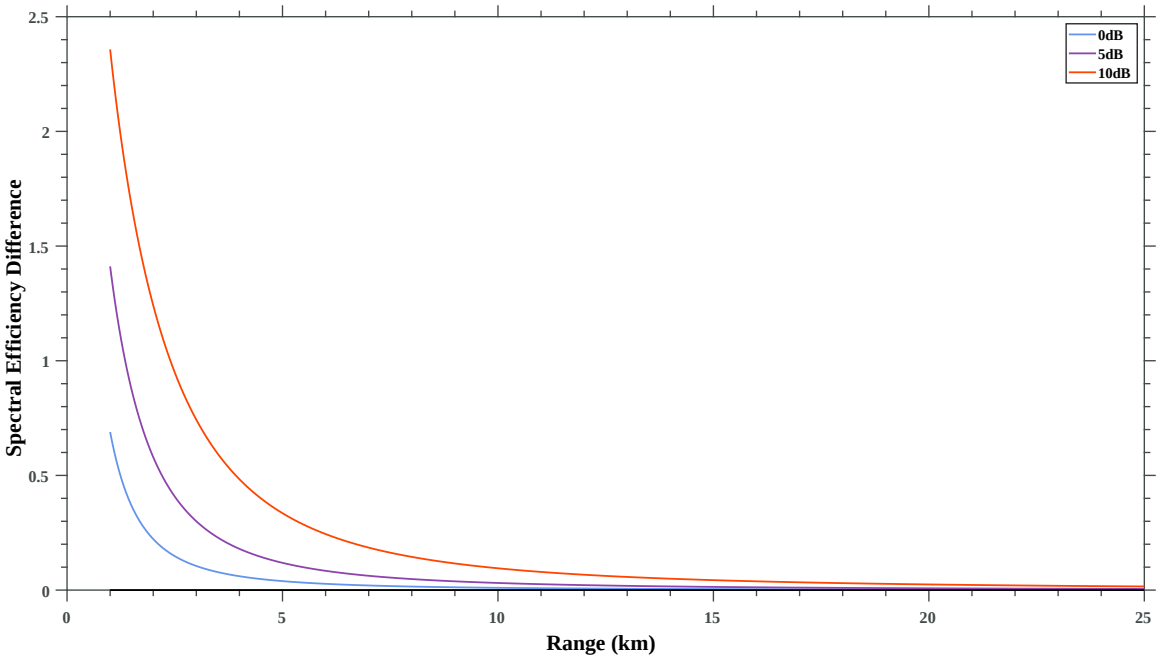

Figure 4.11: Plot showing the spectral efficiency difference between timesharing and aperture partitioning. The legend values are the SNR values at a range of 1000 meters. The radar ERP fraction (α) is fixed at 0.3, $T_p = 20\mu s$, PRF = 2000, and $\gamma = 1$.

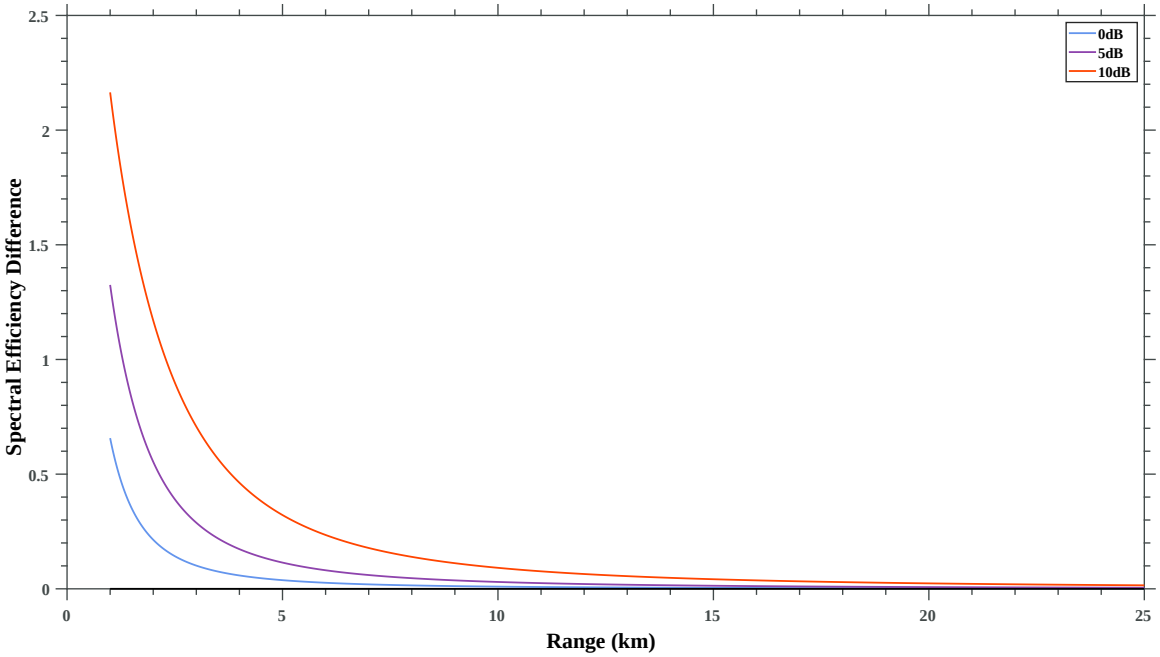

Figure 4.12: Plot showing the spectral efficiency difference between timesharing and aperture partitioning. The legend values are the SNR values at a range of 1000 meters. The radar ERP fraction (α) is fixed at 0.3, $T_p = 20\mu s$, PRF = 8000, and $\gamma = 1$.

Figures 4.11 and 4.14 illustrate the spectral efficiency difference between timesharing and aperture partitioning (with positive values meaning timesharing is more efficient) as a function of duty cycle by varying the PRF. For Figures 4.11 and 4.13 the PRF is set to 2000 Hz, for and for Figures the PRF is set to 8000 Hz. For Figures 4.11 and 4.12 the communications waveform is transmitted at full power. In Figure 4.11, the spectral efficiency difference for the 10dB curve at 1km is approximately 2.357 bits/s/Hz, while in Figure 4.12 it, is 2.164 bits/s/Hz. Figures 4.13-4.14 show the same scenario but with $\gamma = D$ (i.e., the average communications power is limited to the average radar power).

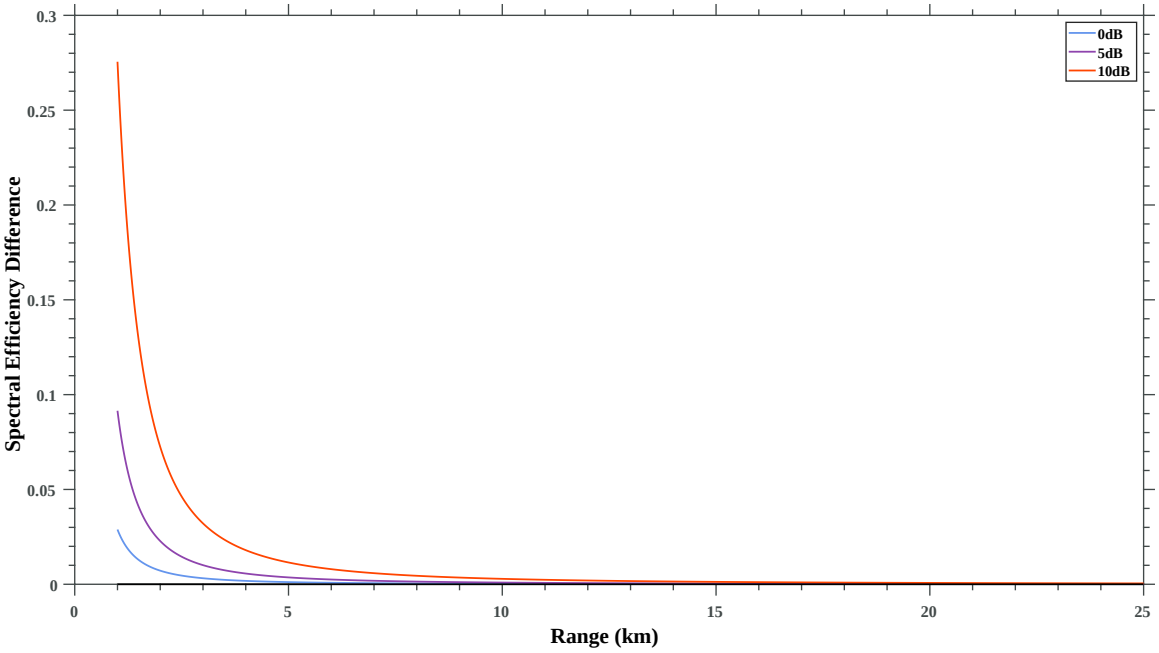

Figure 4.13: Plot showing the spectral efficiency difference between timesharing and aperture partitioning. The legend values are the SNR values at a range of 1000 meters. The radar ERP fraction (α) is fixed at 0.3, $T_p = 20\mu s$, PRF = 2000, and $\gamma = D$.

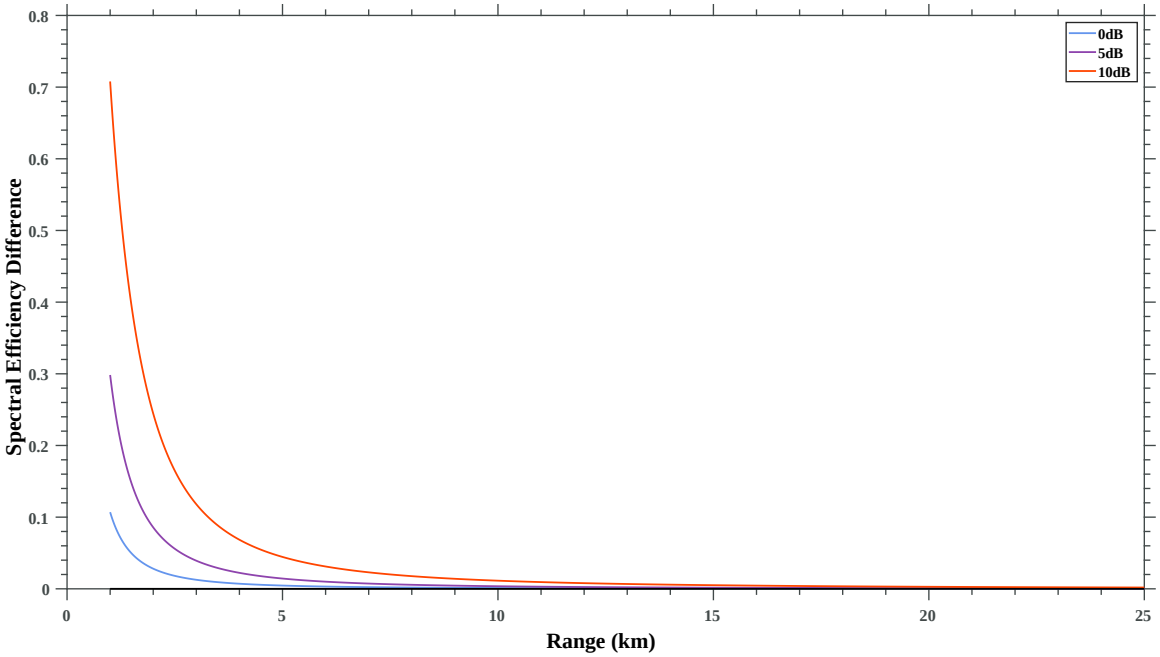

Figure 4.14: Plot showing the spectral efficiency difference between timesharing and aperture partitioning. The legend values are the SNR values at a range of 1000 meters. The radar ERP fraction (α) is fixed at 0.3, $T_p = 20\mu s$, PRF = 8000, and $\gamma = D$.

The values of spectral efficiency difference for the 10dB curves are now 0.275 bits/s/Hz for Figure 4.13 (i.e., PRF=2000 Hz) and 0.707 for Figure 4.14 (i.e., PRF=8000 Hz). It is shown that increased PRF makes a larger difference when the communications transmit power is limited. Next, the cases examined in Figures 4.11-4.14 are repeated but the radar ERP fraction is set to $\alpha = 0.9$. The corresponding results are shown in Figures 4.15-4.18.

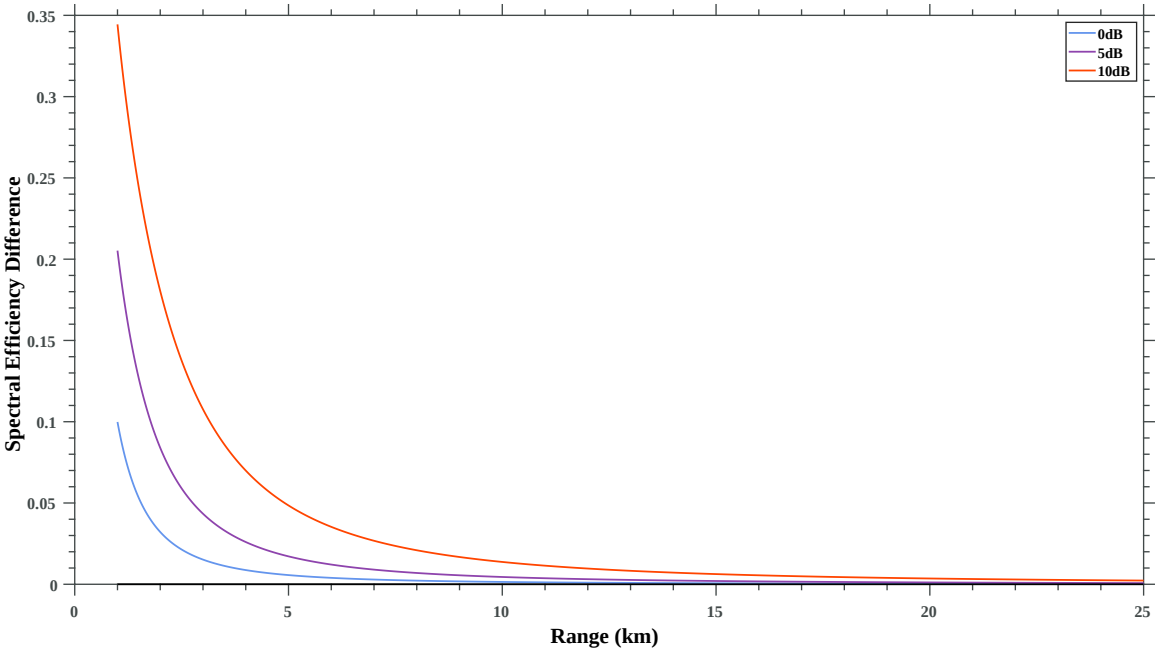

Figure 4.15: Plot showing the spectral efficiency difference between timesharing and aperture partitioning. The legend values are the SNR values at a range of 1000 meters. The radar ERP fraction (α) is fixed at 0.9, $T_p = 20\mu s$, PRF = 2000, and $\gamma = 1$.

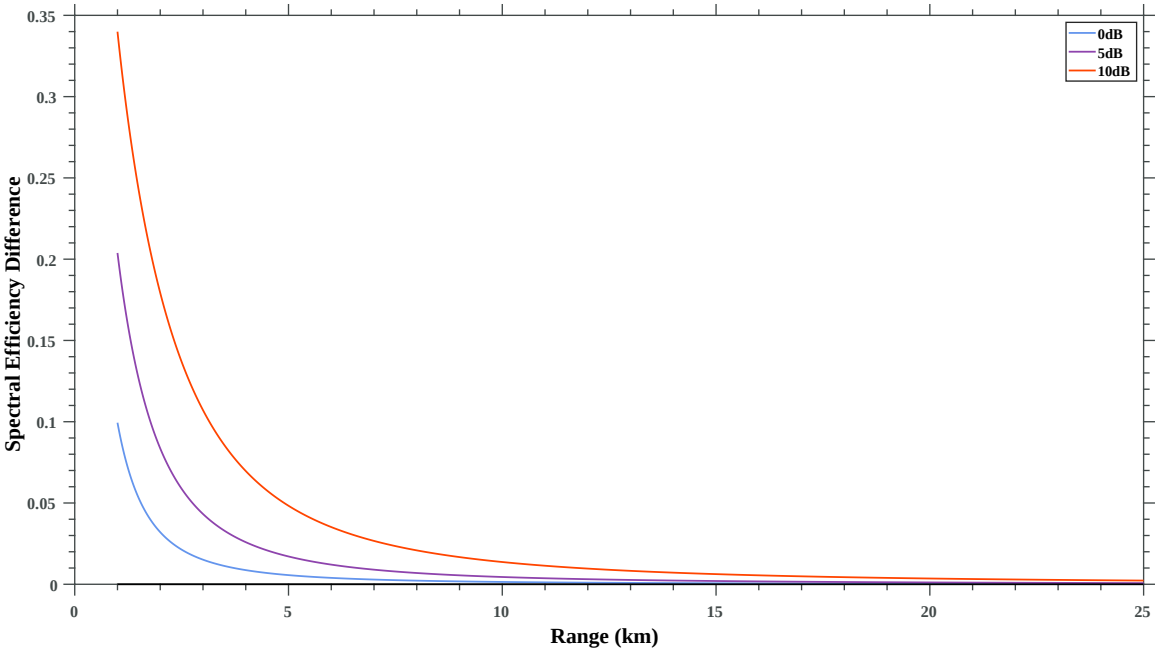

Figure 4.16: Plot showing the spectral efficiency difference between timesharing and aperture partitioning. The legend values are the SNR values at a range of 1000 meters. The radar ERP fraction (α) is fixed at 0.9, $T_p = 20\mu s$, PRF = 8000, and $\gamma = 1$.

At this value of α, the spectral efficiency difference for the 10dB curve at 1km is approximately 0.344 bits/s/Hz for Fig. 4.15 and is 0.340 bits/s/Hz for Fig. 4.16.

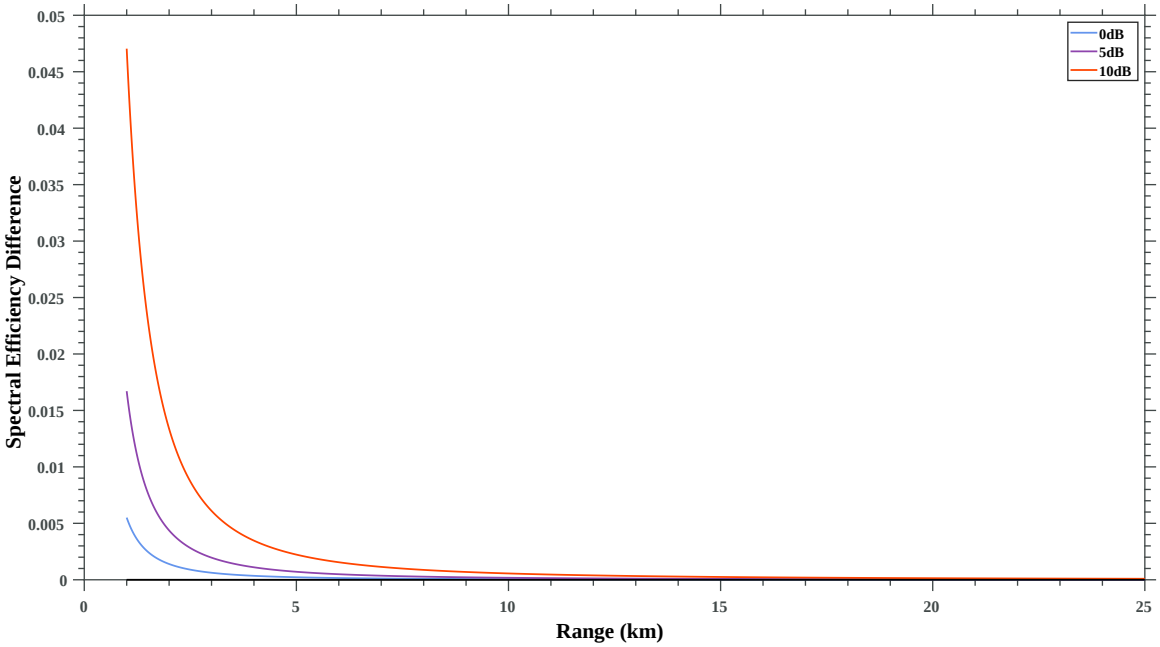

Figure 4.17: Plot showing the spectral efficiency difference between timesharing and aperture partitioning. The legend values are the SNR values at a range of 1000 meters. The radar ERP fraction (α) is fixed at 0.9, $T_p = 20\mu s$, PRF = 2000, and $\gamma = D$.

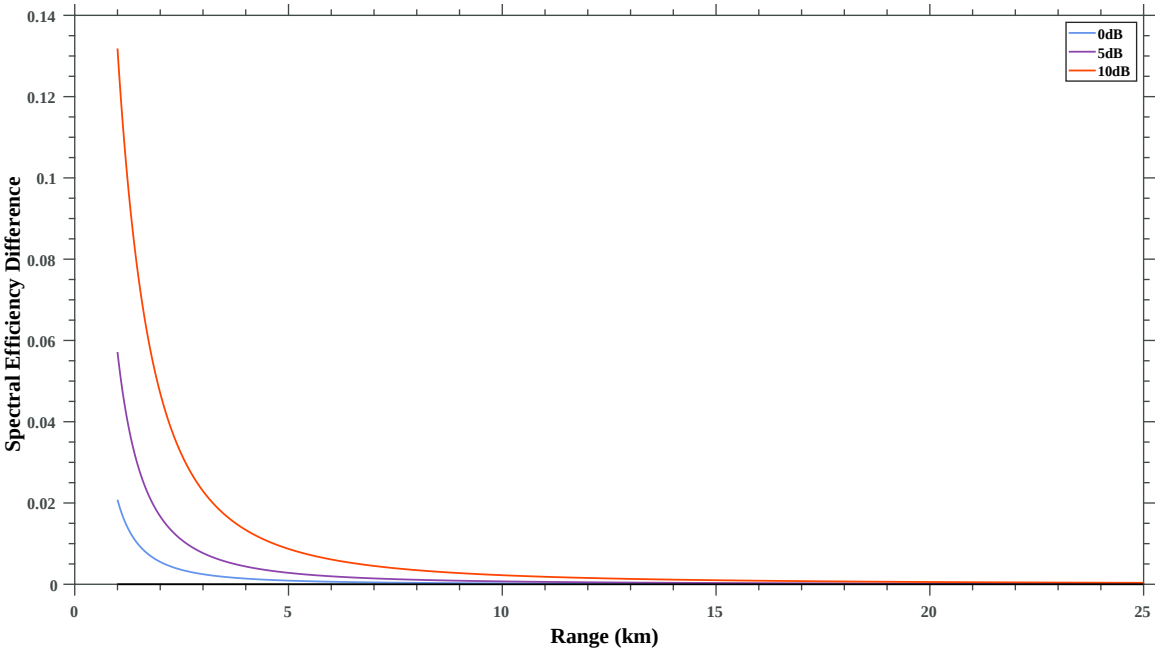

Figure 4.18: Plot showing the spectral efficiency difference between timesharing and aperture partitioning. The legend values are the SNR values at a range of 1000 meters. The radar ERP fraction (α) is fixed at 0.9, $T_p = 20\mu s$, PRF = 8000, and $\gamma = D$.

Showing a similar effect, the values of spectral efficiency difference for the 10dB curves at 1km are now 0.047 bits/s/Hz for Fig. 4.17 and 0.132 bits/s/Hz for Fig. 4.18. Next, the duty cycle is varied for high SNR cases. Specifically, Figures 4.19-4.21 consider SNRs of $[15, 25, 28]$ dB for duty cycles of $D = [0.4, 0.608, 0.8]$, respectively. Further, the percentage transmit power of the timesharing case is limited to the duty cycle of the aperture partitioning case. From Figure 4.20 and 4.21 it is seen that for high duty cycles and SNRs partitioning may become the better choice, as was seen in the previous examination of the continuous wave case considered in Chapter 3.

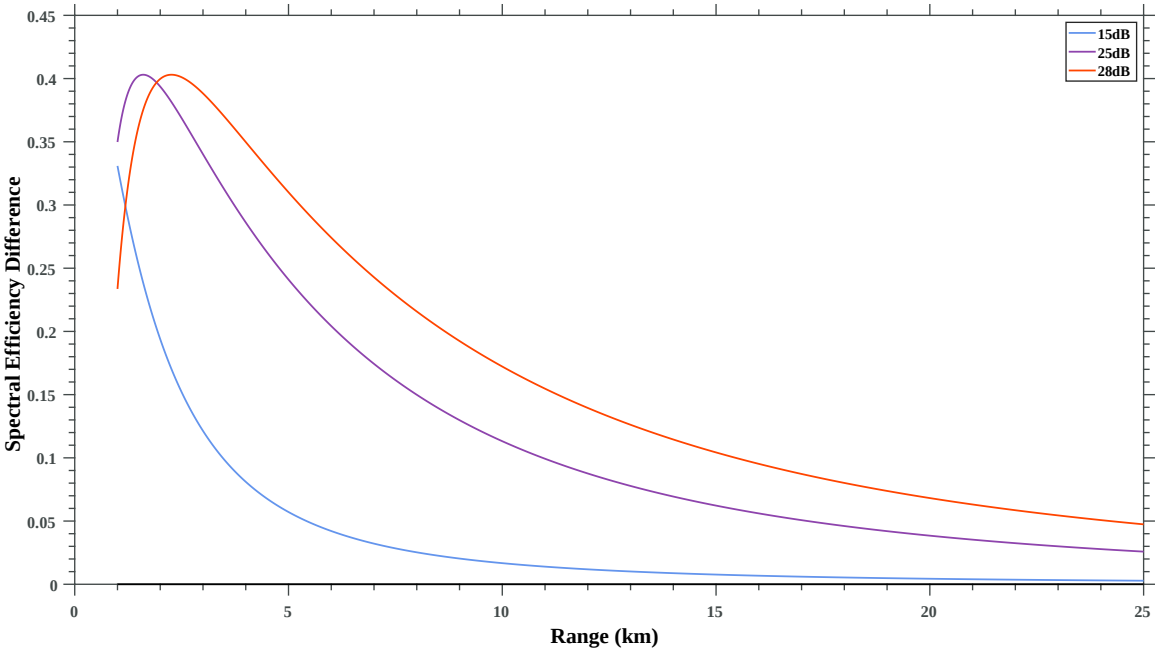

Figure 4.19: Plot showing the spectral efficiency difference between timesharing and aperture partitioning. The legend values are the SNR values at a range of 1000 meters. The radar ERP fraction (α) is fixed at 0.9, $T_p = 50\mu s$, PRF = 8000, and $\gamma = D = 0.4$.

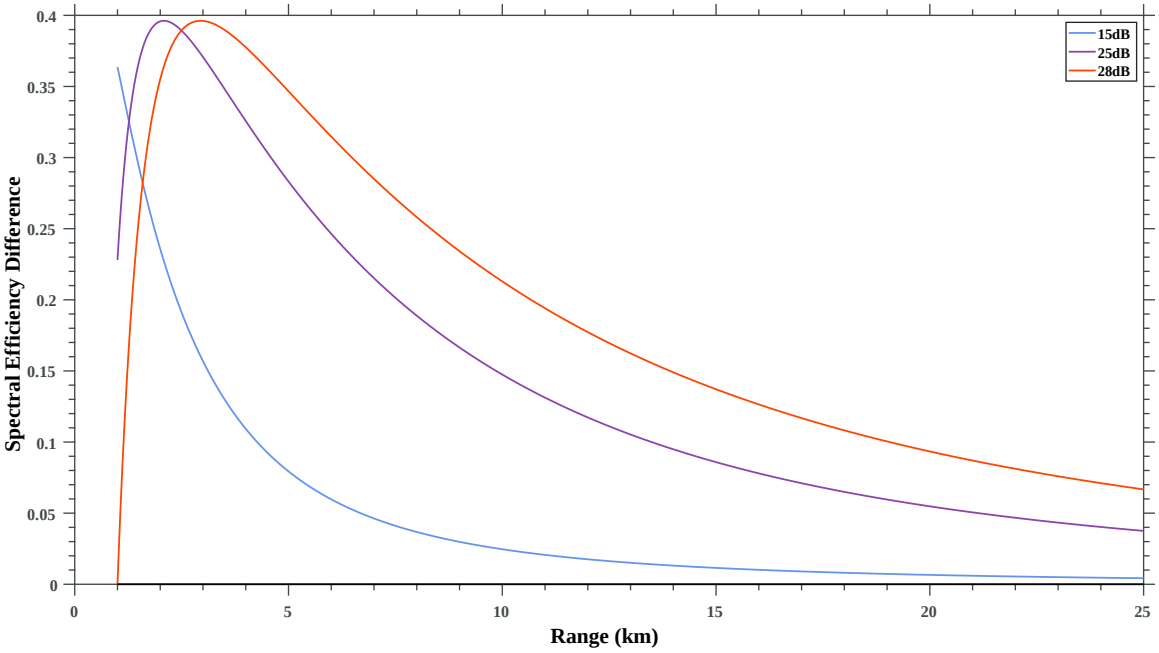

Figure 4.20: Plot showing the spectral efficiency difference between timesharing and aperture partitioning. The legend values are the SNR values at a range of 1000 meters. The radar ERP fraction (α) is fixed at 0.9, $T_p = 76\mu s$, PRF = 8000, and $\gamma = D = 0.608$.

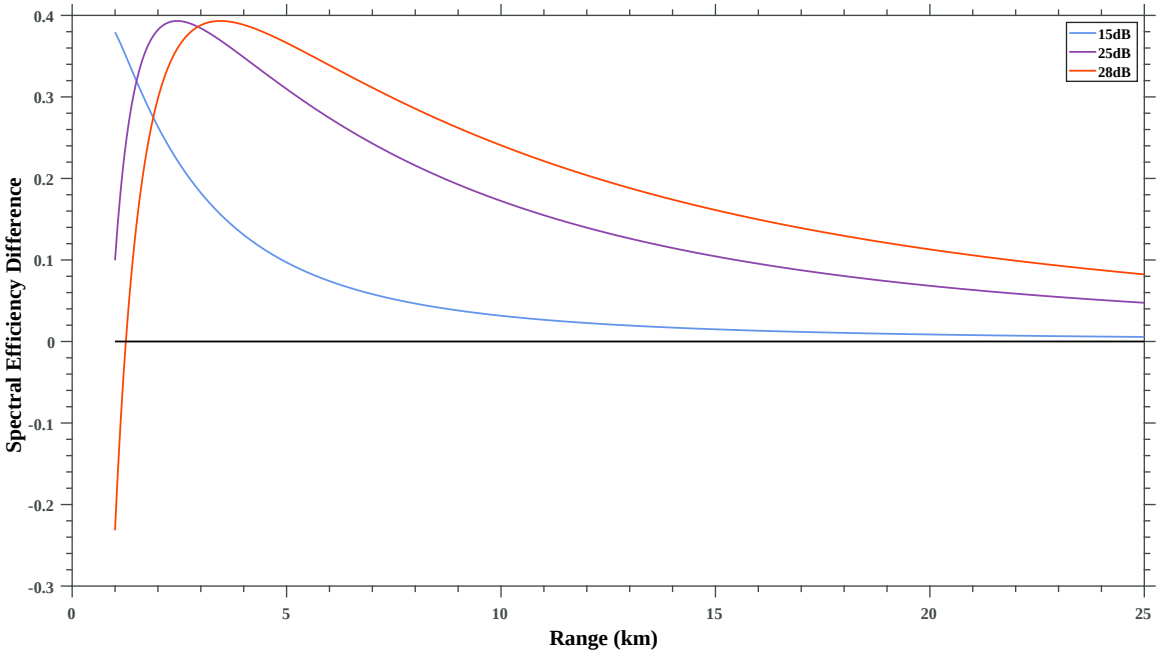

Figure 4.21: Plot showing the spectral efficiency difference between timesharing and aperture partitioning. The legend values are the SNR values at a range of 1000 meters. The radar ERP fraction (α) is fixed at 0.9, $T_p = 100\mu s$, PRF = 8000, and $\gamma = D = 0.8$.

As seen in Fig. 4.20, an SNR of 28dB at 1km and a duty cycle of approximately 0.608 marks the transition to aperture-partitioning becoming the better choice. Numerically solving $SE_{ts_p} - SE_{ap_p}$ for $\alpha = 0.9$ and an SNR of 28dB gives a duty cycle of 0.6081; for 25dB, a duty cycle of 0.9406 is required for the two methods to be equal.

4.2.2 Pulsed Spectral Efficiency Difference Between Time Sharing and Simultaneous Dual Beam

Next we analyze the spectral efficiency difference between pulsed SDB and timesharing as a function of duty cycle. Note that for this section a positive spectral efficiency difference corresponds to SDB being the best choice, while a negative spectral efficiency difference means that timesharing is the most spectral efficient. First, Figure 4.22 unsurprisingly shows that the timesharing provides a significant advantage for

low duty cycle SDB as compared to full power, continuous wave timeshared communications. This advantage is significantly lessened when the average power of the timeshared communications is set equal to that of the SDB, as is shown in Figure 4.23. Finally, Figure 4.24 shows that at short ranges and 10 dB SNR the SDB approach may still be advantageous at short ranges.

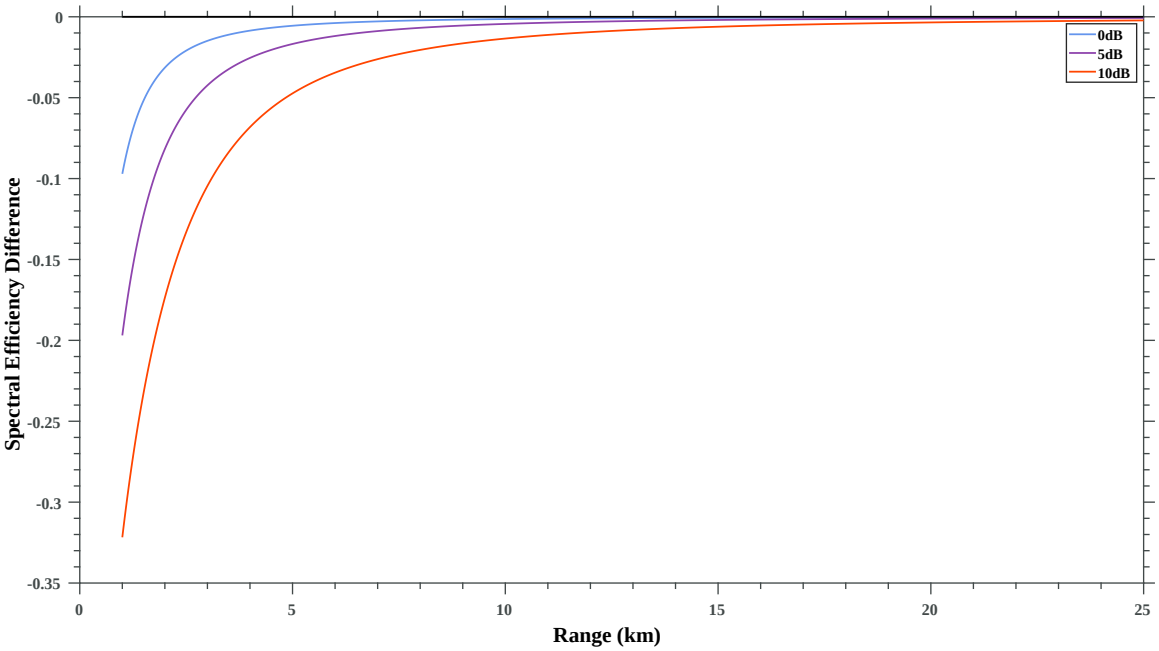

Figure 4.22: Plot showing the spectral efficiency difference between SDB and timesharing. The legend values are the SNR values at a range of 1000 meters. The radar ERP fraction (α) is fixed at 0.9, $T_p = 20\mu s$, PRF = 2000, and $\gamma = 1$.

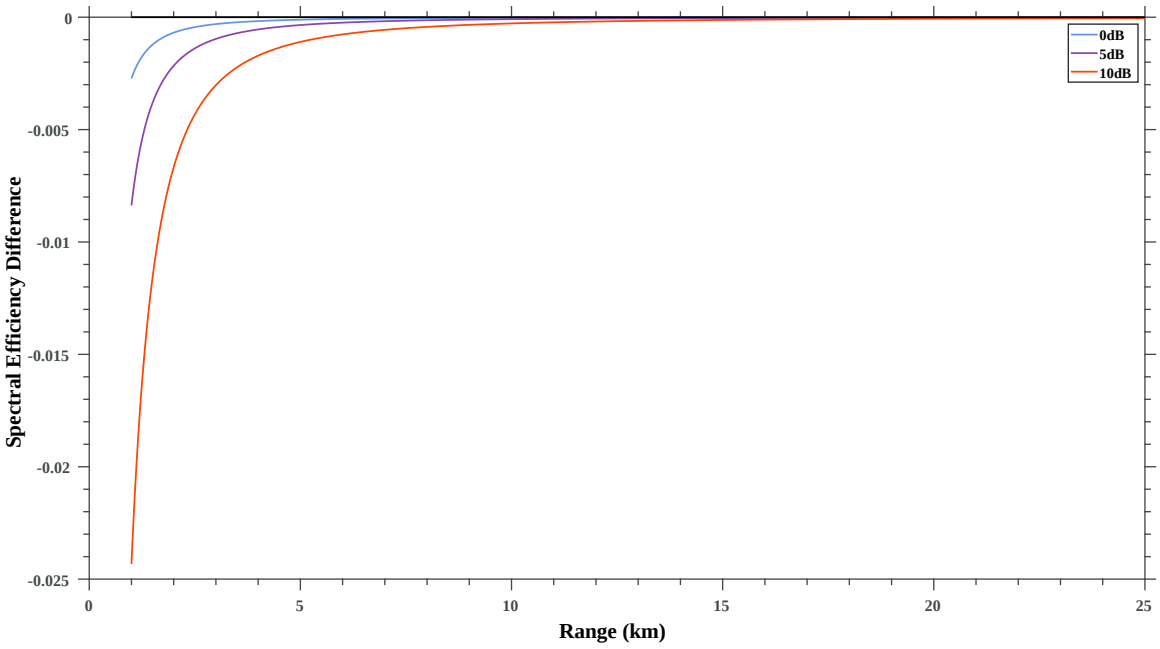

Figure 4.23: Plot showing the spectral efficiency difference between SDB and time-sharing. The legend values are the SNR values at a range of 1000 meters. The radar ERP fraction (α) is fixed at 0.9, $T_p = 20\mu s$, PRF = 2000, and $\gamma = D$.

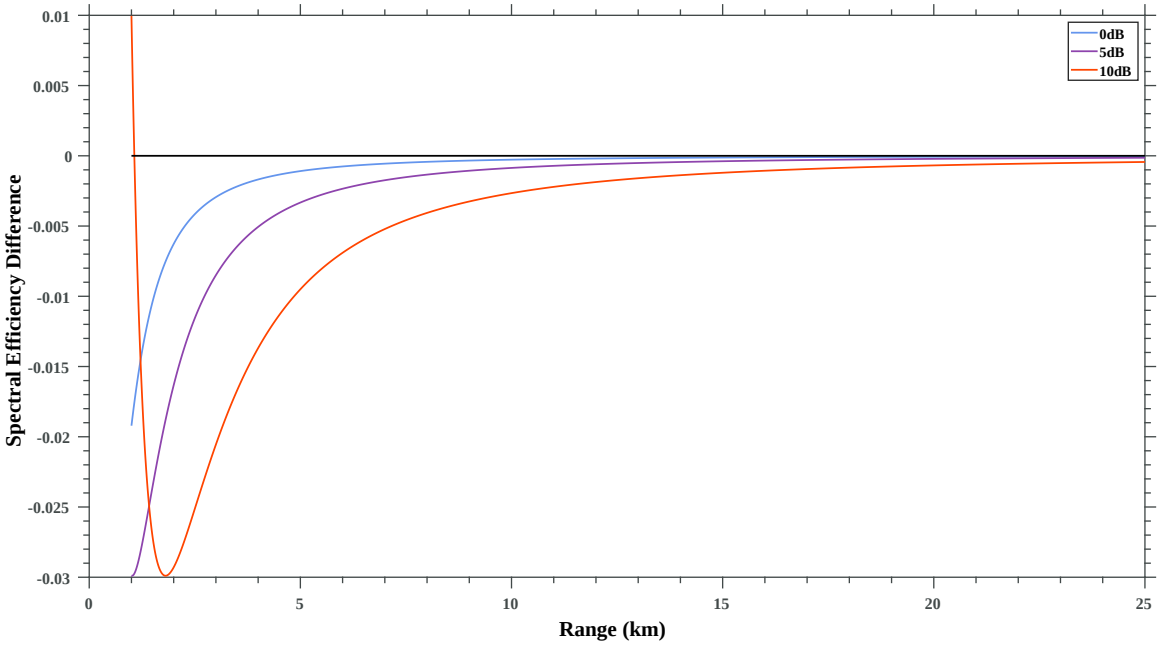

Figure 4.24: Plot showing the spectral efficiency difference between SDB and time-sharing. The legend values are the SNR values at a range of 1000 meters. The radar ERP fraction (α) is fixed at 0.9, $T_p = 200\mu s$, PRF = 2000, and $\gamma = D = 0.4$.

Solving for the value of D where SDB becomes more efficient than timesharing at short distances at 10dB results in a duty cycle of 0.3676. In contrast the continuous wave results shown in Chapter 3, Figures 4.22-4.24 demonstrate that timesharing is largely a better choice than SDB when SDB is pulsed. SDB remains the best choice at shorter distances, high SNR, and high duty cycle as shown in Figures 4.25-4.26.

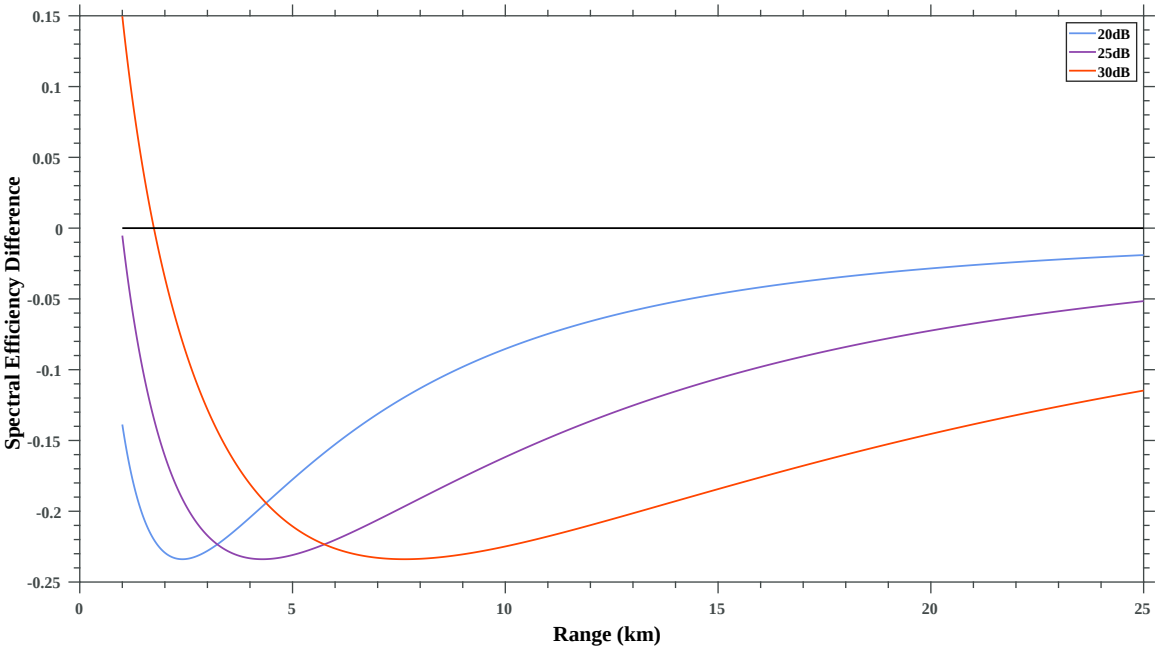

Figure 4.25: Plot showing the spectral efficiency difference between SDB and timesharing. The legend values are the SNR values at a range of 1000 meters. The radar ERP fraction (α) is fixed at 0.9, $T_p = 100\mu s$, PRF = 2000, and $\gamma = 1$.

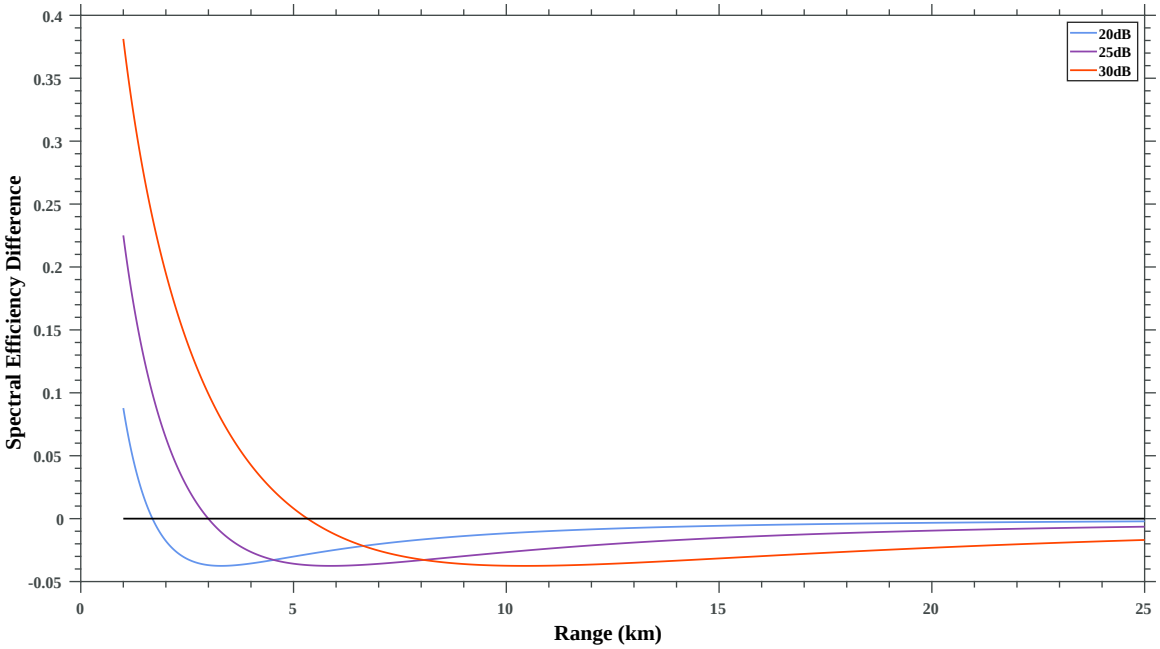

Figure 4.26: Plot showing the spectral efficiency difference between SDB and timesharing. The legend values are the SNR values at a range of 1000 meters. The radar ERP fraction (α) is fixed at 0.9, $T_p = 100\mu s$, PRF = 2000, and $\gamma = D = 0.2$.

It is worth noting that since D determines the curves in the previous figures, a higher PRF and an appropriately lower T_p will produce the same figure. For example, with a PRF of 8000 and a T_p of $25\mu s$ replicates Fig. 4.26 if the transmit power of the continuous communications beam is limited to a fraction D of full power. Figures 4.25 and 4.26 also show that decreasing the transmit power of the timesharing mode decreases the SNR at which SDB becomes more efficient than timesharing.

4.3 Performance Across PRF

Since pulsed radar is being discussed, a brief overview on how PRF affects performance should be covered. Future work could cover how PRF affected quantities such as blind range or velocity determine which DFRC method is optimum.

4.3.1 Comparing the Spectral Efficiency of Time Sharing and Aperture Partitioning as a Function of Pulse Repetition Frequency

First, Figures 4.27-4.30 show traces of spectral efficiency difference for SNR values of $[0, 10, 20]$ dB across short and long pulses for the case where the timeshared communications is continuous wave, and the aperture partitioning uses a PRF varied from 1000-8000 Hz. Specifically, Figures 4.27 and 4.28 examine the case of a $20\mu s$ pulse and Figures 4.29 and 4.30 considers a $100\mu s$ pulse duration. The percentage of ERP allocated to radar for the aperture partitioning is varied from $\alpha = 0.3$ in Figures 4.27 and 4.29 to $\alpha = 0.9$ in Figures 4.28 and 4.30. A slight downward trend in spectral efficiency difference can be seen when the duty cycle is increased (i.e., for the long pulse) and the SNR is 20 dB in Figures 4.29 and 4.30.

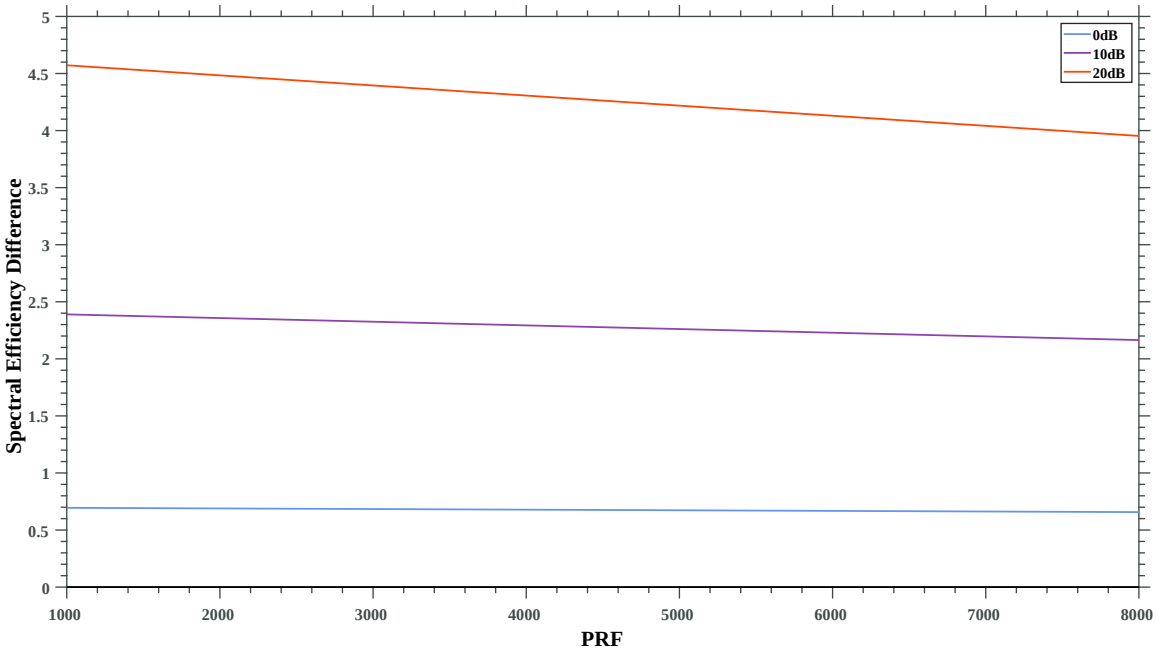

Figure 4.27: Plot showing the spectral efficiency difference between timesharing and aperture partitioning. The legend values are the SNR values at a fixed range. The radar ERP fraction (α) is fixed at 0.3, $T_p = 20\mu s$, and $\gamma = 1$.

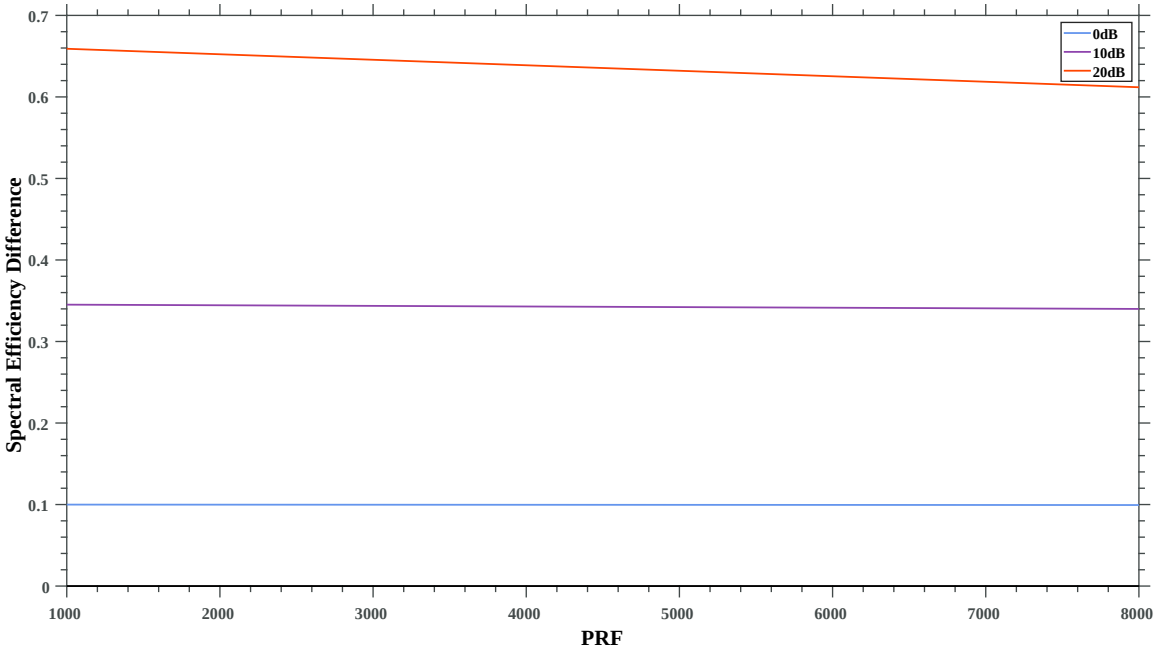

Figure 4.28: Plot showing the spectral efficiency difference between timesharing and aperture partitioning. The legend values are the SNR values at a fixed range. The radar ERP fraction (α) is fixed at 0.9, $T_p = 20\mu s$, and $\gamma = 1$.

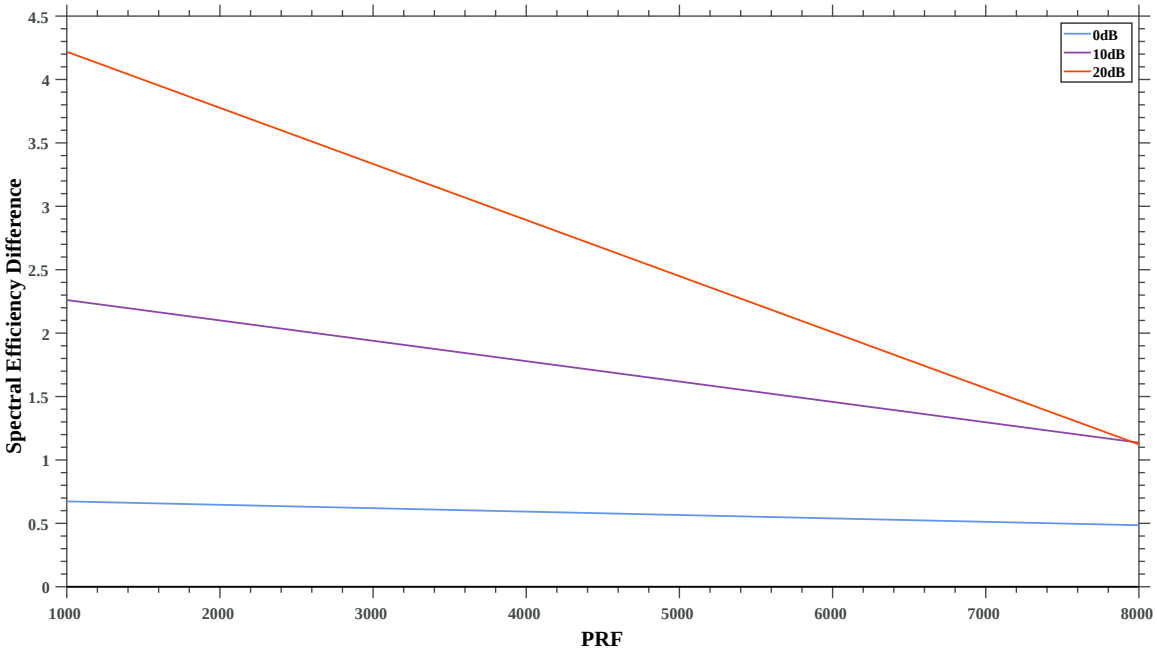

Figure 4.29: Plot showing the spectral efficiency difference between timesharing and aperture partitioning. The legend values are the SNR values at a fixed range. The radar ERP fraction (α) is fixed at 0.3, $T_p = 100\mu s$, and $\gamma = 1$.

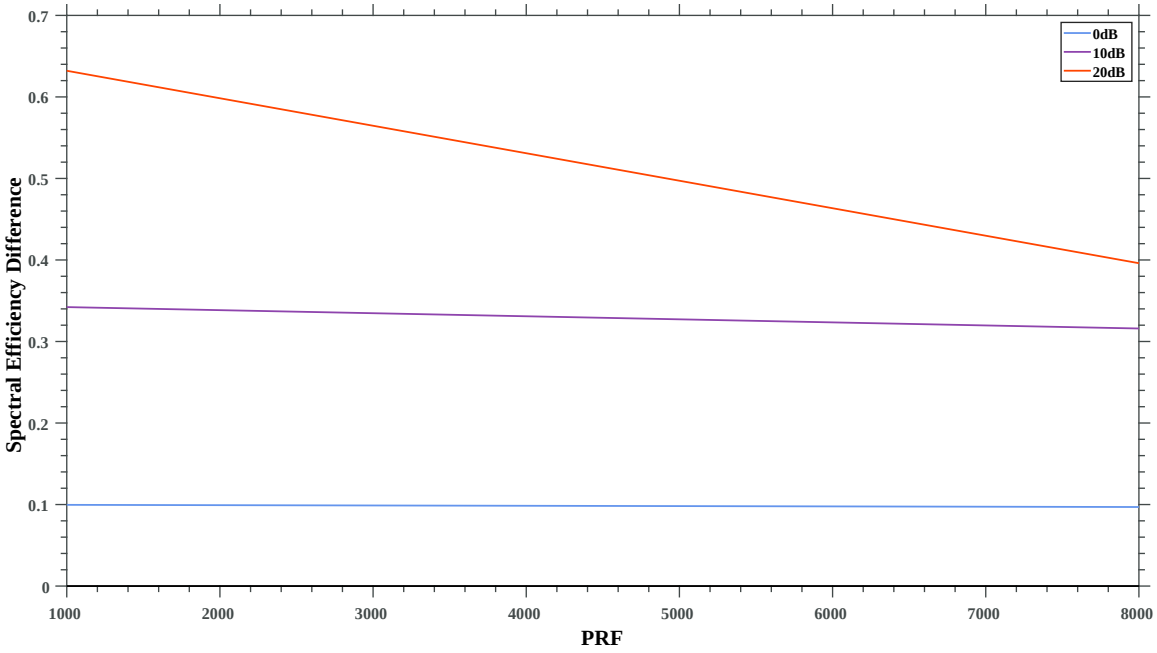

Figure 4.30: Plot showing the spectral efficiency difference between timesharing and aperture partitioning. The legend values are the SNR values at a fixed range. The radar ERP fraction (α) is fixed at 0.9, $T_p = 100\mu s$, and $\gamma = 1$.

Next, an additional trace is added for a high SNR of 27 dB. It can be seen in Figure 4.31 that the long pulse ($100\mu s$) and high radar ERP ($\alpha = 0.9$) enables the aperture partitioning to be more efficient than timesharing at high PRFs ($>\approx$ 7400 Hz).

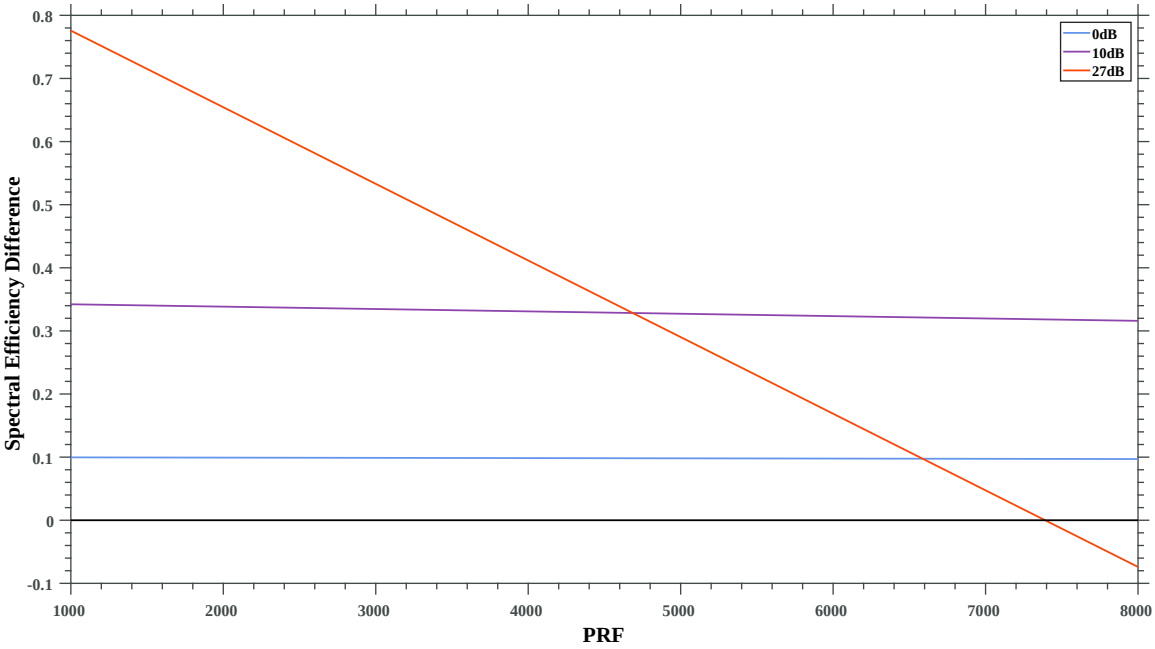

Figure 4.31: Plot showing the spectral efficiency difference between timesharing and aperture partitioning. The legend values are the SNR values at a fixed range. The radar ERP fraction (α) is fixed at 0.9, $T_p = 100\mu s$, and $\gamma = 1$.

However, reducing the radar ERP to $\alpha = 0.3$ reduces the relative spectral efficiency of aperture partitioning, and Figure 4.32 shows timesharing is the more efficient choice in this regime.

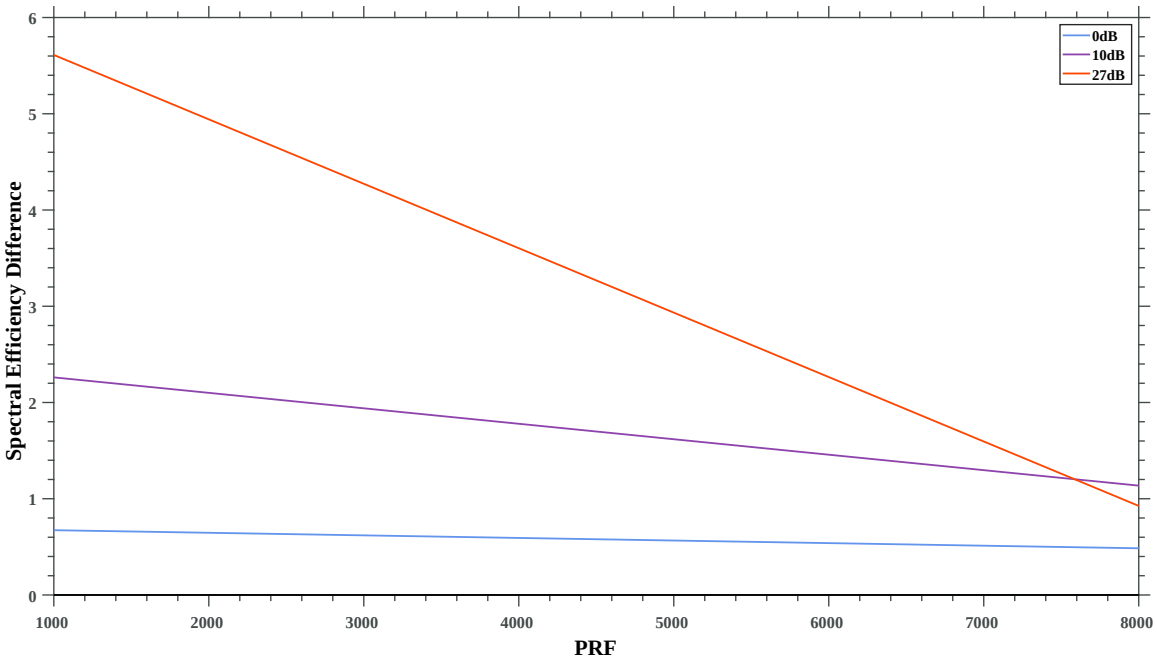

Figure 4.32: Plot showing the spectral efficiency difference between timesharing and aperture partitioning. The legend values are the SNR values at a fixed range. The radar ERP fraction (α) is fixed at 0.3, $T_p = 100\mu s$, and $\gamma = 1$.

Finally, Figures 4.33-4.37 explore the relative advantage of timesharing over aperture partitioning when the timeshared communications average percentage power is set to the duty cycle of the radar waveform for the aperture partitioning case. Figure 4.33 shows the spectral efficiency for the $T_p = 20\mu s$ and $\alpha = 0.9$ case and the $T_p = 100\mu s$ case with $\alpha = 0.3, 0.9$ is shown in Figures 4.34 and 4.35, respectively. It is seen that in all of these cases, there is no PRF considered that has a spectral efficiency advantage for aperture partitioning relative to timesharing. Even when higher SNRs are considered in conjunction with an $\alpha = 0.3$, as is the case in Figure 4.36, timesharing remains the better choice.

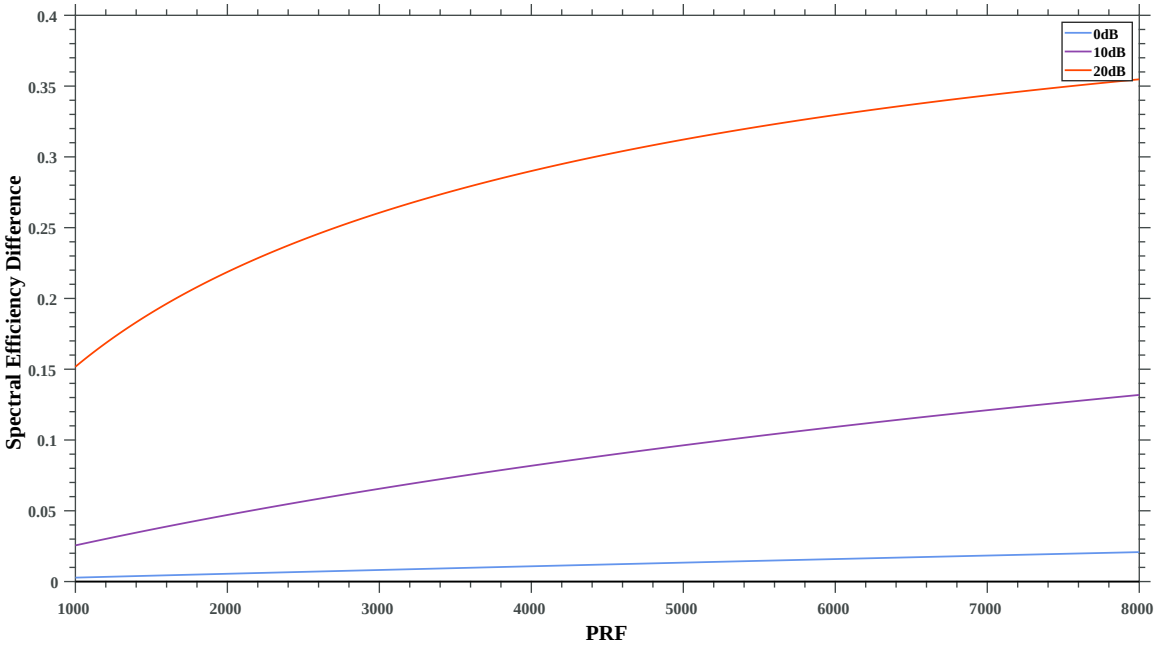

Figure 4.33: Plot showing the spectral efficiency difference between timesharing and aperture partitioning. The legend values are the SNR values at a fixed range. The radar ERP fraction (α) is fixed at 0.9, $T_p = 20\mu s$, and $\gamma = D$.

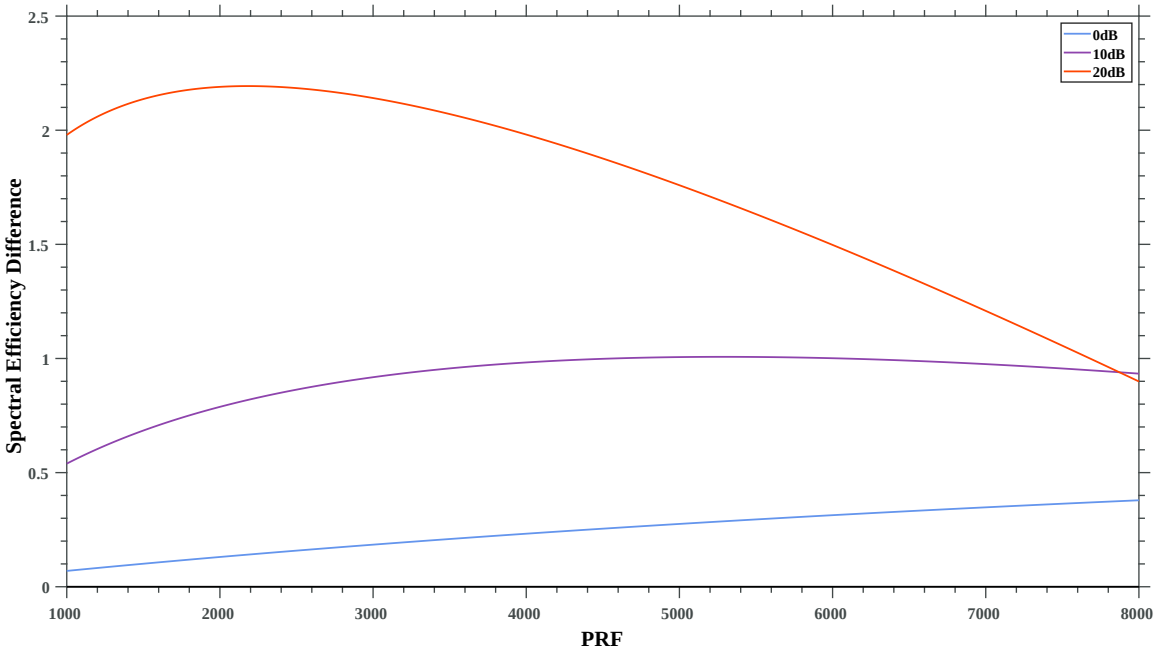

Figure 4.34: Plot showing the spectral efficiency difference between timesharing and aperture partitioning. The legend values are the SNR values at a fixed range. The radar ERP fraction (α) is fixed at 0.3, $T_p = 100\mu s$, and $\gamma = D$.

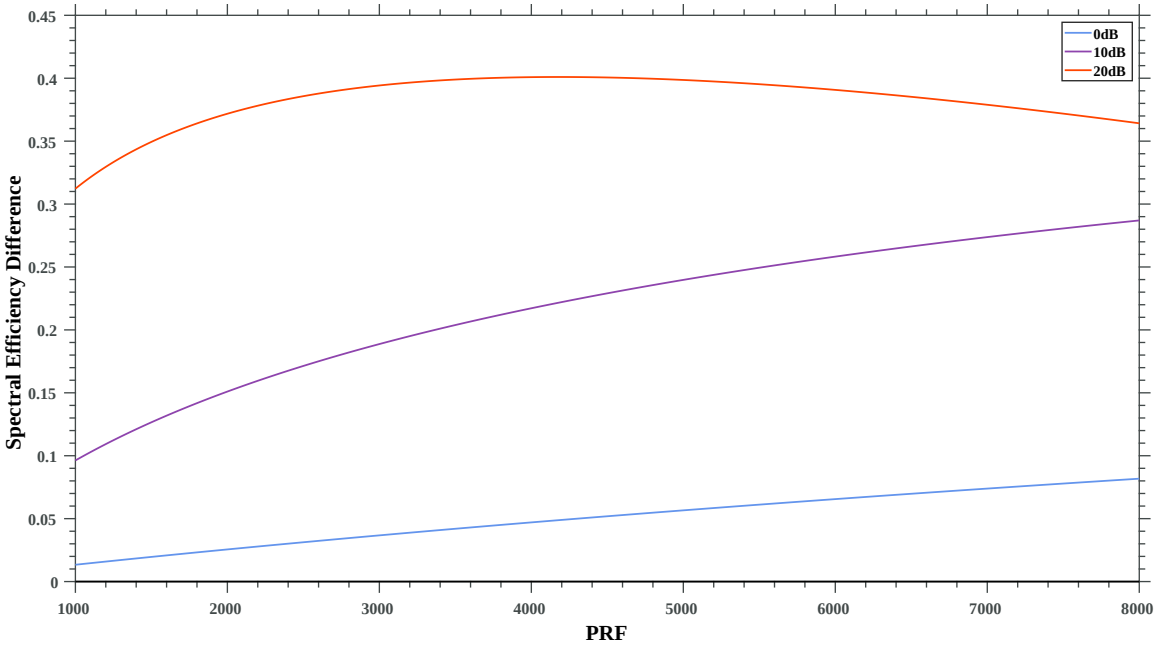

Figure 4.35: Plot showing the spectral efficiency difference between timesharing and aperture partitioning. The legend values are the SNR values at a fixed range. The radar ERP fraction (α) is fixed at 0.9, $T_p = 100\mu s$, and $\gamma = D$.

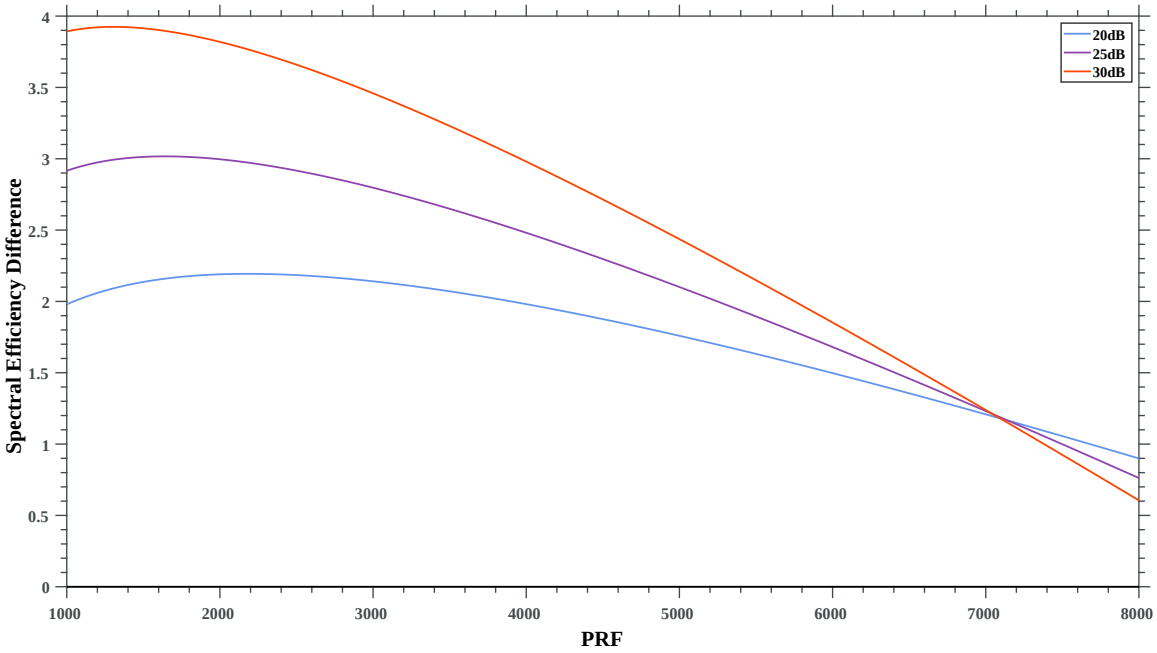

Figure 4.36: Plot showing the spectral efficiency difference between timesharing and aperture partitioning. The legend values are the SNR values at a fixed range. The radar ERP fraction (α) is fixed at 0.3, $T_p = 100\mu s$, and $\gamma = D$.

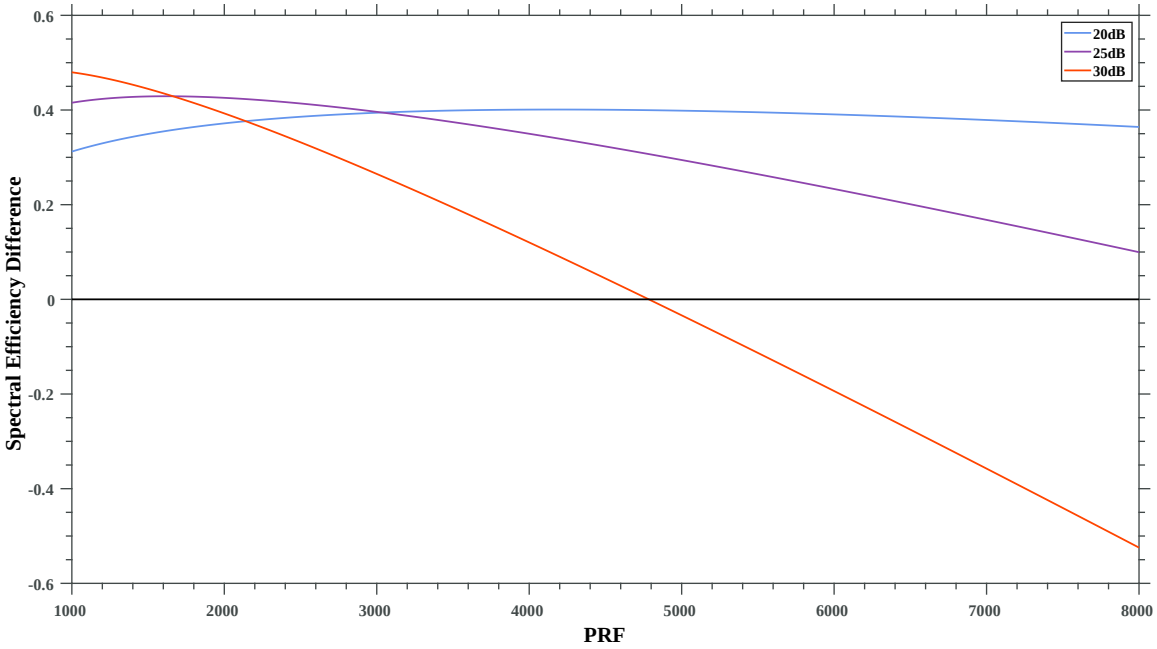

Figure 4.37: Plot showing the spectral efficiency difference between timesharing and aperture partitioning. The legend values are the SNR values at a fixed range. The radar ERP fraction (α) is fixed at 0.9, $T_p = 100\mu s$, and $\gamma = D$.

However, when $\alpha = 0.9$ and $T_p = 100\mu s$, aperture partitioning can be the best choice for very high SNR, as seen in the 30 dB trace in Figure 4.37.

4.3.2 Comparing the Spectral Efficiency of Time Sharing and Simultaneous Dual Beam as a Function of Pulse Repetition Frequency

In this section the spectral efficiency of pulsed SDB and timesharing is compared. First, in Figures 4.38-4.40 the pulse duration is set to $T_p = 20\mu s$. The radar ERP is set to $\alpha = 0.3$ for Figure 4.38 and $\alpha = 0.9$ for Figures 4.39 and 4.40. It can be seen from Figures 4.38 and 4.39 that for both choices of α, if the timesharing communications waveform uses the full power it is the more efficient choice. However, if the communications waveform average power is limited by the radar duty cycle, as

is the case in Figure 4.40, for high PRFs (greater than approximately $7800Hz$) SDB may be more efficient.

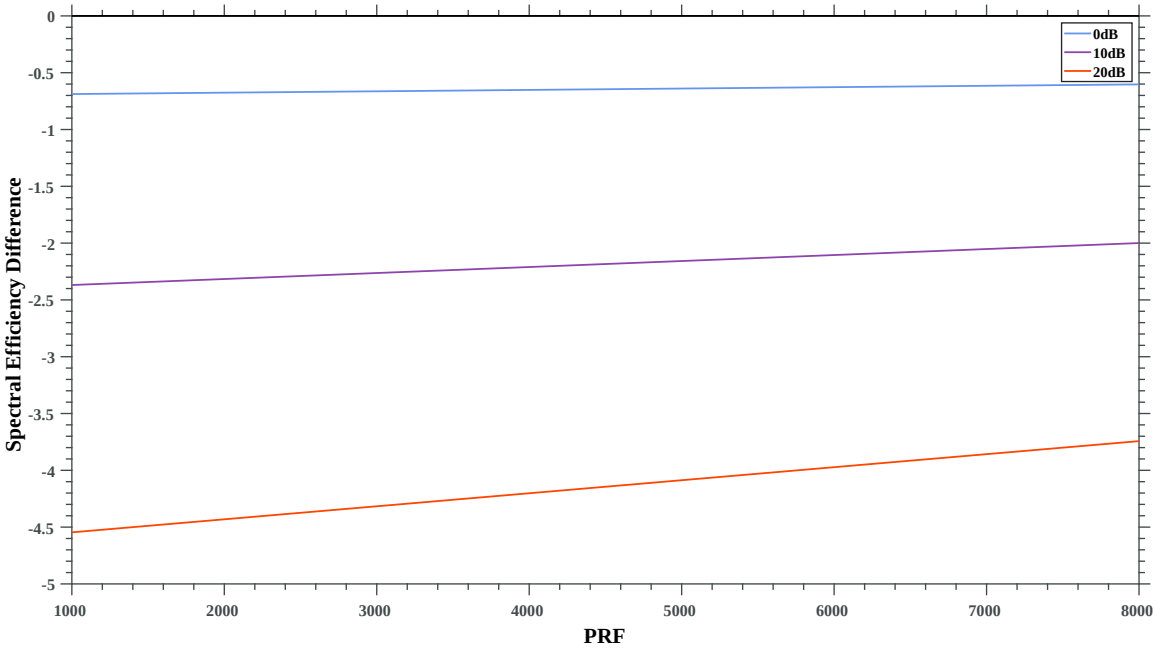

Figure 4.38: Plot showing the spectral efficiency difference between SDB and time-sharing. The legend values are the SNR values at a fixed range. The radar ERP fraction (α) is fixed at 0.3, $T_p = 20\mu s$, and $\gamma = 1$.

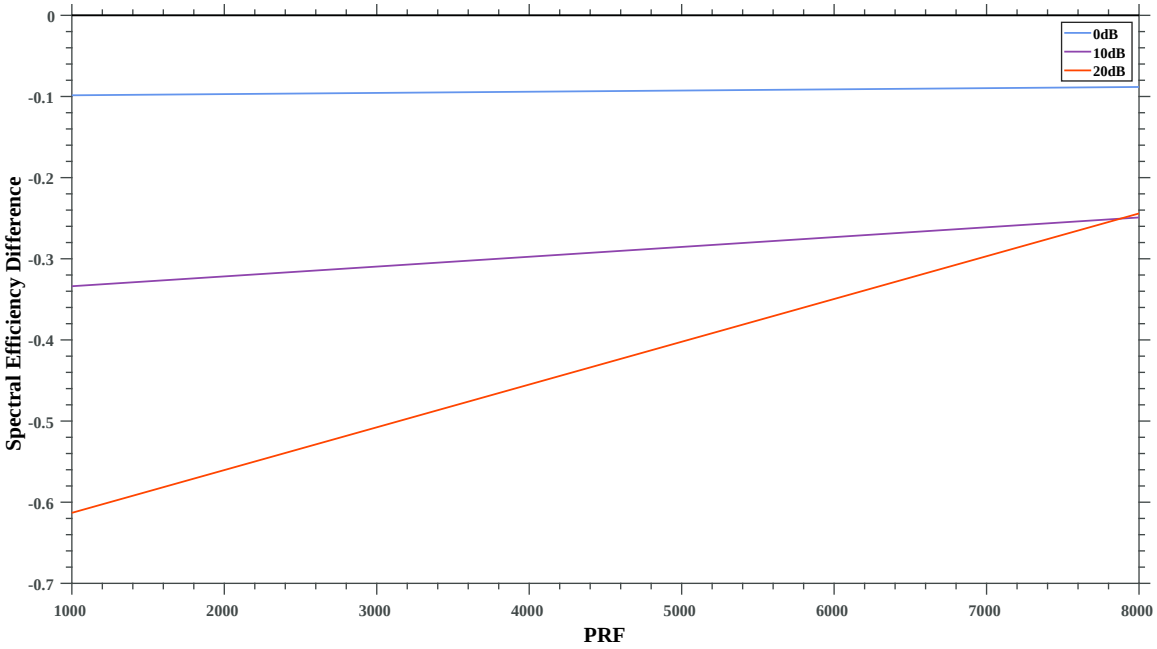

Figure 4.39: Plot showing the spectral efficiency difference between SDB and time-sharing. The legend values are the SNR values at a fixed range. The radar ERP fraction (α) is fixed at 0.9, $T_p = 20\mu s$, and $\gamma = 1$.

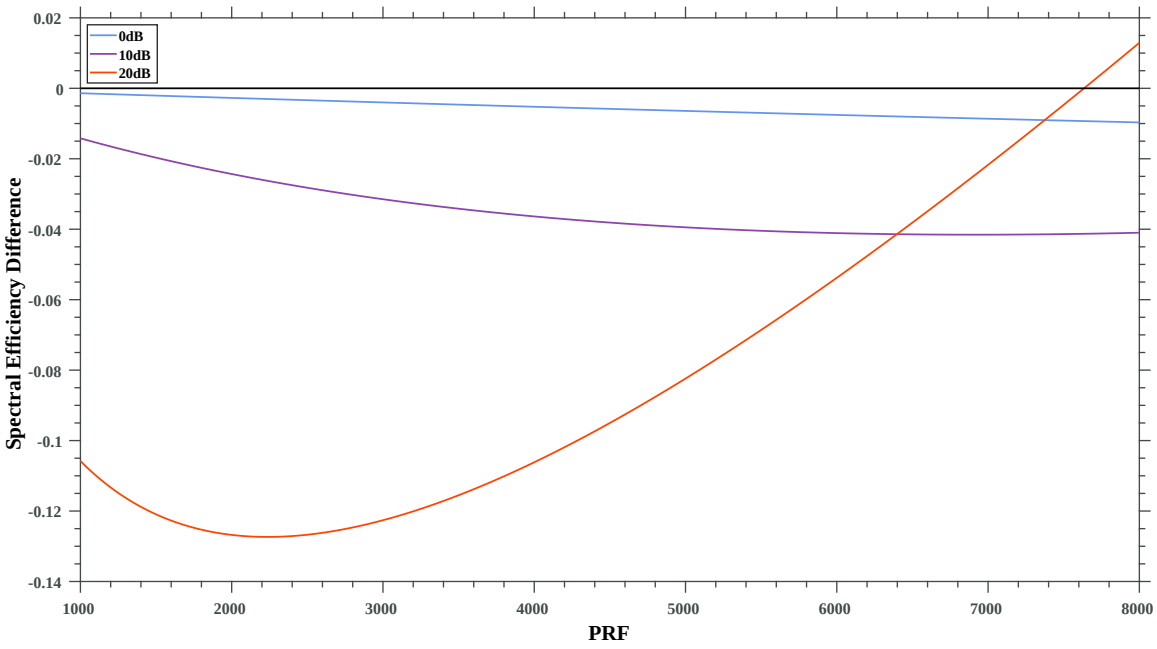

Figure 4.40: Plot showing the spectral efficiency difference between SDB and time-sharing. The legend values are the SNR values at a fixed range. The radar ERP fraction (α) is fixed at 0.9, $T_p = 20\mu s$, and $\gamma = D$.

Finally, in Figures 4.41-4.7 the pulse duration is extended to $T_p = 100\mu s$. Figure 4.41 shows that if the radar ERP is high, with $\alpha = 0.9$, then the SDB is more spectrally efficient after a PRF of ≈ 2600. Unsurprisingly this advantage for SDB arises at even lower PRFs when the timesharing communications power is limited to the duty cycle, as is the case in Figure 4.42. However, even if the communications power is limited to the duty cycle, if $\alpha = 0.3$ the SDB approach is more efficient only for high PRF values. The latter scenario is shown in Figure 4.43.

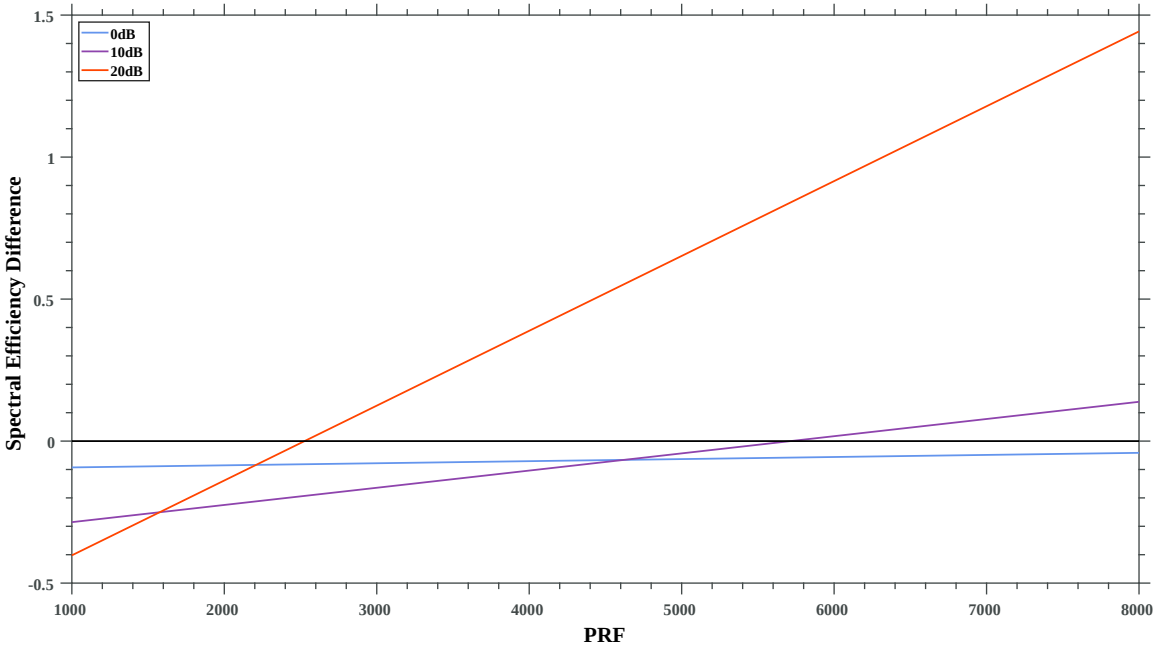

Figure 4.41: Plot showing the spectral efficiency difference between SDB and timesharing. The legend values are the SNR values at a fixed range. The radar ERP fraction (α) is fixed at 0.9, $T_p = 100\mu s$, and $\gamma = 1$.

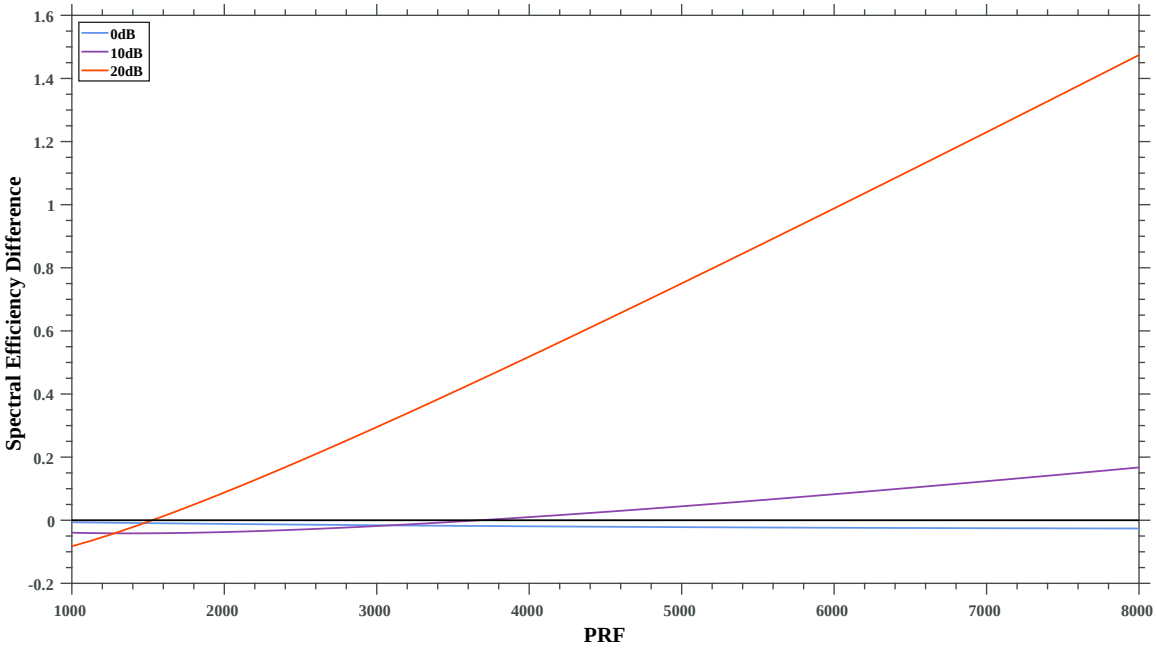

Figure 4.42: Plot showing the spectral efficiency difference between SDB and time-sharing. The legend values are the SNR values at a fixed range. The radar ERP fraction (α) is fixed at 0.9, $T_p = 100\mu s$, and $\gamma = D$.

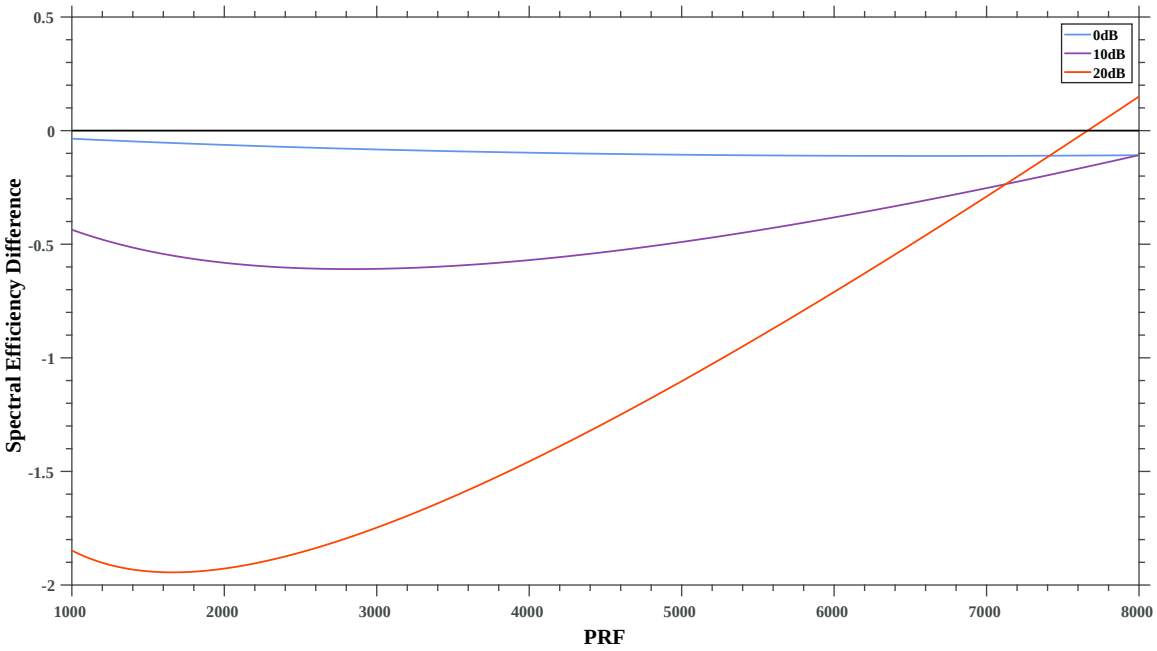

Figure 4.43: Plot showing the spectral efficiency difference between SDB and time-sharing. The legend values are the SNR values at a fixed range. The radar ERP fraction (α) is fixed at 0.3, $T_p = 100\mu s$, and $\gamma = D$.

Finally, we examine high SNR cases for the comparison between pulsed SDB and timesharing. Interestingly, by comparing Figures 4.44 and 4.45, the ERP fraction appears to dominate the results. In other words, even with high SNR (up to 30 dB) the SDB requires an extremely high duty cycle (nearly 80%) before it is more efficient as compared to continuous wave timesharing for the case of $\alpha = 0.3$, as is shown in Figure 4.44. However, if $\alpha = 0.9$, as is the case in Figure 4.45, the SDB approach is more efficient for the majority of the PRFs considered.

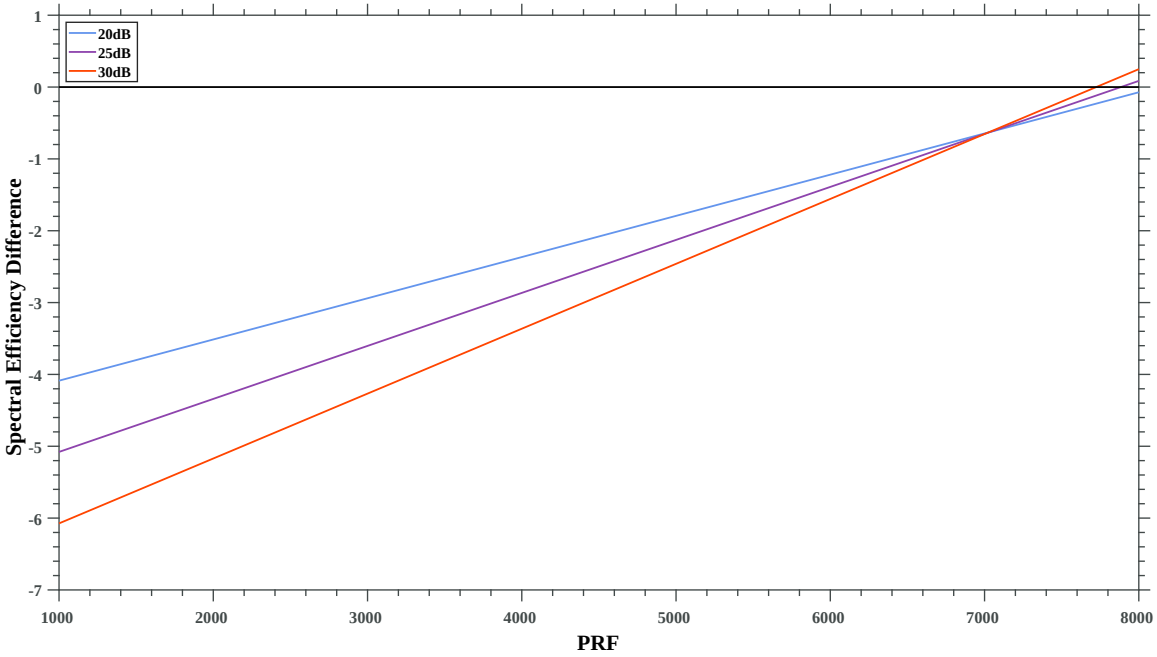

Figure 4.44: Plot showing the spectral efficiency difference between SDB and timesharing. The legend values are the SNR values at a fixed range. The radar ERP fraction (α) is fixed at 0.3, $T_p = 100\mu s$, and $\gamma = 1$.

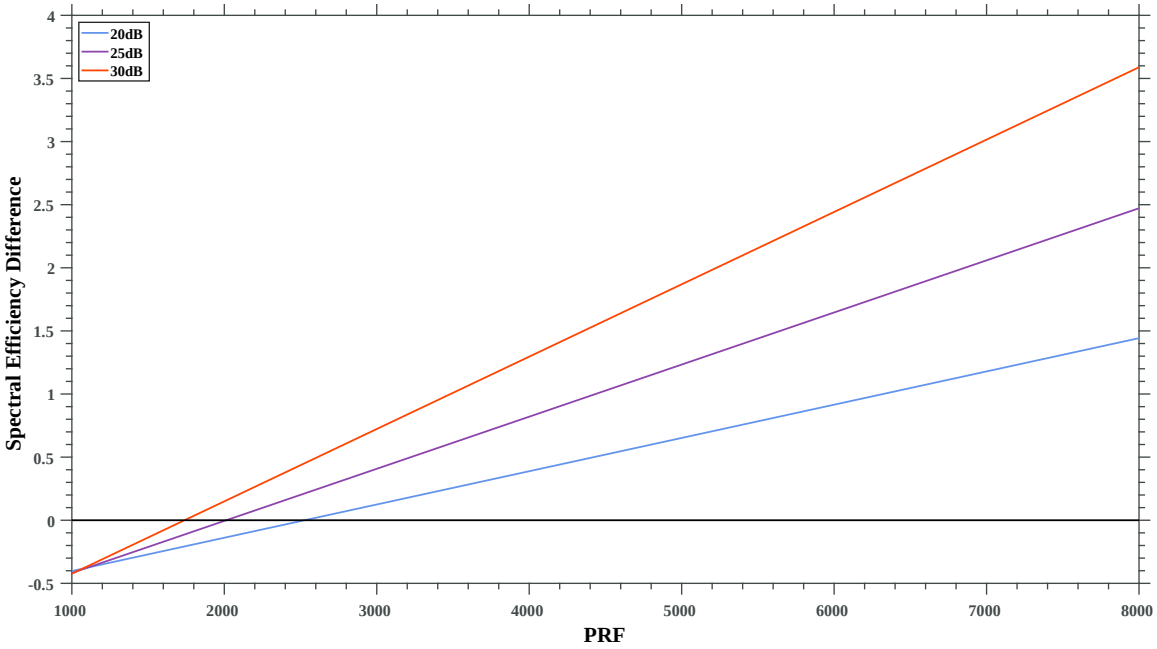

Figure 4.45: Plot showing the spectral efficiency difference between SDB and timesharing. The legend values are the SNR values at a fixed range. The radar ERP fraction (α) is fixed at 0.9, $T_p = 100\mu s$, and $\gamma = 1$.

The same trend continues in Figures 4.46 and 4.47, which show the same scenario as Figures 4.44 and 4.45, except the average communications power is limited based on the radar duty cycle. Even in this case, the low radar ERP case of Figure 4.46 shows that SDB is not more efficient than timesharing unless the duty cycle and SNR are very high. Therefore, if the radar function must receive the majority of the power and the communications SNR is high, the SDB approach is likely to be the best approach, regardless of whether the emission is pulsed or continuous wave. However, unless both of these conditions are met, timesharing is likely to be the best approach.

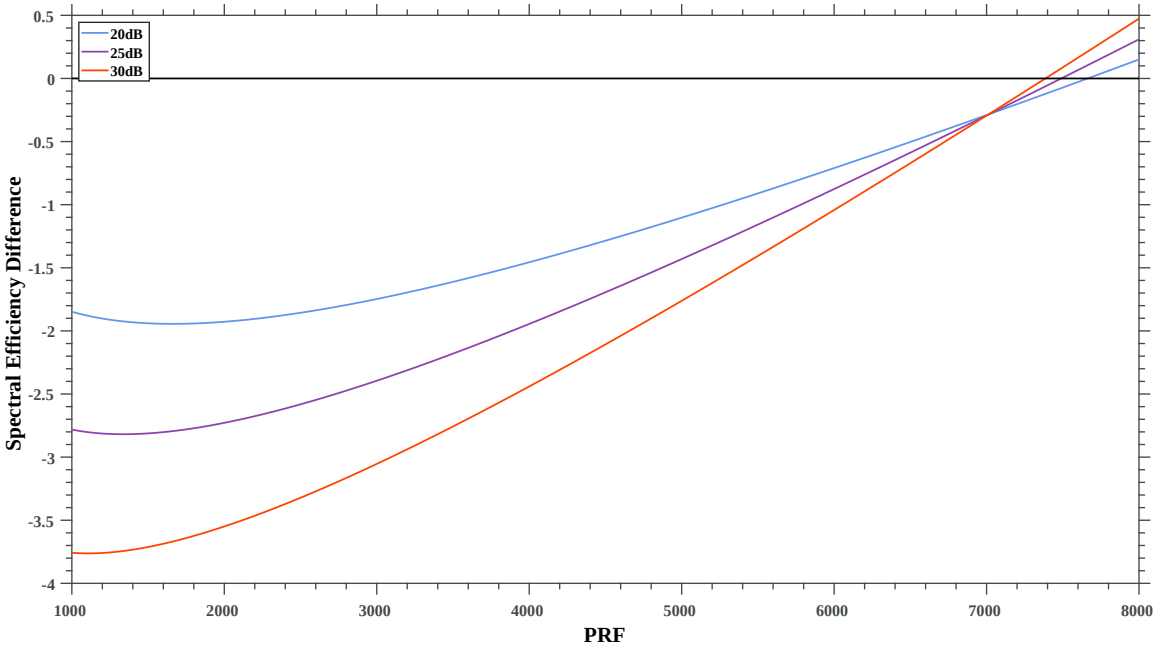

Figure 4.46: Plot showing the spectral efficiency difference between SDB and time-sharing. The legend values are the SNR values at a fixed range. The radar ERP fraction (α) is fixed at 0.3, $T_p = 100\mu s$, and $\gamma = D$.

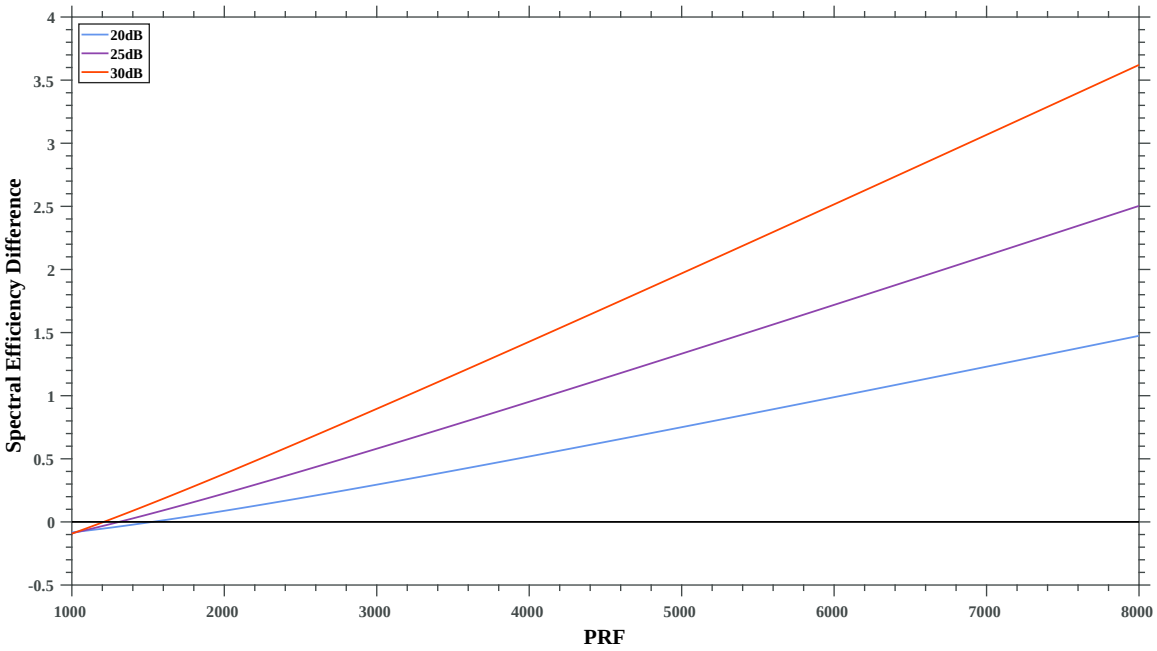

Figure 4.47: Plot showing the spectral efficiency difference between SDB and time-sharing. The legend values are the SNR values at a fixed range. The radar ERP fraction (α) is fixed at 0.9, $T_p = 100\mu s$, and $\gamma = D$.

Chapter 5

Beamwidth Effects

This chapter covers how beamwidth is affected by aperture partitioning and SDB which will lead into topics covered in chapters 7 and 9.

5.1 Beamwidth Equations

A key performance parameter of an antenna element is the achievable beamwidth of the emission, where the majority of the transmitted (or received) energy is contained [6]. Two measures of beamwidth include the null-to-null (or Rayleigh) beamwidth and the 3-dB (or half power) beamwidth. The 3-dB beamwidth is the measure considered here. Assuming a constant aperture current where D is the aperture length, in meters, of a linearly shaped antenna (e.g., a dipole or one dimension of a rectangular shaped aperture), an approximation of the 3-dB beamwidth can be derived from the far-field normalized voltage pattern [6],

$$E(\theta) = sinc\left(\pi \frac{D}{\lambda} sin\theta\right), \tag{5.1}$$

where λ is the wavelength of the emission and θ is the angle from boresight. By finding the half-power point $E(\theta) = 1/\sqrt{2}$ and doubling the result, the approximate

3-dB beamwidth is found as:

$$\theta_3 \approx 0.89\frac{\lambda}{D} \text{ radians.} \tag{5.2}$$

For a uniform linear array (ULA), the aperture length may be set to $D = Nd$ where N is the number of elements and d is the inter-element spacing in meters. Electronically steering the beam can be viewed as shortening the effective aperture length when viewed from an off-normal angle leading to $D = Nd\cos\theta$. If the inter-element spacing is taken to be $\lambda/2$, the 3-dB beamwidth becomes

$$\theta_3 \approx \frac{1.78}{N\cos\theta}\text{radians.} \tag{5.3}$$

In Balanis [7], a common approximation for the 3dB beamwidth is [7]

$$\theta_3 \approx \arccos\left[\cos\left(90-\theta\right) - \frac{2.782}{N\pi}\right] - \arccos\left[\cos\left(90-\theta\right) + \frac{2.782}{N\pi}\right] \text{radians.} \tag{5.4}$$

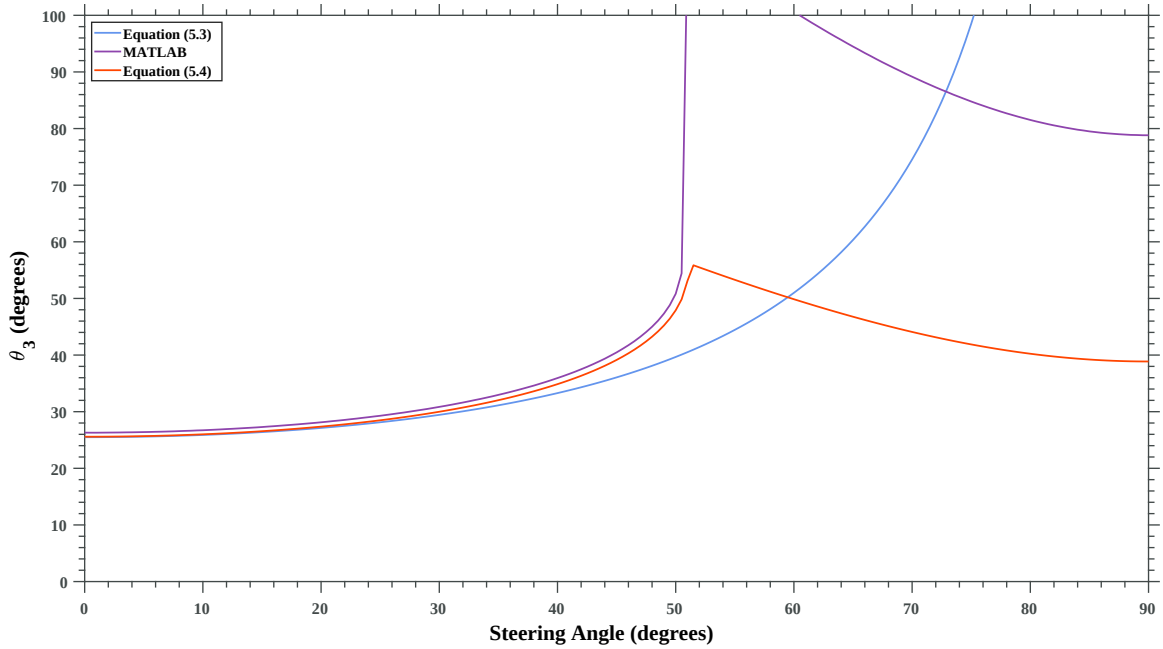

Figure 5.1: Comparing the beamwidth approximations for θ_3 for a 4 element ULA.

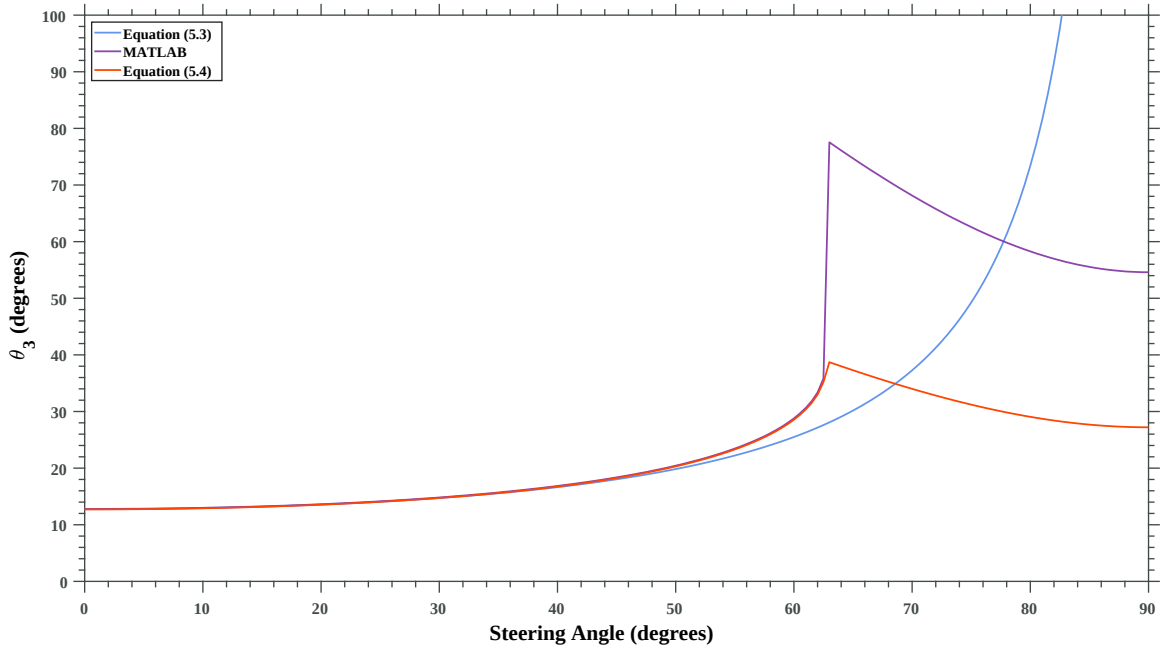

Figure 5.2: Comparing the beamwidth approximations for θ_3 for an 8 element ULA.

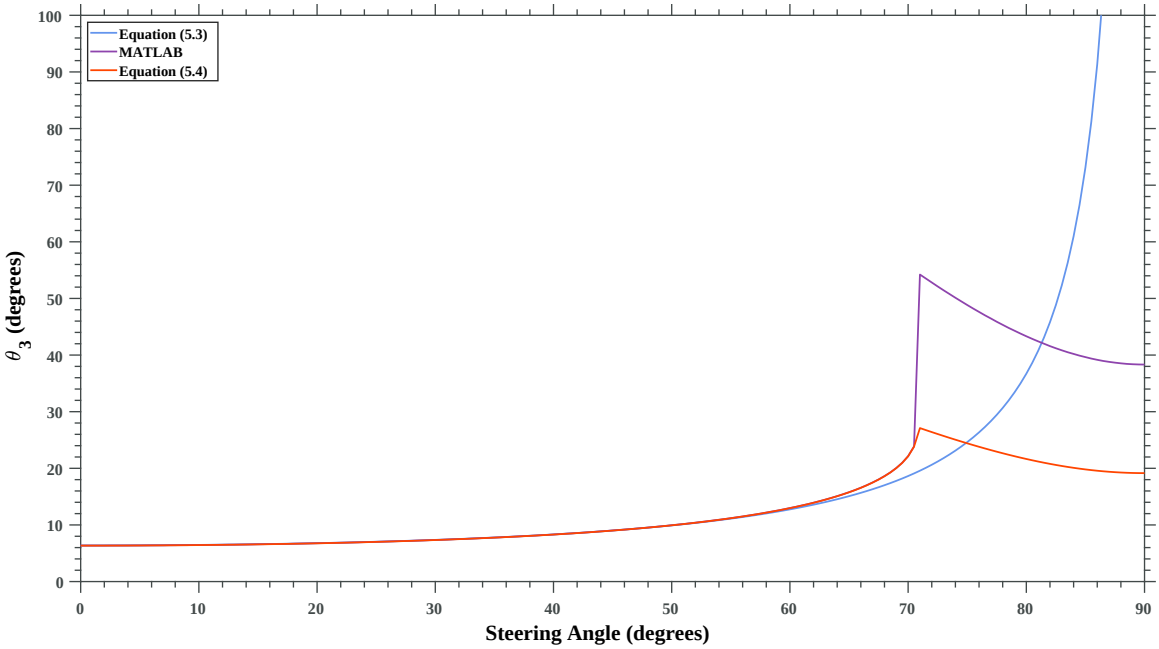

Figure 5.3: Comparing the beamwidth approximations for θ_3 for a 16 element ULA.

To explore the limits of these assumptions an analysis was conducted as a function of the number of antenna elements in the array and the steering angle. The beamwidth approximations (5.3 and 5.4) were compared to MATLAB's approximation, which was found using the Phased Array Toolbox for MATLAB [8]. From Figures 5.1-5.3 it can be seen that 5.3 and 5.4 are good approximations for ULAs greater than 16 elements in length and for steering angles not exceeding 60° to avoid singularities and large errors. This result allows for the use of simplified approximations in later analysis and optimizations.

If a radar is to sample some search space in angle, the sampling interval in angle, according to Nyquist, is given by

$$T_\theta \leq \frac{\theta_3}{1.78}, \tag{5.5}$$

with θ_3 in radians [6].

The effect of the number of antenna elements and steering angle on the beamwidth will have consequences on search, detection, tracking, and communications, especially when aperture partitioning, and will be explored in the next sections and later chapters.

5.2 Aperture Partitioning

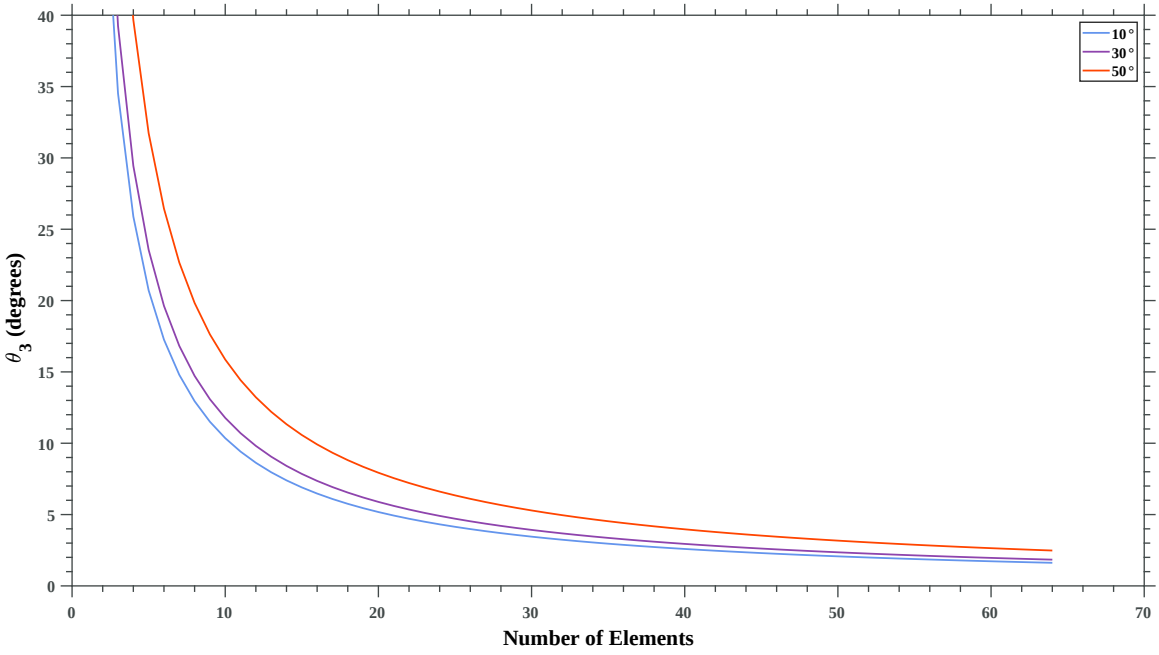

Figure 5.4: A ULA with 64 elements showing the communications beam 3dB beamwidth as increasingly more elements are allocated to the communications beam in the case of aperture partitioning. The three different curves show when the beam is steered to the corresponding value in the legend.

A higher number of elements leads to more communications elements being supported if some beamwidth is to not be exceeded; allowing for more gain, privacy, etc.

Describing θ_3 as a function of α for aperture-partitioning leads to the equation

$$\theta_3 = \frac{1.78}{\alpha N \cos\theta}. \tag{5.6}$$

This is illustrated in the following plot at different steering angles and element numbers.

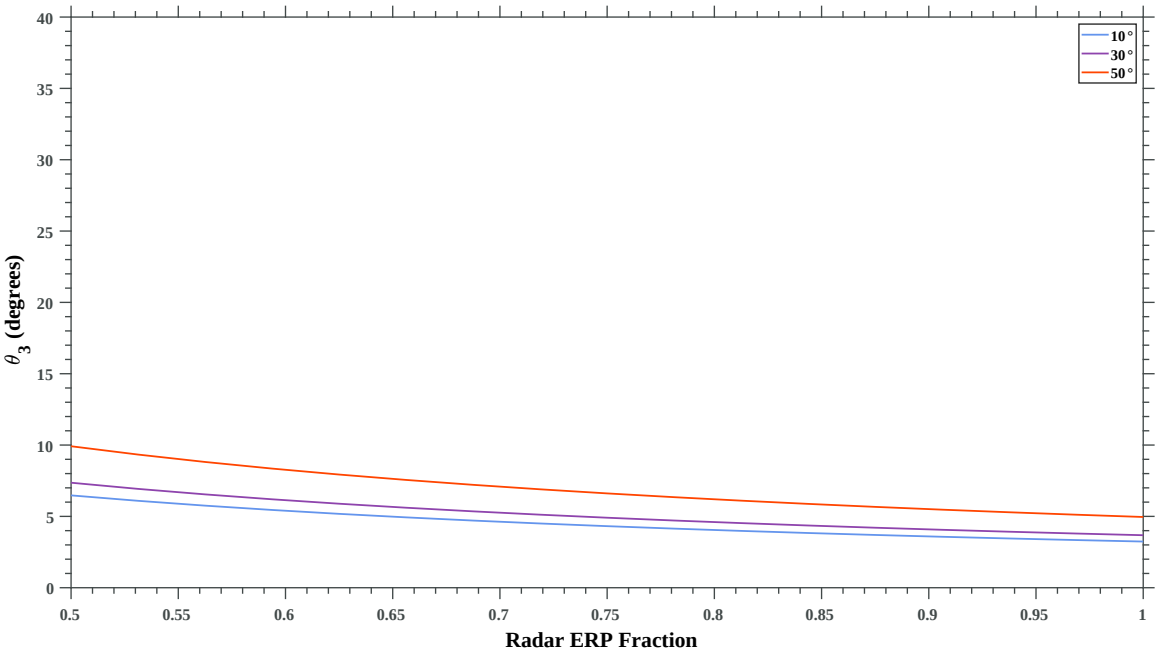

Figure 5.5: 3dB beamwidth as function of radar ERP for aperture-partitioning. The legend values are the angles the radar beam is steered to with the communications beam at 45° for all cases. The number of elements is 32.

5.3 SDB

The 3dB-beamwidth for SDB is simulated from [5] and is shown for a communications beam constantly at 45° and various radar beam positions and powers. Figures 5.3 and 5.4 show the beamwidth for several angles of illumination.

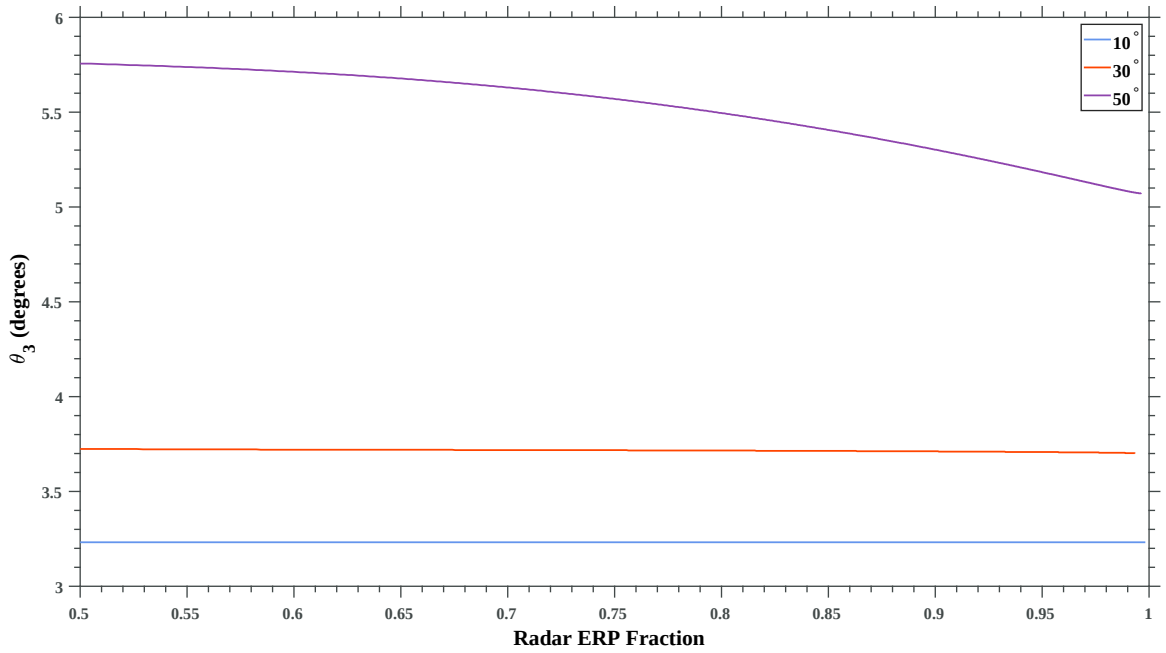

Figure 5.6: 3dB beamwidth as function of radar ERP for SDB. The legend values are the angles the radar beam is steered to with the communications beam at 45° for all cases. The number of elements is 32 and all other parameters are the same as mentioned in the literature review.

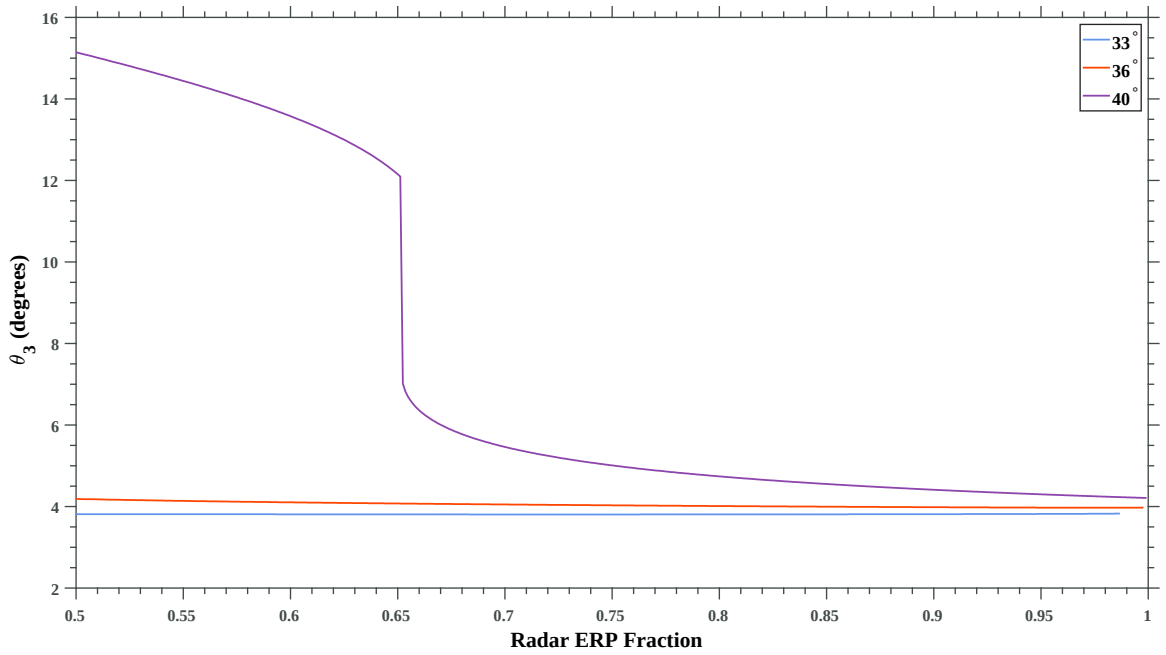

Figure 5.7: 3dB beamwidth as function of radar ERP for SDB. The legend values are the angles the radar beam is steered to with the communications beam at 45° for all cases. The number of elements is 32 and all other parameters are the same as mentioned in the literature review.

The sharp jump in θ_3 is presumably due to the radar being being placed so closely to the communications beam (within 5 degrees). Therefore, the SDB approach may not always be a viable technique, depending on the desired angles of the radar and communications emissions.

Figures 5.5 and 5.6 show the same scenario, except with an aperture twice as large (i.e., with 64 elements). In this case, the beamwidth is narrow enough that the radar beam can be transmitted at 40 degrees without interfering with the communications beam at 45 degrees, as seen in Figure 5.6.

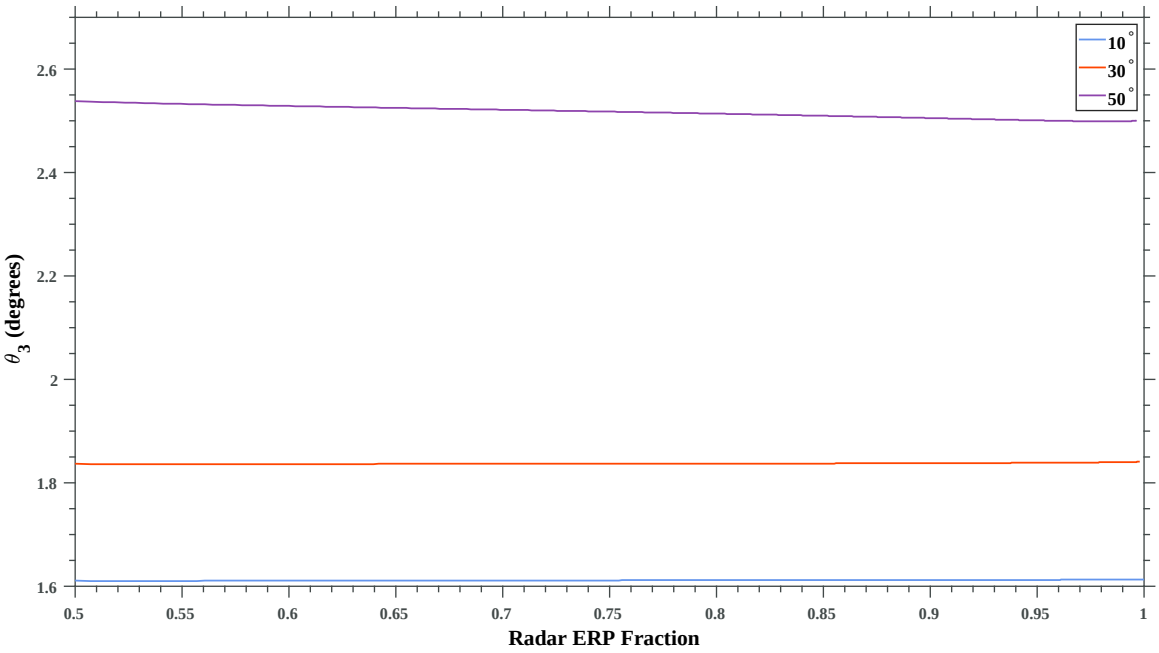

Figure 5.8: 3dB beamwidth as function of radar ERP for SDB. The legend values are the angles the radar beam is steered to with the communications beam at 45° for all cases. The number of elements is 64 and all other parameters are the same as mentioned in the literature review.

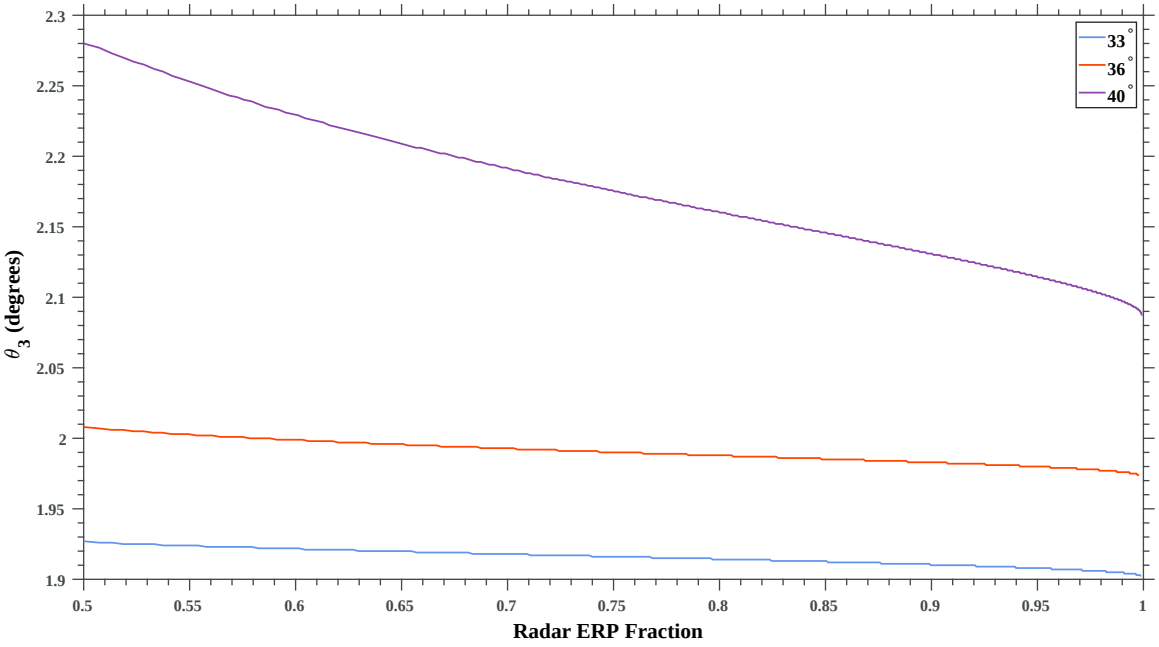

Figure 5.9: 3dB beamwidth as function of radar ERP for SDB. The legend values are the angles the radar beam is steered to with the communications beam at 45° for all cases. The number of elements is 64 and all other parameters are the same as mentioned in the literature review.

The beamwidth values used for these figures will be used in chapter 7 to determine the impact on the track revisit interval.

Chapter 6

Estimators

An important value to consider when using estimators is the minimum possible variance of the estimator, known as the Cramer-Rao Lower Bound(CRLB). For example, for a complex sampled signal with a peak SNR of χ and a constant of proportionality k; the CRLB is [6]

$$\sigma^2_{\hat{\Theta}} \geq \begin{cases} \frac{1}{2k\chi} & \text{(complex signals)} \\ \frac{1}{k\chi} & \text{(real signals)} \end{cases} \tag{6.1}$$

It should be noted that, in this case, the parameter of interest is not the amplitude of the signal. If the parameter of interest is the amplitude and the variance of the amplitude is considered to be normalized with respect to the amplitude, then $k = 1$. As an exploration, since SNR is affected differently by each DFRC method, investigating how this CRLB, among others with more specific parameters of interest, could provide more insight into how DFRC affects radar performance.

RMS values for certain quantities are typically used (when using the LFM waveform) with $\Delta R_{rms} = c/2B_{rms}$. Instead of B_{rms}, $B_{rms} = B/\sqrt{12}$ may be used to keep CRLB equations more in line with typical radar signal processing equations. The CRLB for a time delay estimator for complex signals with B_{rms} being the waveform

RMS bandwidth for an LFM waveform with 3 dB bandwidth B is [6]

$$\sigma^2_{\hat{t_0}} \geq \frac{1}{8\pi^2 \chi B^2_{rms}} \geq \frac{12}{8\pi^2 \chi B^2}, \tag{6.2}$$

leading to the CRLB for range estimation becoming

$$\sigma^2_{\hat{R_0}} \geq \frac{\Delta R^2_{rms}}{8\pi^2 \chi} \geq \frac{3c^2}{8\pi^2 \chi B^2}. \tag{6.3}$$

The CRLB for the estimation of wavenumber, where M is the number of pulses is. [6]:

$$\sigma^2_{\hat{k_\theta}} \geq \frac{6}{\chi M(M^2-1)} \approx \frac{6}{M^3 \chi} \tag{6.4}$$

Similarly, the CRLB for frequency of a complex sinusoid is [6]

$$\sigma^2_{\hat{f}_0} \geq \frac{6}{(2\pi)^2 \chi M(M^2-1)} \approx \frac{6}{(2\pi)^2 M^3 \chi}. \tag{6.5}$$

The CRLB for the angle of arrival for an array with half-wavelength element spacing is [6]:

$$\sigma^2_{\hat{\theta}} \geq \frac{24}{\chi N^3 (2\pi cos(\theta))^2}. \tag{6.6}$$

6.1 Range

6.1.1 Range Estimators

For an altered CRLB, if using M pulses to refine the estimate, the CRLB would change by a factor of $\frac{1}{M}$ leading to

$$\sigma^2_{\hat{R}_0,ts} \geq \frac{3c^2}{8\pi^2 \lfloor \alpha M \rfloor \chi B^2}. \tag{6.7}$$

Where χ is the per pulse SNR.

The range CRLB for the aperture-partitioning method, since transmit power and transmit gain are linearly affected by α, becomes

$$\sigma^2_{\hat{R}_0,ap} \geq \frac{3c^2}{8\pi^2 \alpha^2 M \chi B^2}. \tag{6.8}$$

Lastly, for SDB, the range CRLB is given by

$$\sigma^2_{\hat{R}_0,sdb} \geq \frac{3c^2}{8\pi^2 \alpha M \chi B^2}. \tag{6.9}$$

Below are graphs comparing the minimum range variances for each DFRC method.

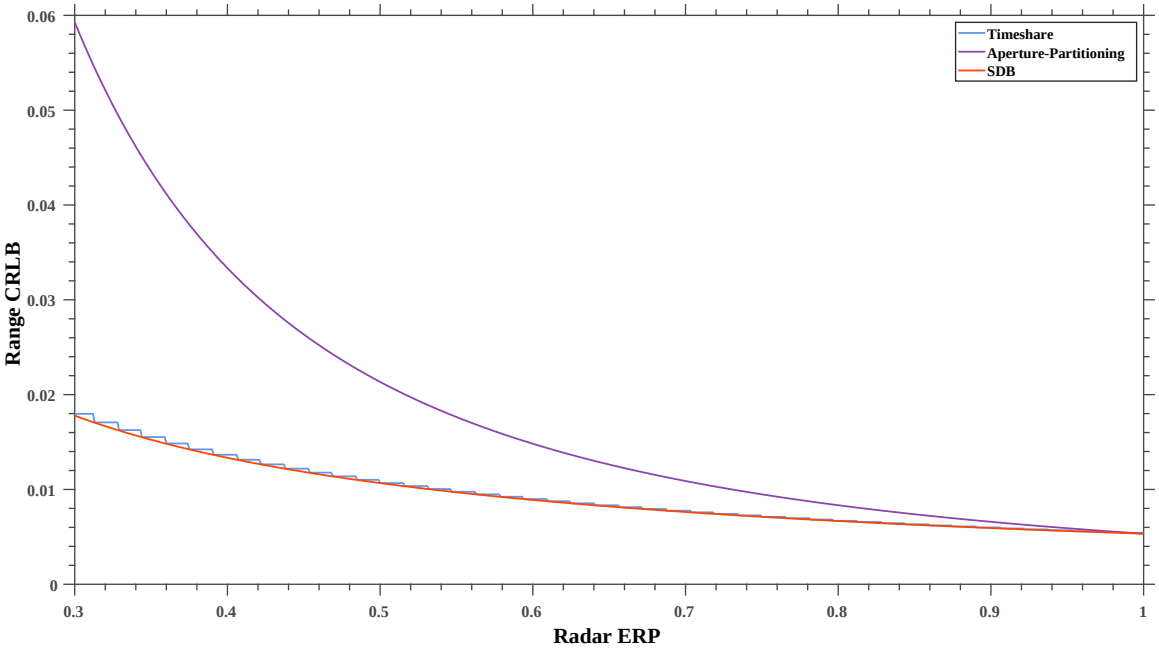

Figure 6.1: Range CRLB for each DFRC method for a target with a per pulse SNR of 0dB, a radar bandwidth of $100MHz$, and M = 64.

6.2 Frequency

The CRLB for frequency estimation (across pulses) is given by [6]

$$\sigma^2_{\hat{f}_0} \geq \frac{6}{4\pi^2 M^3 \chi}. \tag{6.10}$$

This expression is also the same for $\sigma^2_{\hat{f}_0,ts}$ if the number of pulses remains constant. The effect on frequency CRLB in aperture-partitioning and SDB due to SNR change is given by

$$\sigma^2_{\hat{f}_0,ap} \geq \frac{6}{4\pi^2 M^3 \alpha^2 \chi}, \tag{6.11}$$

and

$$\sigma^2_{\hat{f}_0,sdb} \geq \frac{6}{4\pi^2 M^3 \alpha \chi}. \tag{6.12}$$

The above three equations are similar enough to the CRLB for range estimation so a plot is not included at this point.

However, if a given spectral efficiency is required with a communications target, this can reduce SNR in the aperture-partitioning and SDB method while reducing the number of pulses (M) in the timesharing case. As a function of spectral efficiency, the fraction of time allocated to radar in the timesharing case is

$$\alpha_{ts} = -\frac{SE}{\log_2(1+\gamma\chi_{comm})} + 1, \tag{6.13}$$

for continuous communications transmission, and

$$\alpha_{ts} = -\frac{SE}{D\log_2(1+\chi_{comm})} + 1 \tag{6.14}$$

for pulsed transmission. The fraction of power allocated to radar for aperture-partitioning is

$$\alpha_{ap} = \left[-\sqrt{\frac{2^{\frac{SE}{D}}-1}{\chi_{comm}}} + 1\right]^2. \tag{6.15}$$

While the fraction of power allocated to communications for SDB is

$$\beta_{SDB}(\alpha) = \frac{2^{\frac{SE}{D}}-1}{\chi_{comm}}. \tag{6.16}$$

The obtained values for β will be associated with an appropriate α via MATLAB's *interp*1 function using the α and β values from implementing [5].

A maximum number of pulses hitting a target needs to defined so that any imposed spectral efficiency or bit rate reduces the number of pulses for the timesharing case only. The new CRLB for frequency in the timesharing case becomes

$$\sigma^2_{\hat{f}_0,ts} \geq \frac{6}{4\pi^2 \lfloor (M\alpha)^3 \rfloor \chi}. \tag{6.17}$$

This seems similar to the aperture-partitiong method, however, different spectral efficiencies lead to different α values; the CRLB expressions for the other DFRC methods remain the same. Also, spectral efficiency values outside of a certain range (depending on the scenario) leads to the fraction of power for radar or communications being outside of the interval (0,1), meaning these spectral efficiencies are not allowed.

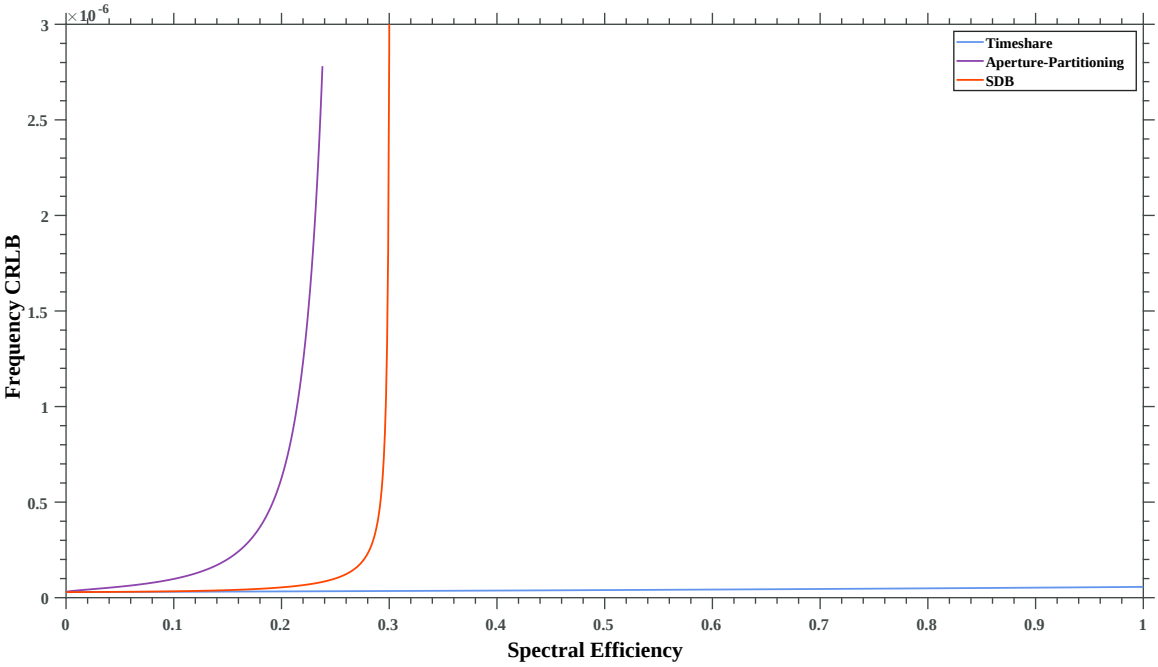

Figure 6.2: PRF $= 3000$, $\chi_{comm} = 15dB$, $\chi = 13dB$, $T_p = 20\mu s$, $\gamma = 1$, and $M = 64$.

As seen in Figures 6.2 and 6.3, if the communications beam can continuously transmit at full power, timesharing maintains a lower CRLB for a much larger amount of allowable spectral efficiency.

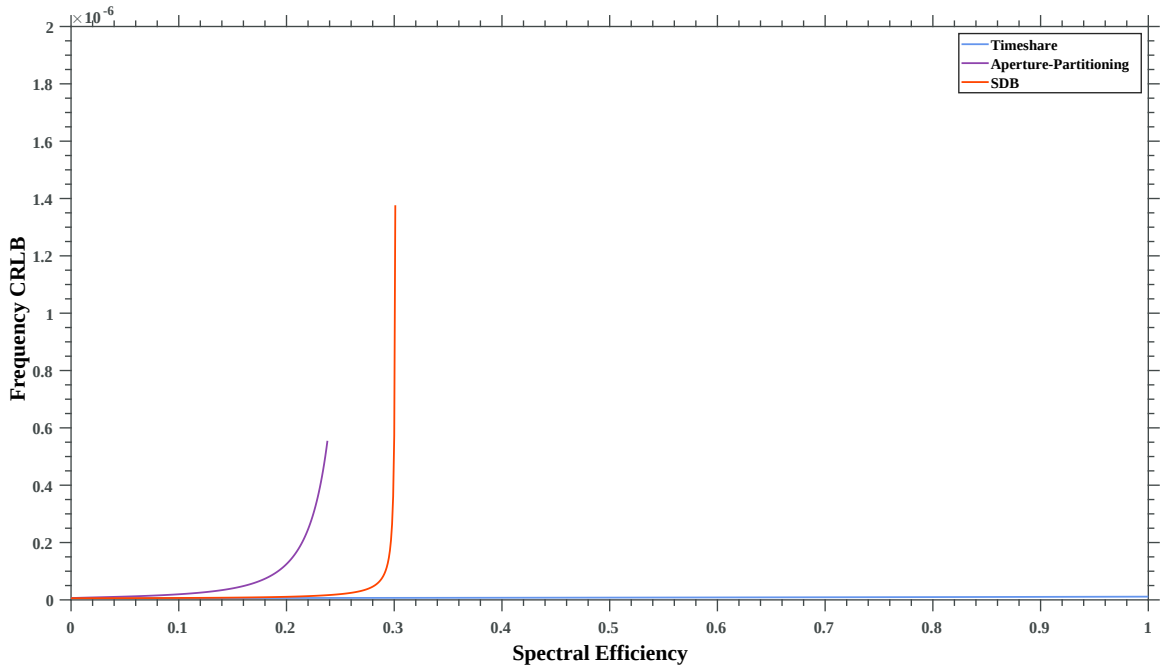

Figure 6.3: PRF $= 3000$, $\chi_{comm} = 15dB$, $\chi = 20dB$, $T_p = 20\mu s$, $\gamma = 1$, and $M = 64$.

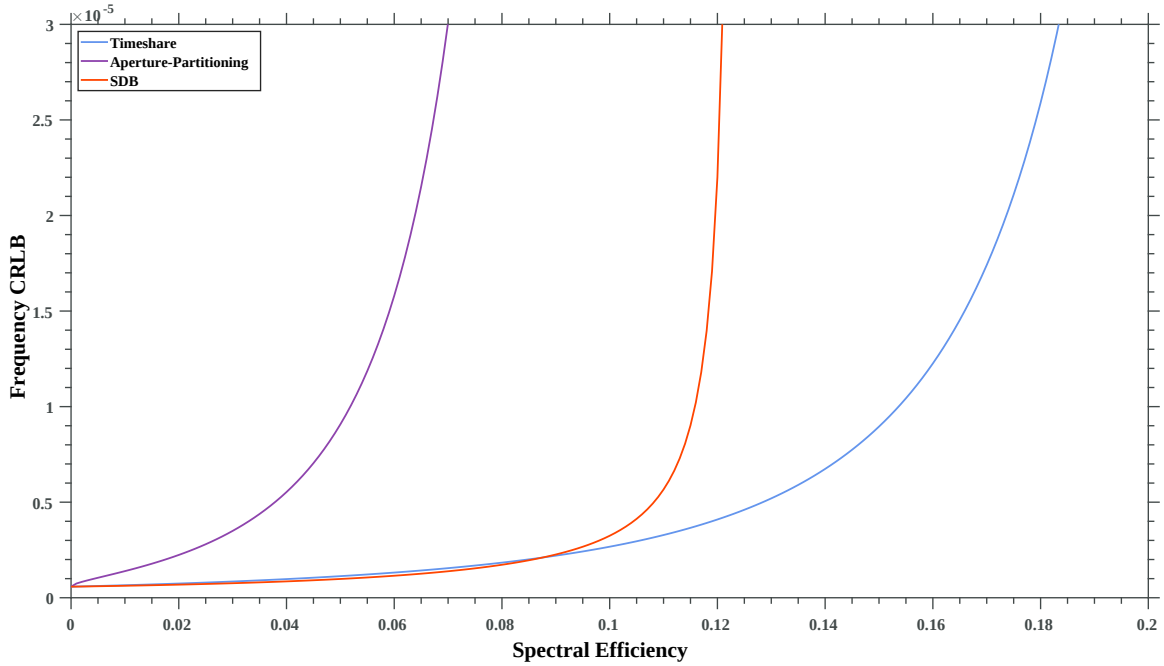

Figure 6.4: PRF $= 3000$, $\chi_{comm} = 5dB$, $\chi = 0dB$, $T_p = 20\mu s$, $\gamma = D$, and $M = 64$.

Replicating the above figure with $\chi_{comm} = 10dB$ leads to the following figure

that increases the allowable spectral efficiencies with timesharing gaining a larger advantage.

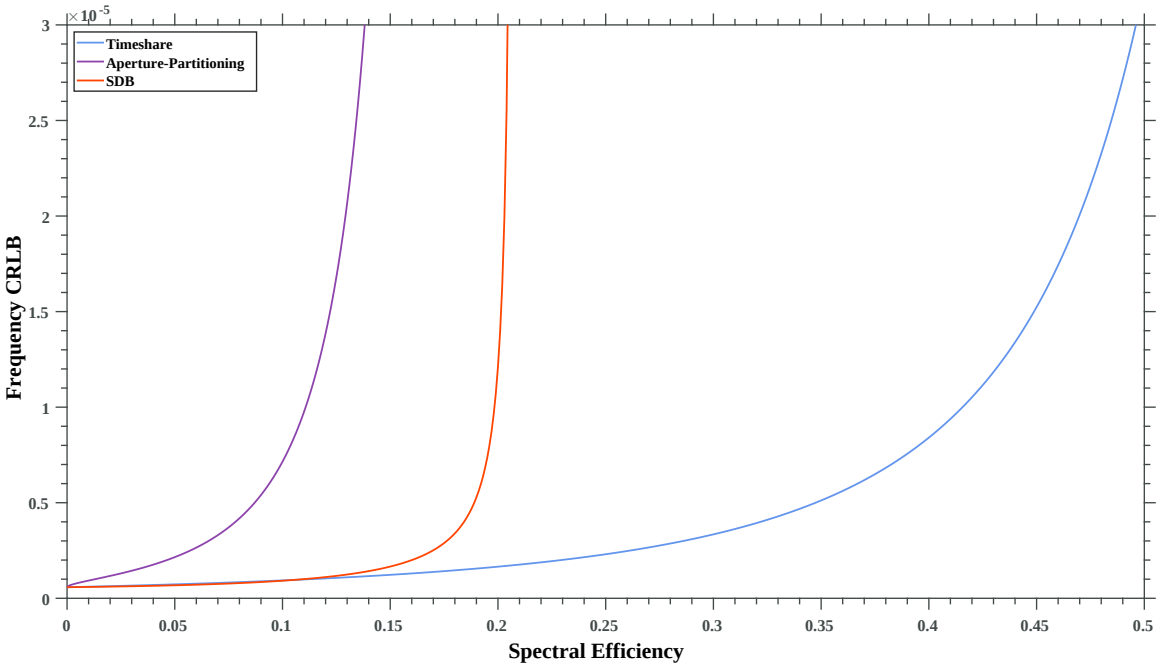

Figure 6.5: PRF $= 3000$, $\chi_{comm} = 10dB$, $\chi = 0dB$, $T_p = 20\mu s$, $\gamma = D$, and $M = 64$.

Changing only the PRF to 8000 from the above figure shows how the supported spectral efficiencies increase while improving the frequency CRLB.

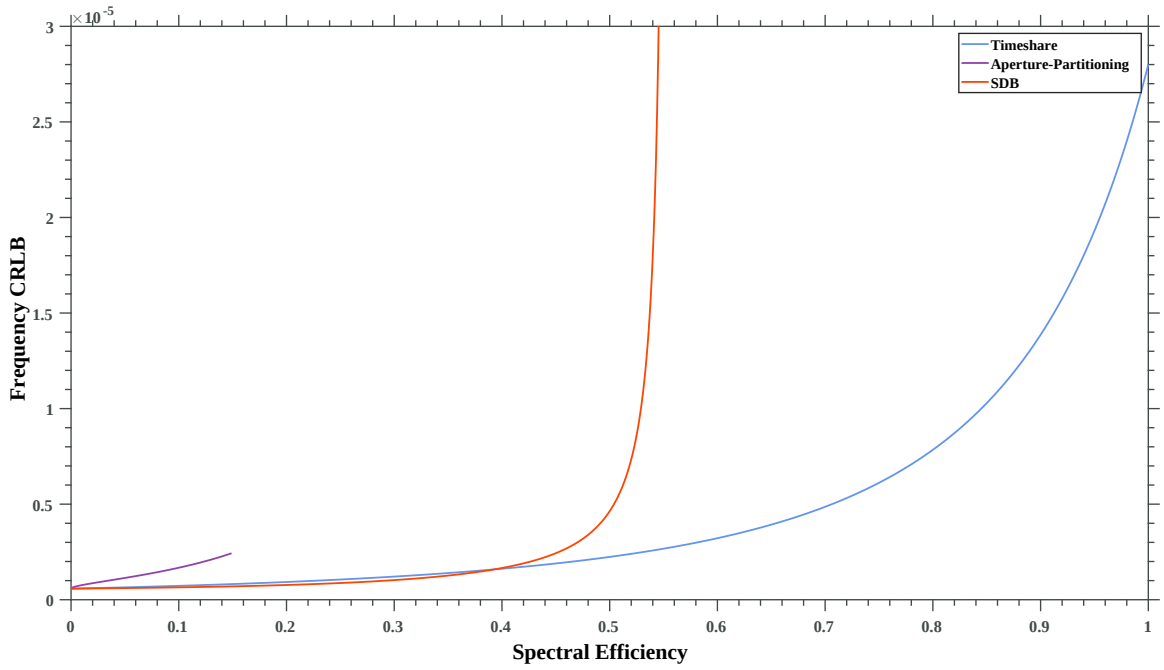

Figure 6.6: PRF $= 8000$, $\chi_{comm} = 10dB$, $\chi = 0dB$, $T_p = 20\mu s$, $\gamma = D$, and $M = 64$.

Interestingly, there is a region where SDB outperforms timesharing below a spectral efficiency of approximately 0.388.

6.3 Angle of Arrival (AOA)

The CRLB for AOA is a fairly simple consideration since aperture-partitioning is the only DFRC method that could affect the number of samples (array elements).

The CRLB for AOA for aperture-partitioning is

$$\sigma_{\hat{\theta}}^2 \geq \frac{24}{\chi\alpha^3 N^3 (2\pi cos(\theta))^2}. \tag{6.18}$$

The figure below shows the AOA CRLB various incoming angles and α values.

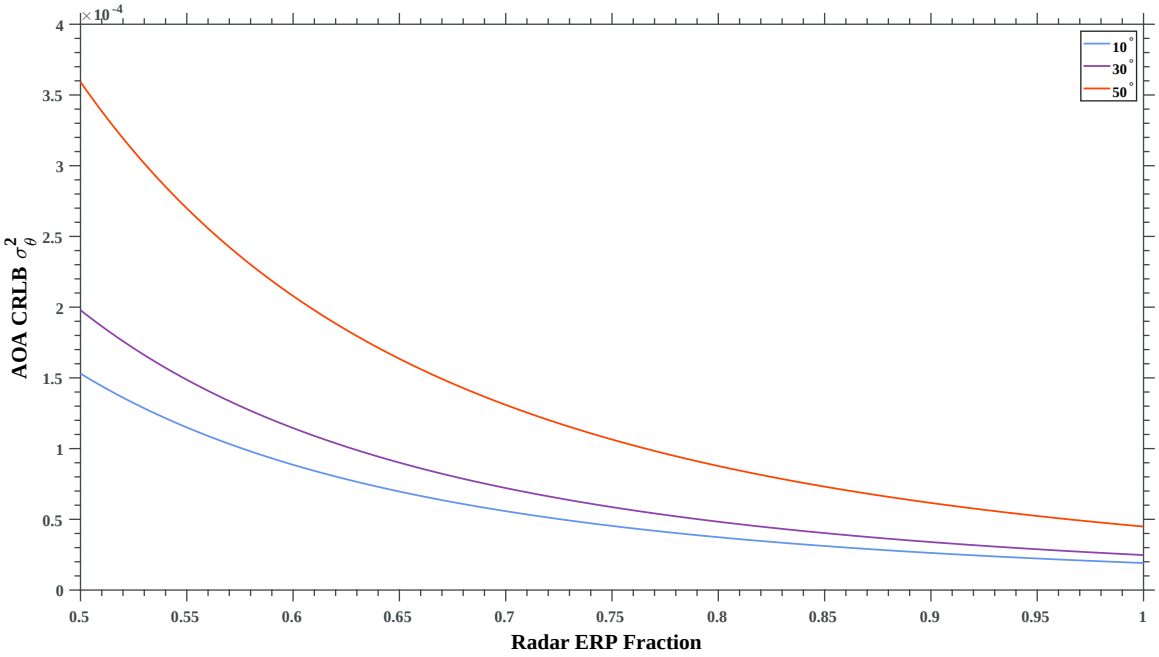

Figure 6.7: Minimum $\sigma^2_{\hat{\theta}}$ for aperture-partitioning for an SNR of 0dB and a 32 element array. The legend values are the angles of arrival.

Chapter 7

Tracking

7.1 Van Keuk Background

Van Keuk and Blackman [3] define ΔT as the time between target updates for a search-while-track application. If ΔT is small, the track will be more accurate and it will not be necessary to search around the expected position to re-detect the target since the beamwidth may be much smaller than the target variance; however, this leads to a potential waste of resources in a surveillance mode of operation. On the other hand, increasing ΔT too much will waste resources on searching around the expected target position for a re-detection. The target is modeled in Cartesian coordinates and is driven by three independent Markov acceleration processes. They use the major axis of the state covariance ellipsoid in u,v space, G, to define

$$G(k+1|k) = V_0\theta_3. \tag{7.1}$$

Where V_0 is a number that sets the maximum amount of track inaccuracy in u, v coordinates. Van Keuk and Blackman use filters in r, u, v coordinates for linearity in measurement and later exclude r.

The search strategy for re-detecting a target that won was forming a normal

distribution with a mean of the predicted position and a variance of $V_0\theta_3$ and then using Bayes' rule to update the pdf if no detection occurs. This results in

$$pdf(2) = c(1 - P_D)pdf(1). \tag{7.2}$$

Where c is a normalizing constant and P_D is defined by

$$P_D = P_{FA}^{\frac{1}{1+\chi}} \tag{7.3}$$

and where

$$\chi = Aexp\Big[- 2\frac{(u - u(1))^2 + v - v(1))^2}{\theta_3^2}\Big] \tag{7.4}$$

with A being the SNR for no angular pointing error.

Searching the entire surveillance space is not considered and the paper concludes with an optimum V_0 of approximately 0.3 and an SNR of 15-18dB.

By simulation, an approximation for the expected number of beam positions, n, is given by

$$E[n] \approxeq \frac{1}{P_D}\sqrt{1 + (\gamma V_0^2)^2} \tag{7.5}$$

where

$$\gamma \approxeq 1 + 14\sqrt{\frac{|\ln P_{FA}|}{\chi}} \tag{7.6}$$

ΔT eventually converges to a constant value, given the process noise is constant. The steady-state value is given by

$$\begin{aligned} T &\approx 0.4 \left(\frac{rR}{Q\sqrt{\alpha_{corr}}} \right)^{0.4} \frac{U^{2.4}}{1 + 0.5U^2} \\ U &= \frac{\theta_3 V_0}{R}. \end{aligned} \tag{7.7}$$

where Q is the process noise (acceleration) standard deviation, R is the radar position measurement noise, α_{corr} is the signal correlation time, and r is the range to the target. The process autocorrelation is assumed to be exponentially decaying with

$$E[q_i(t)q_j(t+\tau)] = Q^2 e^{-\alpha_{corr}|\tau|}. \tag{7.8}$$

and the measurement noise variance is given by

$$R^2 = \frac{\theta_3^2}{SNRT} \tag{7.9}$$

where SNRT is the signal's instantaneous SNR given by the estimate

$$SNRT = \frac{\chi - \ln(P_{FA})}{1 + 2V_0^2}. \tag{7.10}$$

7.2 Implementation

Using the tracking equations from the literature review from [3] and the beamwidth equations and plots from Chapter 5, the converged track revisit time or expected number of beam positions for each DFRC method can be investigated.

The SNR in the previous Van Keuk tracking equations scales with the square of α in the aperture-partitioning case and linearly in the SDB method. Consider how the

SNR would be affected by aperture-partitioning. Transmit power would be scaled by α, transmit gain will be scaled by α assuming isotropic elements, and receive gain would be unaffected if the whole array is used to form the digital beam. This leads to the SNR equation for aperture-partitioning becoming

$$\chi_{ap} = \frac{(\alpha P_t)(\alpha G_t) G_r \lambda^2}{(4\pi R)^2 k_B T_e B F_n}. \tag{7.11}$$

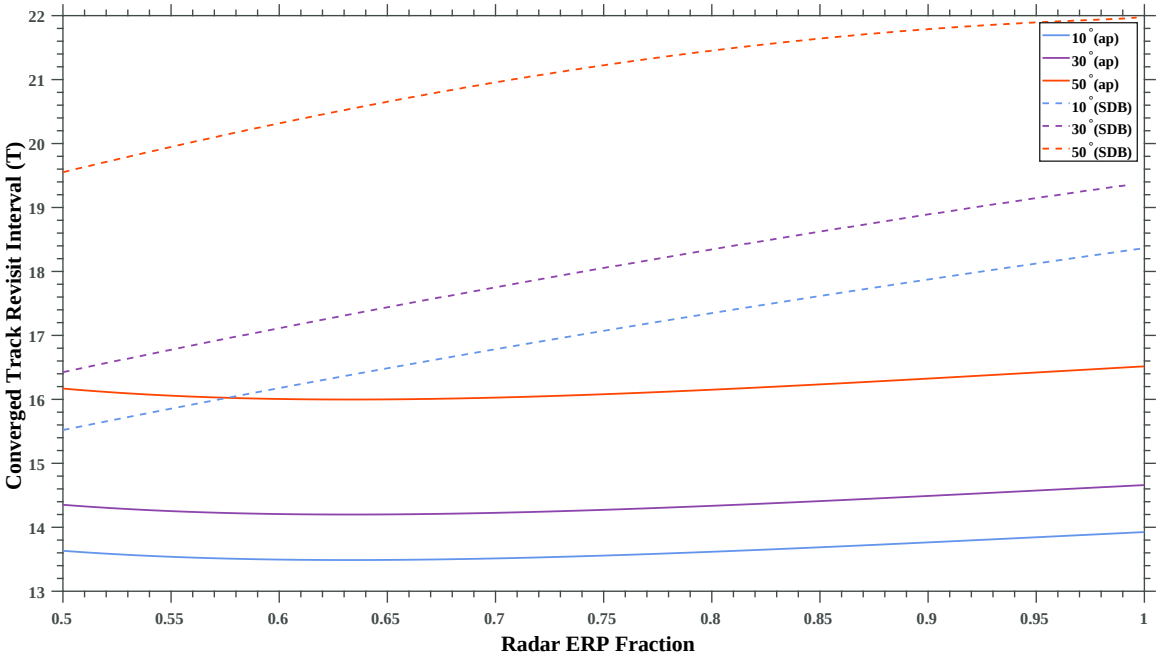

Figure 7.1: Converged revisit interval for aperture-partitioning and SDB where the legend values give the angle the radar beam is steered to.$\chi = 13dB$, $P_{FA} = 10^{-6}$, $N = 32$, $\alpha_{corr} = \frac{1}{30}$, $Q = 10$, and $r = 20km$.

The next figure shows a scenario when the number of elements increases to 64.

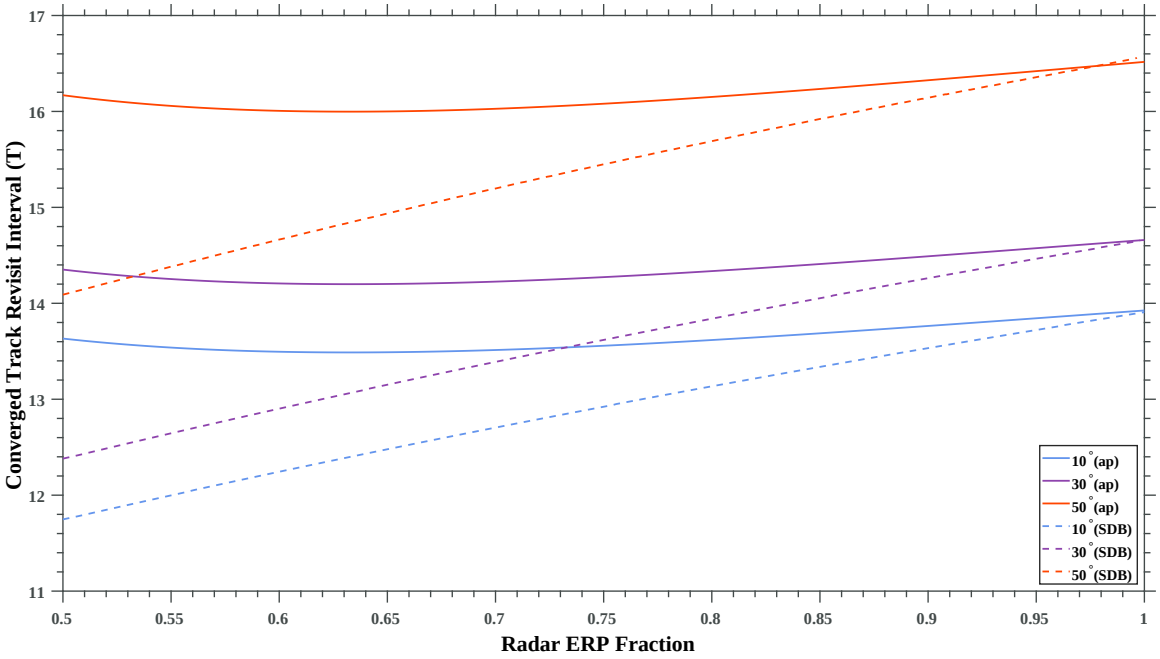

Figure 7.2: Converged revisit interval for aperture-partitioning and SDB where the legend values give the angle the radar beam is steered to.$\chi = 13dB$, $P_{FA} = 10^{-6}$, $N = 64$, $\alpha_{corr} = \frac{1}{30}$, $Q = 10$, and $r = 20km$.

The scenario when SDB receives a large jump in beamwidth naturally increases the revisit interval as shown below.

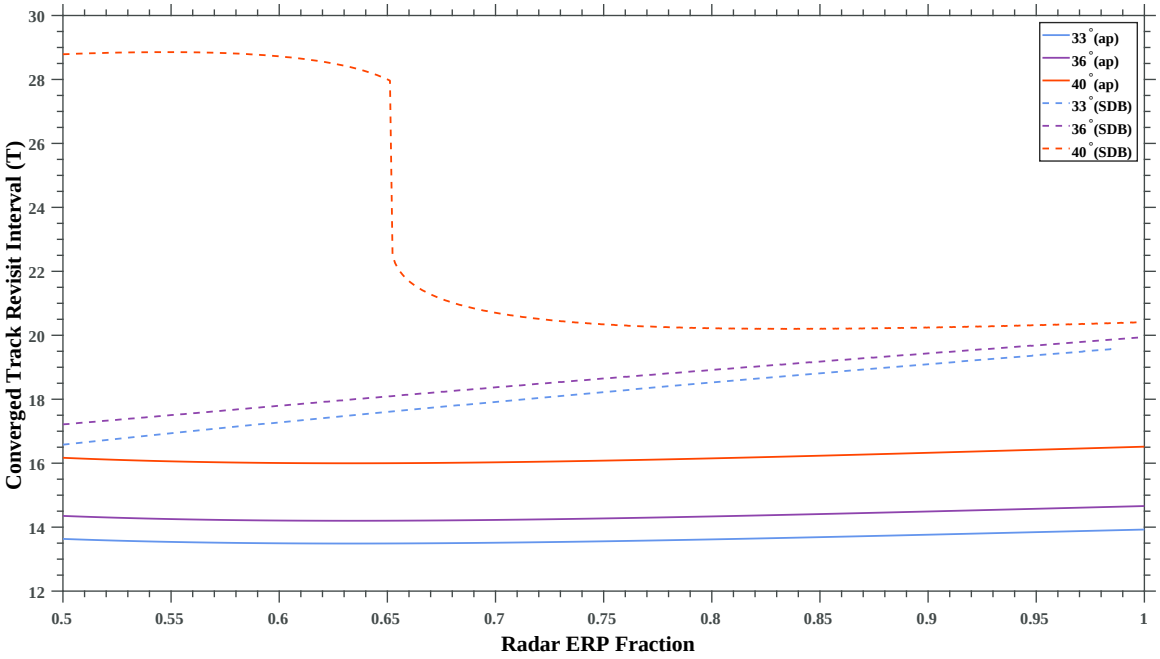

Figure 7.3: Converged revisit interval for aperture-partitioning and SDB where the legend values give the angle the radar beam is steered to.$\chi = 13dB$, $P_{FA} = 10^{-6}$, $N = 32$, $\alpha_{corr} = \frac{1}{30}$, $Q = 10$, and $r = 20km$.

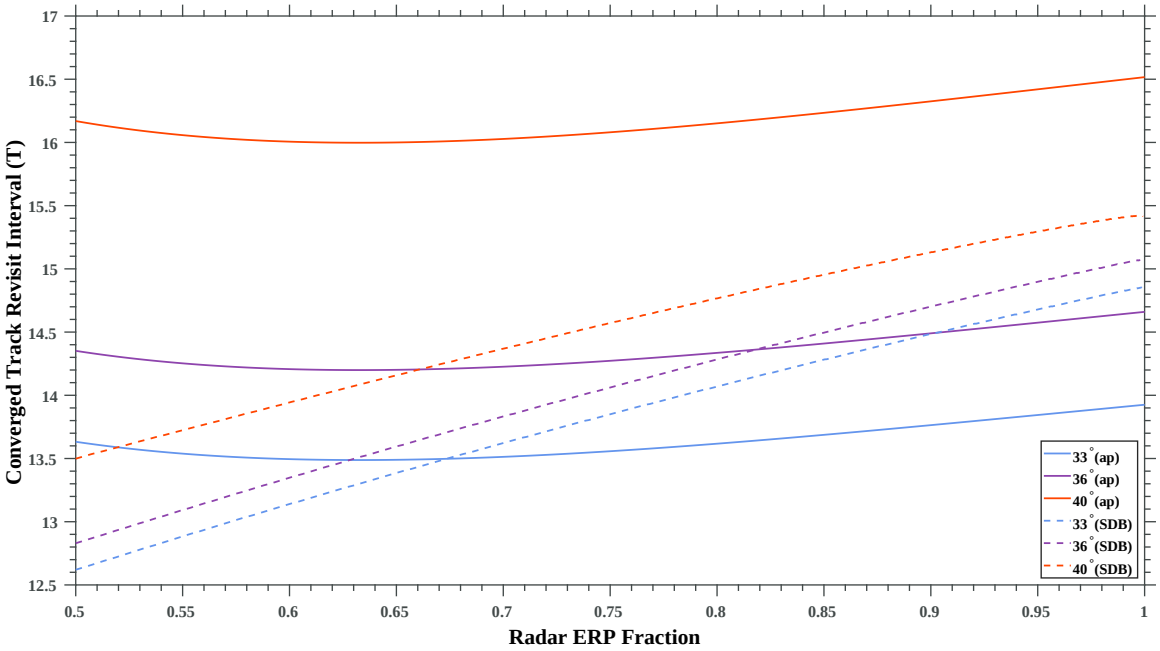

Figure 7.4: Converged revisit interval for aperture-partitioning and SDB where the legend values give the angle the radar beam is steered to.$\chi = 13dB$, $P_{FA} = 10^{-6}$, $N = 64$, $\alpha_{corr} = \frac{1}{30}$, $Q = 10$, and $r = 20km$.

Aperture partitioning's revisit interval initially decreases until it eventually increases around a ERP fraction of 0.6, presumably due to the increasing beamwidth out-competing the reduced SNR.

Chapter 8

Detection

This thesis will focus on the Neyman-Pearson decision rule for detection topics. Since radar power, number of pulses, etc affect the SNR of a given target, trade-offs relating to which DFRC method is used and how it affects the probability of detection (P_D) will be investigated. Relevant probability distribution functions (pdfs) for P_D that will be discussed include the real constant in Gaussian noise:

$$P_D = \frac{1}{2} erfc\left[erfc^{-1}(2P_{FA}) - \sqrt{\frac{\chi}{2}}\right], \tag{8.1}$$

the Gaussian case for coherent receivers with i.i.d noise samples:

$$P_D = \frac{1}{2} erfc\left[erfc^{-1}(2P_{FA}) - \sqrt{\chi}\right], \tag{8.2}$$

and unknown phase, where Q_M is Marcum's Q function:

$$P_D = Q_M\left(\sqrt{2\chi}, \sqrt{-2lnP_{FA}}\right). \tag{8.3}$$

Marcum's Q function is defined as

$$Q_M(\alpha, \gamma) = \int_{\gamma}^{\infty} t \exp\left[-\frac{1}{2}(t^2 + \alpha^2)\right] I_0(\alpha t)\, dt, \tag{8.4}$$

where $I_0(\alpha t)$ is the modified Bessel function of the first kind. However, Marcum's Q function is implemented by using MATLAB's *marcumq* function.

As mentioned in the previous chapter, SNR SSscales with the square of α, for aperture-partitioning and scales linearly with α and for SDB and timesharing since, for timesharing, the number of pulses on target is assumed to be proportional to α. The probability of detection of a target with some nominal SNR at $\alpha = 1$ will decrease faster for aperture partitioning as α decreases. However, if P_D is plotted against β or spectral efficiency, each DFRC method will be different.

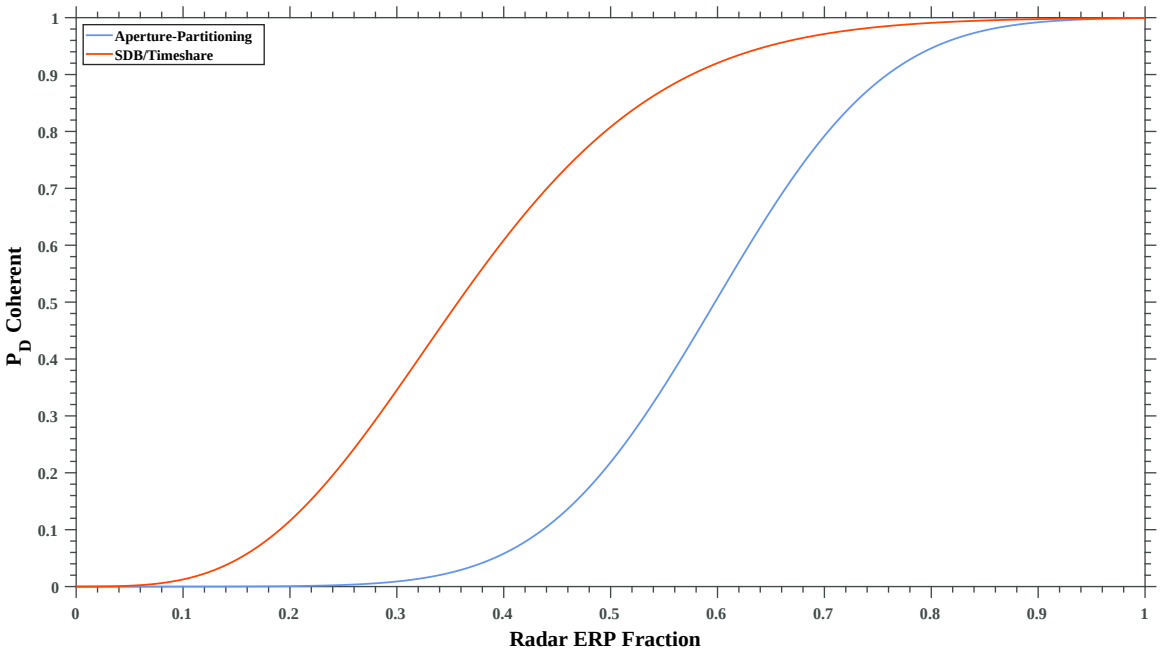

Figure 8.1: Probability of detection for a coherent receiver and Gaussian noise. SNR at $\alpha = 1$ is 15dB and $P_{FA} = 10^{-6}$.

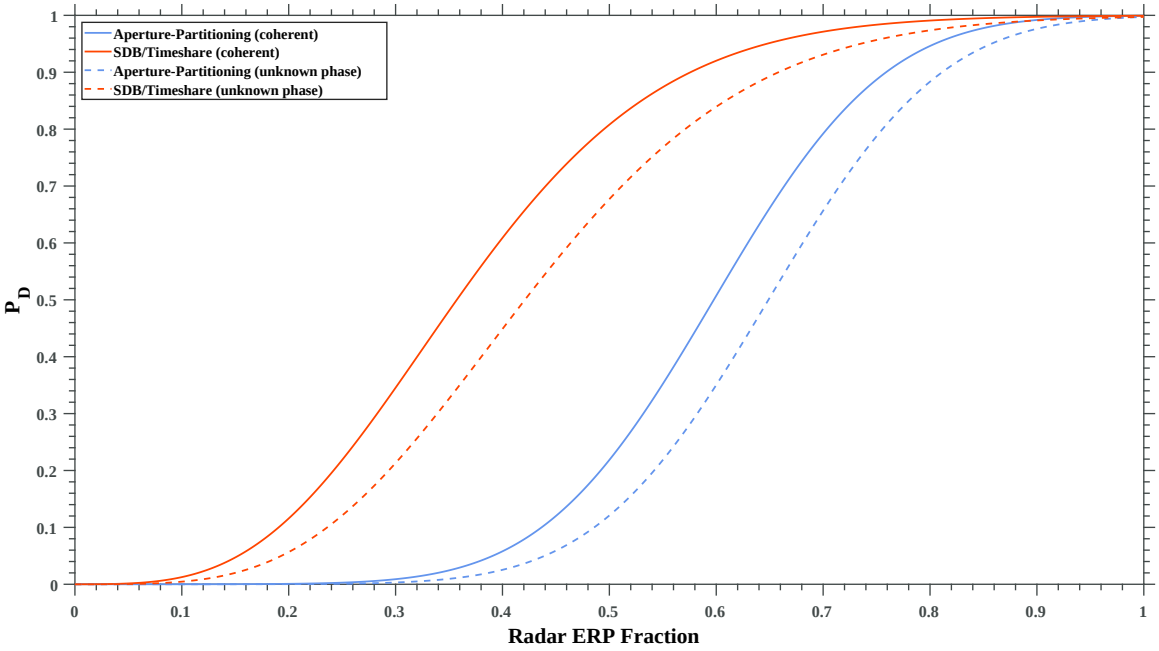

Figure 8.2: Probability of detection for a coherent receiver and Gaussian noise with unknown phase. SNR at $\alpha = 1$ is 15dB and $P_{FA} = 10^{-6}$.

The difference between the two detectors is shown for each DFRC method in the next figure.

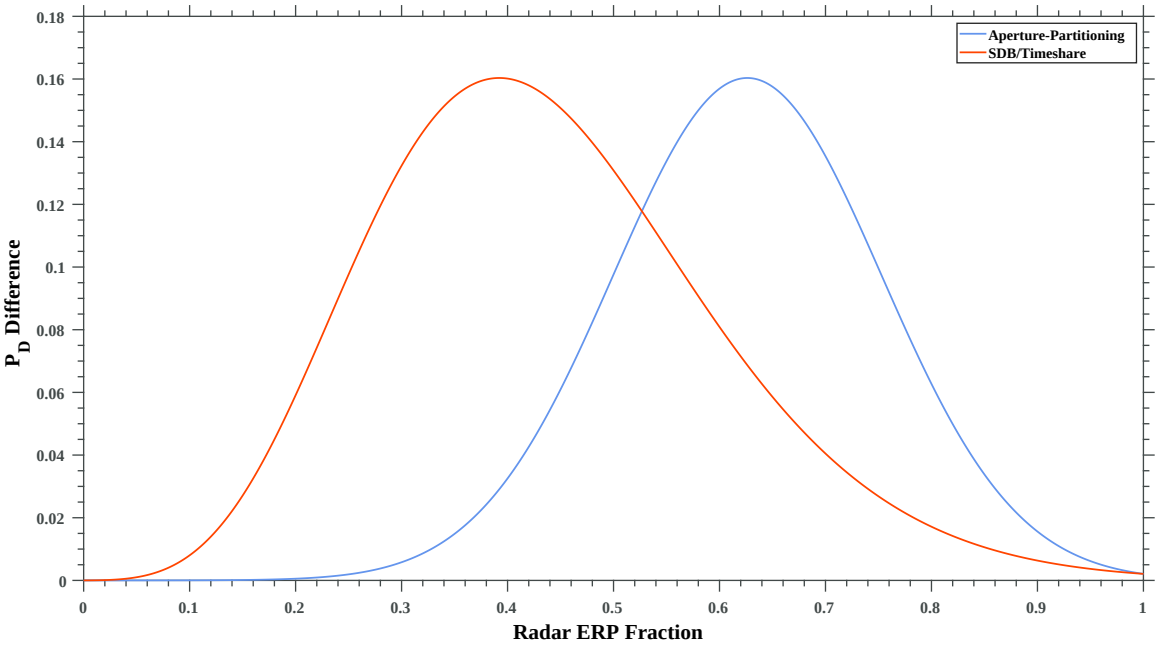

Figure 8.3: $P_{D_{coh}} - P_{D_{phase}}$. SNR at $\alpha = 1$ is 15dB and $P_{FA} = 10^{-6}$.

As expected, SDB and timesharing outperforms aperture partitioning in terms of detection performance due to aperture partitioning's decrease in gain.

Chapter 9

Search

This chapter covers further attempts to incorporate information or capacity into radar operation and using the beamwidth results from chapter 5 and equations from [10] and [11] to look at how each DFRC method affects the results.

9.1 Search Radar Capacity

Guerci et al. [10] suggest a definition of radar capacity as

$$C_r = \log N, \tag{9.1}$$

where N is the number of resolution cells a periodically searching MTI radar produces for a given minimum SNR. The total number of cells is given by

$$N \propto (BR_{max}) \left(\frac{2\pi}{\Delta\theta}\right) \left(\frac{PRF}{\Delta F_D}\right), \tag{9.2}$$

where $\Delta\theta$ is the angular resolution and ΔF_D is the doppler resolution.

Substituting the expression for R_{max} (from the radar range equation) into the above equation results in

$$C_r = \frac{1}{T_s}\left(\frac{B\kappa}{\sqrt{\sigma_n}\sqrt[4]{SNR_{min}}}\right)\left(\frac{2\pi}{\Delta\theta}\right)\left(\frac{PRF}{\Delta F_D}\right); \tag{9.3}$$

where T_s is the scan time, κ is a constant that incorporates all radar losses, and σ_n is the noise standard deviation. This can be combined with communications capacity to obtain the final expression for total capacity,

$$C_r = \frac{1}{T_s}\left(\frac{\beta\kappa}{\sqrt{\sigma_n}\sqrt[4]{SNR_{min}}}\right)\left(\frac{2\pi}{\Delta\theta}\right)\left(\frac{PRF}{\Delta F_D}\right) + \beta\log\left(1+SNR_c\right). \tag{9.4}$$

The above equation will be altered by the different DFRC methods of timesharing, aperture partitioning, and SDB. The implications will be explored in Section 9.3.

9.2 Radar Detection Capacity

A second information-theoretic approach to search radar capacity was presented recently from the perspective of the radar detector [11]. If the probability of false alarm and the probability of detection are viewed as a binary asymmetric channel, the following expression for mutual information is obtained:

$$\begin{aligned} I(H;u) = {} & P_0(1-P_{FA})\left[\log(1-P_{FA}) - \log(P_{u_0})\right] \\ & + (1-P_0)(1-P_D)\left[\log(1-P_D) - \log(P_{u_0})\right] \\ & + (1-P_0)(P_D)\left[\log(P_D) - \log(P_{u_1})\right] \\ & + P_0 P_{FA}\left[\log(P_{FA}) - \log(P_{u_1})\right]. \end{aligned} \tag{9.5}$$

Where P_0 is the probability of no target, P_{u_0} is the probability of deciding no target is detected, P_{u_1} is the probability of detecting a target, H is the random variable of

whether a target is present or not, and u is the decision of whether a target is present or not. These values are given by

$$P_{u_0} = P_0(1 - P_{FA}) + (1 - P_0)(1 - P_D) \tag{9.6}$$

and

$$P_{u_1} = P_0 P_{FA} + (1 - P_0) P_D. \tag{9.7}$$

P_D is then related to P_{FA} through the equations in Chapter 8.

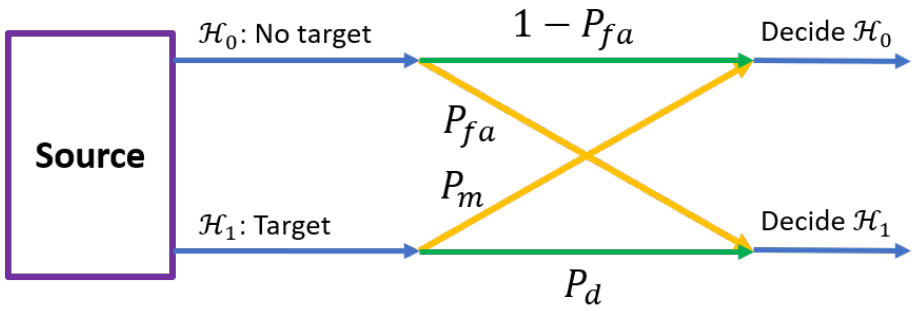

Figure 9.1: Model of radar detection as a binary asymmetric channel.

9.3 Examination of Search Radar Capacity

Given a minimum SNR, χ_{min}, and a signal processing gain of G_{sp}, the maximum range of a radar is given by [6]

$$R_{max} = \sqrt[4]{\frac{P_t G^2 \lambda^2 \sigma G_{sp}}{(4\pi)^3 \chi_{min} k_b T_0 B F_n L_s}}. \tag{9.8}$$

For pulsed timesharing, the total capacity becomes

$$C_{tot} = \frac{R_{max}B}{T_s\alpha}\left(\frac{2\pi}{\Delta\theta}\right)\left(\frac{PRF}{\Delta F_D}\right) + (1-\alpha)BD\log\left(1+\gamma\chi_{comm}\right). \tag{9.9}$$

As mentioned in Chapter 7, aperture partitioning will affect the radar's transmit power and gain. Assuming 100% efficient isotropic elements, this reduces the maximum range as described by

$$R_{max_{ap}} = \sqrt[4]{\frac{(\alpha P_t)(\alpha G_t)G_r\lambda^2\sigma G_{sp}}{(4\pi)^3\chi_{min}k_bT_0BF_nL_s}}. \tag{9.10}$$

This results in the total capacity for aperture-partitioning becoming

$$C_{tot} = \frac{BR_{max}\alpha^{\frac{1}{2}}}{T_s}\left(\frac{2\pi}{\Delta\theta}\right)\left(\frac{PRF}{\Delta F_D}\right) + BD\log\left(1+(1-\sqrt{\alpha})^2\chi_{comm}\right). \tag{9.11}$$

Lastly, the total capacity for SDB is given by

$$C_{tot} = \frac{BR_{max}\alpha^{\frac{1}{4}}}{T_s}\left(\frac{2\pi}{\Delta\theta}\right)\left(\frac{PRF}{\Delta F_D}\right) + BD\log\left(1+\beta_{SDB}(\alpha)\chi_{comm}\right), \tag{9.12}$$

where $\beta_{SDB}(\alpha)$ is obtained by implementing [5].

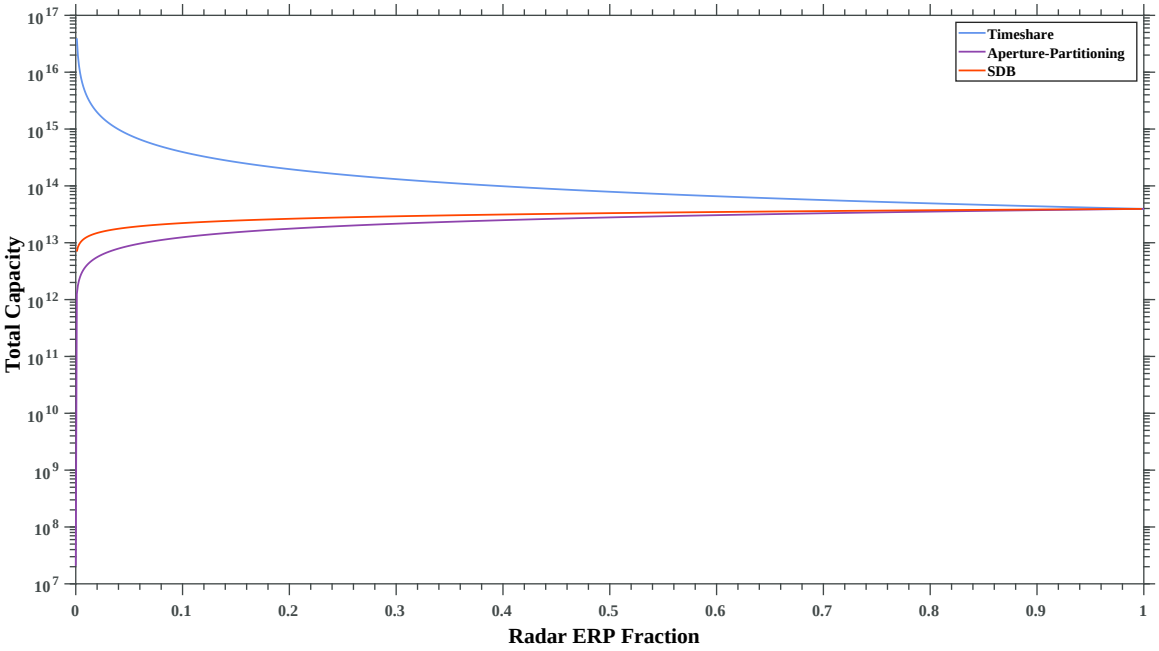

Figure 9.2: C_{tot} vs α for each DFRC method. $\chi_{comm} = 10dB, \chi_{min} = 13dB, PRF = 3000, L_s = 3dB, F_n = 4$, $\gamma = 1$, $T_s = 4$, and $T_p = 20\mu s$.

Reducing the transmit power for the timesharing method does not noticeably affect the results

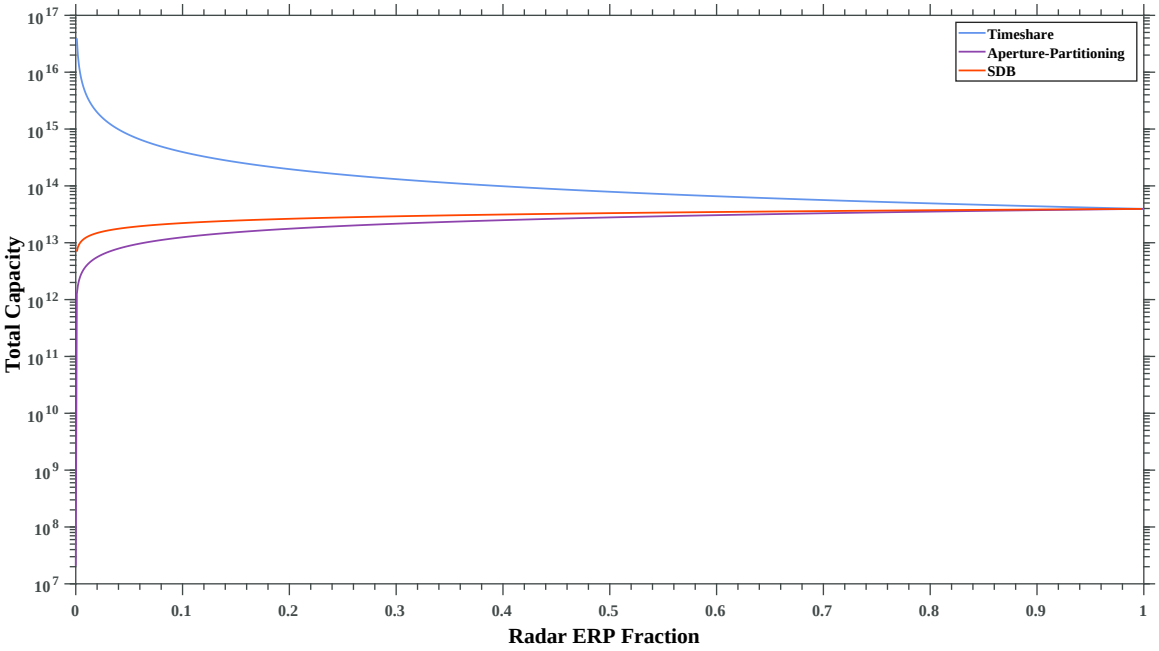

Figure 9.3: C_{tot} vs α for each DFRC method. $\chi_{comm} = 10dB, \chi_{min} = 13dB, PRF = 3000, L_s = 3dB, F_n = 4$, $\gamma = D$, $T_s = 4$, and $T_p = 20\mu s$.

Most likely due to the loss in maximum range, aperture partitioning is always has the lowest C_{tot} value with all methods being fairly close at high values of α

9.4 Detector Mutual Information

Implementing Metcalf's [11] method and using the P_D values obtained in the detection chapter, $I(H;u)$ is plotted for each detector and DFRC method.

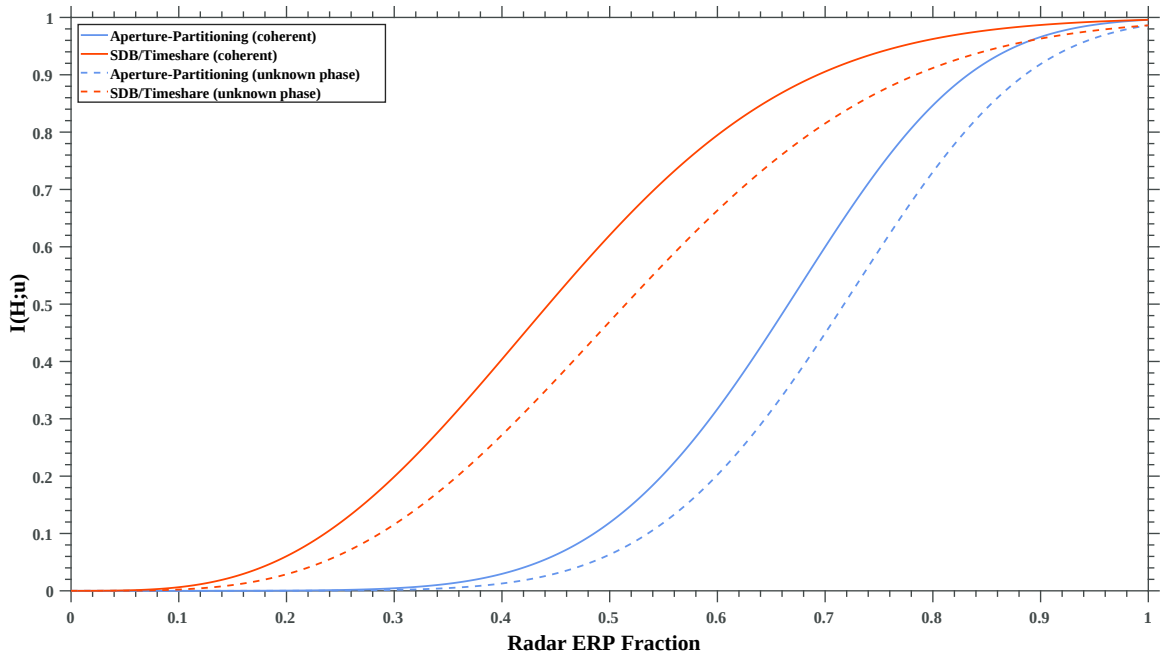

Figure 9.4: $P_0 = 0.5$, $P_{FA} = 10^{-6}$, and SNR at full radar power is 15dB.

As expected, aperture partitioning under performs the other DFRC methods due to its comparatively decreased probability of detecting a target.

Chapter 10

Conclusions and Future Work

In terms of spectral efficiency, SDB was shown to be the optimal DFRC method for the continuous wave scenario if the SNR at the receiver is above approximately 6dB. Since SNR is affected by range, plots were shown that SDB eventually loses efficiency as compared to timesharing as distance increases. For example, if a receiver at 1km has an SNR of 25dB, timesharing will be the superior approach at approximately 10km. It was also shown SDB consistently outperforms aperture partitioning across distance.

For pulsed radar, the optimal method can drastically change if, for timesharing, the communications beam is allowed to continuously transmit. Timesharing still outperforms SDB at reduced transmit power as long as the duty cycle is low and α is low. However, SDB does outperform timesharing at high PRFs at moderate to high communications SNR. Across distance, timesharing remains the optimal method compared against aperture partitioning unless the duty cycle is in very high regimes (larger than 0.6 in shown figures). Likewise, timesharing outperforms SDB, unless the communications SNR is fairly large and the duty cycle is moderate. For example, SDB initially outperforms timesharing at at SNR of 10dB and a duty cycle of 0.4 until only 1.05km. SDB can remain optimal for approximately 2km if timesharing transmit power is reduced and SNR is greater than 25dB.

Across PRF, for a target at a constant distance, timesharing outperforms aperture partitioning unless at high PRFs, SNR, and pulse lengths. If timesharing transmit power in limited to be proportional to the duty cycle, aperture partitioning wins at a PRF of approximately 5000 and an SNR of 30dB. This effect is similar when comparing SDB and timesharing with SDB only winning at high PRFs when the transmit power for timesharing is reduced or the pulse length is increased. For example, with $T_p = 100\mu s$, $\alpha = 0.9$, an SNR of 20dB, and transmit power limited to be proportional to D, SDB is optimal at a PRF of approximately 1600. Future work may be exploring at how limitations to some PRF affected quantities like blind range or doppler changes the optimal DFRC method.

SDB has more advantages when considering that its beamwidth is not affected as much as aperture partitioning when communication is desired while also being able to performs radar tasks simultaneously, although there is some wasted power that is not used by either beam. Furthermore, aperture partitioning while simultaneously emitting two beams was not fully simulated or considered mathematically, this leaves room for future work to better quantify interference effects for aperture partitioning.

For range estimators, each DFRC method is fairly similar as long as most power is dedicated to radar, otherwise aperture partitioning performs very poorly at low α values. As for frequency CRLB, timesharing naturally outperforms other methods if high spectral efficiency is demanded. However, all methods do converge at low spectral efficiency values with SDB outperforming timesharing if PRF is large. Future work would be to look at other CRLBs as a function of spectral efficiency.

As for basic tracking and detection effects, due to beamwidth effects, SDB initially has a larger converged track revisit interval than aperture partitioning until aperture partitioning's power issues increases the revisit interval. Also, a larger interval is not necessarily good since the error in location of a target will be larger with a larger

beamwidth.

Detection performance for each method is also rather unsurprising with aperture partitioning performing the worse out of each method with aperture partitioning acquiring a greater effect of P_D on larger α values than SDB or timesharing.

Looking at experimental measures of radar capacity, timesharing has the highest while aperture partitioning has the lowest. Due to the P_D effects of each method, the mutual information for aperture partitioning is lower than the other methods.

References

[1] A. Hassanien, M. G. Amin, E. Aboutanios, and B. Himed, "Dual-function radar communication systems: A solution to the spectrum congestion problem," *IEEE Signal Processing Magazine*, vol. 36, no. 5, pp. 115–126, 2019.

[2] A. C. O'Connor and N. A. O'Donoughue, "Amplifier performance limits on dual function radar and communication," in *2020 IEEE International Radar Conference (RADAR)*, 2020, pp. 454–459. DOI: 10.1109/RADAR42522.2020.9114680.

[3] G. van Keuk and S. Blackman, "On phased-array radar tracking and parameter control," *IEEE Transactions on Aerospace and Electronic Systems*, vol. 29, no. 1, pp. 186–194, 1993. DOI: 10.1109/7.249124.

[4] T. Cover and J. Thomas, *Elements of Information Theory*, 2nd. John Wiley & Sons, 2006.

[5] N. A. O'Donoughue, "Analysis of dual-transmit beams," in *2017 IEEE Radar Conference (RadarConf)*, 2017, pp. 1233–1238. DOI: 10.1109/RADAR.2017.7944393.

[6] M. A. Richards, *Fundamentals of Radar Signal Processing*. McGraw-Hill, 2005.

[7] C. A. Balanis, *Antenna Theory: Analysis and Design*, 4th. John Wiley and Sons, Inc, 2016.

[8] I. The MathWorks, *Phased array system toolbox*, Natick, Massachusetts, United State, 2022. [Online]. Available: https://www.mathworks.com/products/phased-array.html.

[9] A. Charlish, "Autonomous agents for multi-function radar resource management," Ph.D. dissertation, University College London, 2011.

[10] J. R. Guerci, R. M. Guerci, A. Lackpour, and D. Moskowitz, "Joint design and operation of shared spectrum access for radar and communications," in *2015 IEEE Radar Conference (RadarCon)*, 2015, pp. 0761–0766. DOI: 10.1109/RADAR.2015.7131098.

[11] J. G. Metcalf, "An examination of the spectral utility of radar," in *2022 IEEE Radar Conference (RadarConf22)*, 2022, pp. 1–6. DOI: 10.1109/RadarConf2248738.2022.9764206.